الجـــــــــــــــــــمـهـوريـــــة الجـــــــــــــزائـريـة الديمـــــــقـراطيـة الـشـــــــــعبيـة

PEOPLE'S DEMOCRATIC REPUBLIC OF ALGERIA

وزارة التـــــــــــــــــــــــــــعـليـم العـــــــالي و البـــــــــحث العـــــلـمـــي

Ministry of Higher Education and Scientific Research

جـــــــــــــامعة أبي بكـــر بـلـقـايد – تـلمســـــــــــــان –

University Aboubakr Belkaïd – Tlemcen –
Faculty of TECHNOLOGY

THESIS

Presented for obtaining the **degree** of **DOCTORATE 3rd Cycle**
In: Civil engineering

Speciality: Steel and composite construction

By: Almoutaz Bellah Asem Abdulwahab Mohamed Alsamawi

Subject

Behaviour of composite steel-concrete columns subjected to cyclic loads

Supported publicly, the 21/ 05/ 2022, in front of the jury composed of:

Dr. Zahira Benadla	Professor	Univ. Tlemcen	President
Dr. Nadir Boumechra	Professor	Univ. Tlemcen	Supervisor
Dr. Karim Hamdaoui	Professor	Univ. Tlemcen	Co- Supervisor
Dr. Anis Abidelah	Professor	Univ. USTO-MB	First Examiner
Dr. Bachir Nasser	Professor	Univ. USTO-MB	Second Examiner

ACKNOWLEDGMENTS

In the name of Allah, the most Gracious and the most Merciful

I sincerely express my deepest gratitude to the Almighty.

First and foremost, I would like to express thanks to my supervisor **Dr. Nadir Boumechra**, Professor, Department of Civil Engineering, UABT. It has been an honour to be his PhD student. His guidance on the research methods, deep knowledge, motivation, encouragement and patience in all the stages of this research work has been made the task of the author less difficult and made it possible to complete the thesis work.

I also wish to express his deepest gratitude to my co-supervisor **Dr. Karim Hamdaoui**, Professor, Department of Civil Engineering, UABT for his constant guidance, invaluable suggestions, motivation in difficult times and affectionate encouragement, which were extremely helpful in accomplishing this study.

I am also grateful to all the most respected members of the Doctoral committee (**Dr. Zahira benadla, Dr. Anis Abidellah, Dr. Bachir Nasser**) for their valuable and constructive advice and suggestions throughout this research works.

I also appreciatively remember the assistance and encouragement of my friends and well-wishers and everyone related to carrying out and completing this study.

Finally, I wish to express my deep gratitude to my family members: my **father**, my **mother**, my sister (**Maram**), my **brothers** (**Moutassem**, **Mohammed**, **Mostafa** and **Amir**) and my uncle (**Eng. Anis Alsamawi**) for their constant support encouragement and sacrifice throughout the research work.

TABLE OF CONTENTS

LIST OF FIGURES

LIST OF TABLES

LIST OF SYMBOLS

A_a cross-sectional area of the structural steel section.

A_c cross-sectional area of concrete.

A_s cross-sectional area of reinforcement.

c the cover concrete.

Coeff the coefficient of the friction.

E energy dissipation.

E_a modulus of elasticity of steel profile.

E_{s2} modulus of elasticity of reinforcement bars.

E_{cm} modulus of elasticity of concrete.

ε_{c1} the strain at reaching the maximum strength.

ε_{cu1} the ultimate strain.

f_y yield strength of steel profile.

f_{sk} yield strength of reinforcement bars.

f_{ck} characteristic compressive cylinder strength of concrete at 28 days.

f_{cm} mean value of concrete cylinder compressive strength.

f_t the value of the design tensile strength.

F_{sk} Characteristic value of the yield strength of reinforcing steel.

h Height of the composite column.

K_y initial stiffness.

k_i structural stiffness.

N the ratio of axial load.

P the axial load.

P_{exp} the maximum load from the experimental test.

P_{FEM} the maximum load from the numerical simulation.

P_m maximum lateral load that can be supported by the composite columns.

P_y yield load.

P_u the ultimate load.

$N_{Pl,Rk}$ characteristic value of the composite section's plastic resistance to compressive normal force.

Δ_y the yielding of the structural steel section displacement.

Δ_u the ultimate displacement.

μ ductility factor.

GENERAL INTRODUCTION

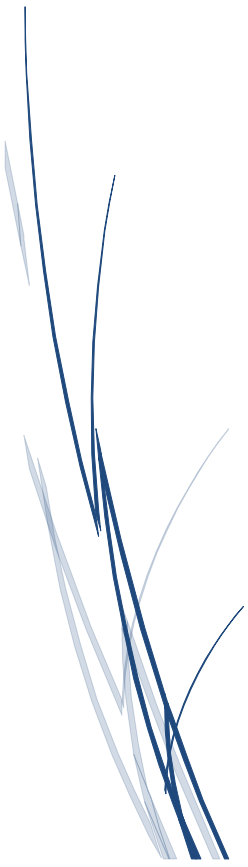

GENERAL INTRODUCTION

A composite column is a load-bearing structural element made out of structural steel shapes, with or without reinforcing steel bars, and concrete to support axial compressive loads alone or a combination of axial and cyclic loads. Both of steel and concrete sections of a composite column resist external loading by interacting with each other through bond and friction. Structural steel is encased in concrete or concrete is encased in structural steel in composite columns. These columns are used in the construction of high-rise buildings all over the globe because they could minimise the size of the building's columns while increasing the floor plan's useable area. Furthermore, the composite column improves the building's overall stiffness and offers great shear resistance against strong earthquakes and other lateral loads.

There are three types of composite column sections more used in high-rise construction: (a) fully encased composite column (FEC), (b) partially encased composite column (PEC) and (c) concrete filled tube (CFT). Figure 0.1 depicts typical cross-sections of these three types of composite columns. The structural steel section of FEC columns is totally encased by surrounding concrete, as indicated in Figure 0.1(a), while the steel section of PEC columns (Figure 0.1 (b)) is partially encased by concrete. On the other hand, in concrete filled tubular composite columns (Figure 0.1 (c)), the concrete is completely contained by the steel section that surrounds the concrete. These composite sections have developed to maximise the benefits of both concrete and steel. Concrete offers compressive strength, stability, stiffness, increased fire proofing, and high corrosion protection in these composite sections, while steel provides tensile strength, ductility and rapid construction speed. Because the steel section is totally encased by concrete, the FEC column provides better fire proofing and corrosion protection than the other two sections. In contrast to PEC and CFT columns, FEC columns do not require fire proofing or corrosion resistance. As a result, due to the humid weather conditions and the seismic activity in Algeria, FEC columns may be the best solution for high-rise constructions in terms of strength, ductility, and economy.

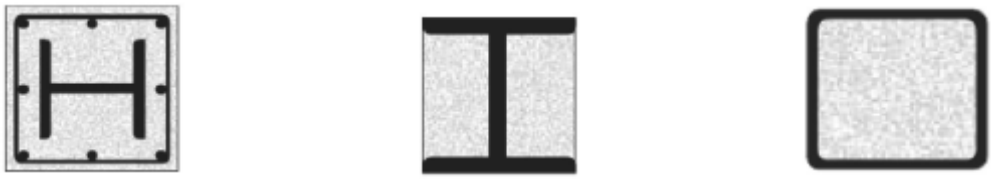

a) b) c)

Figure 0.1: Typical sections of composite columns, (a) FEC; (b) PEC; and (c) CFT.

In comparison to an experimental investigation, numerical analysis takes less time and is more cost-effective. It is also more practical than analytical or theoretical research. Furthermore, finite element (FE) analysis can predict experimental results and separate the contributions of individual FEC column

elements. There have been relatively few studies on FEC columns subjected to cyclic loading using FE analysis and altering various parameters of FEC columns. It was discovered that only a few research had been done on the creation of a filled finite element model on FEC columns with various percentages of structural steel, load axial ratios, spacing of transverse reinforcement and high strength materials, among other things. The effects of axial load, cover concrete, steel-concrete coefficient of friction and boundary conditions have not been well studied. The connectors insert a good adherence between the concrete and the steel so it has good behaviour. The concrete reinforcement bars have great importance in the concrete-steel connection because they reinforce the concrete. There is consideration to combine steel profile and reinforcement bars in an industrial concept.

Even though FEC columns are frequently used in high rise composite buildings, the understanding of their fundamental behaviour is still not sufficient analysis, design methods have not been developed owing to the lack of experimental and numerical research on this type of composite columns. The current design codes such as Eurocode 4 (2004), LRFD (1999) and ACI 318 (2002) do not provide specifications for the design of FEC columns subjected to cyclic loading.

The research aims to develop new numerical models for simulating the nonlinear inelastic behaviour of FEC columns under axial and cyclic loading. The research findings from this project make significant contributions to the analysis and design of FEC columns under axial and cyclic loads. The numerical models were developed to provide structural designers with advanced analysis and design tools that can be used to design safe and economical composite buildings. Furthermore, the proposed numerical models allow the designer to analyse and design FEC columns made with a new type of connection between steel and concrete.

1 Objective of the study

Two main objectives have been defined for this research work:

1- Understand the behaviour of FEC column under cyclic loads.

2- Develop new types of connection between steel and concrete interface in the FEC column.

To achieve these objectives, the work envisaged within the framework of the thesis is as follows:

1. Implementation of 3D columns using ANSYS code.
2. Validation of the global modelling with experimental results.
3. Investigation of the coefficient of friction.
4. Investigation of the cover concrete.
5. Investigation of the effects of longitudinal and transversal bars.

6. Investigation of the effects of the connectors.
7. Investigation of the effects boundary condition.
8. Investigation of the effects of axial load.

To achieve the objectives mentioned above serval numerical studies were conducted. The numerical simulation consisted of seventy-five (75) square FEC columns with the effect of serval geometries, physical and mechanical parametric are analysed as column sizes, coefficient of friction, ratio of axial load, reinforcement bars ratio (longitudinal and transversal bars) and types of shear connectors in the dynamic compound.

Firstly, eight of these columns were constructed with a different size to study the effect of the cover concrete. After those eleven columns were constructed with the same size of 450 mm × 450 mm to investigate the effect of the coefficient of friction. Another thirty-six columns have the same size of composite column with different percentages of concrete reinforcing bars and axial load ratio were built to study the effect of the concrete reinforcing bars and axial load. Also, seventeen columns were constructed with different types of shear connectors in order to verify the effectiveness of the proposed shear connectors. All the columns had a length of 4000 mm. The columns were investigated with axial load applied at the centroid of the column cross-section and the horizontal load is applied with displacement using boundary conditions under different increment steps. Finally, three columns with fixed boundary conditions at the end of the column were built to understand the behaviour of FEC columns under cyclic loading in reality.

The ANSYS finite element software was used to construct the numerical models for FEC columns. Both geometric and materials nonlinearities were included in the FE model. A concrete damage plasticity model capable of predicting both compressive and tensile failures was used to model the concrete material behaviour. To validate the model, some simulations were conducted for both monotonic and cyclic loads test specimens from the current study and test specimens from published literatures, encompassing a variety of lengths and types loads. Comparisons were made between the FE predictions and experimental results available in the literature by Aribert et al. [1] in terms of (load-displacement curve, peak load and failure mode) of the FEC columns. An extensive parametric study was conducted using the numerical model to investigate the influences of some key parameters affecting the behaviour of FEC columns under axial and cyclic loads. The key parameters selected in the present study are a cross-section of the composite column, coefficient of friction, percentage of concrete reinforcing bars, a ratio of axial load and spacing of the shear connectors. The concrete used in the proposed model is stress-strain relation for non-linear analysis, recommended by Eurocode4 [2]. The steel is assumed to behave as an elastoplastic material.

2 Organization of the thesis

This thesis has five chapters, and the following is a summary of the report structure:

Chapter 1 presents an introduction of the FEC column and shear connectors, an extensive literature review on the nonlinear analysis and behaviour of composite columns. Published work on the nonlinear analysis and behaviour of FEC columns under axial load and cyclic loads is firstly reviewed. The study of cyclic horizontal loads and a constant vertical load on partially encased composite columns are summarised in this report. Extensive reviews are then tested and investigated to the preloaded circular and rectangular concrete-filled steel columns. Finally, the studies on the shear connectors are highlighted. The scopes and conclusions of the research work are presented.

Chapter 2 presents the development of the finite element model, including the element selection, mesh description incorporating the built dimensions, steel-concrete interaction modelling, boundary condition simulation, material properties. Loading application and validation of the numerical results used in the models are also included.

Chapter 3 presents the numerical results, including hysteretic behaviour, skeleton curves, energy dissipation, ductility and structural stiffness of the test specimen on the behaviour of FEC column under cyclic loads. Cover concrete, coefficient of friction and effect of boundary conditions in the FEC columns are included.

Chapter 4 presents the numerical results, including hysteretic behaviour, skeleton curves, energy dissipation, ductility and structural stiffness of the test specimen. Discussions about the effect of concrete reinforcing bars (longitudinal and transversal) and the effect of axial load in the FEC columns are presented as well.

Chapter 5 presents the numerical results, including hysteretic behaviour, skeleton curves, energy dissipation, ductility and structural stiffness of the test specimen. Discussions about the performance of the proposed connected reinforming design in the FEC columns are included.

And the thesis is finalized by a conclusion, global synthesis and some presented perspectives for thesis contribution.

Chapter I
LITERATURE REVIEW

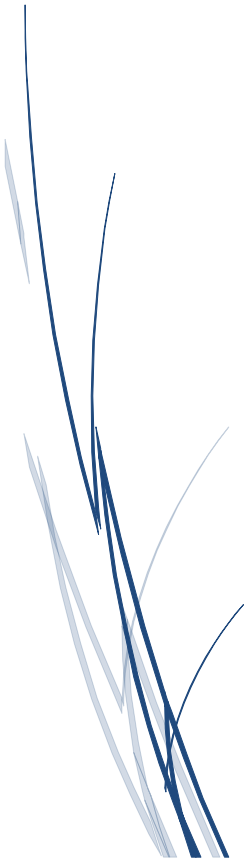

CHAPTER I
LITERATURE REVIEW

I.1 Introduction

Composite columns are constructed using different combinations of structural concrete and steel to take advantage of the beneficial properties of each material. The reactive and integrative behaviour of steel and concrete structural members makes the composite column extremely rigid, more ductile and cost effective, and therefore it is a structurally effective element in building and bridge constructions. Three main types of composite column sections are used in the construction of high-rise buildings. In the early of twentieth century, concrete was used for encasement steel columns and beams, and as a filler material for flooring systems. The first experimental test was performed by Emperger in 1907 on composite columns built under a concentric load [3]. The authors have also proposed formulas for predicting the strength of composite columns Bridge and Roderick [4] and Eggemann [5]. Experimental investigations have been carried out on concrete encased steel composite columns by various researchers long ago. On the other hand, the numerical simulations of reinforced concrete structures using the finite element method has seen significant progress since 1990. Although experimental research is costly and time consuming than numerical research, progress in numerical studies is relatively less. Recently, various researchers have developed nonlinear finite element models that investigate the behaviour of the concentric axial loads and seismic performance of composite columns. A large number of design specifications addressed the design of composite columns. Among these, Eurocode 4 [2], AISC-LRFD [6] and ACI- 318 [7] have been widely used worldwide for composite structure design. Initially, the American Institute of Concrete (ACI) and the American Institute of Steel Constructions (AISC) provided rules for designing these structural elements. In 1978, a Joint Structural Specifications Liaison Committee (SSLC) was organized in the United States of America to evaluate the acceptability of composite column design procedures. Respectively, the numbers of versions of the Eurocode4, AISC-LRFD and ACI-318 specifications were released at various times. Other specifications or codes that have provided composite structure design rules are the Eurocode (ENV 1994), the New Zealand Building Code (8 NZBC1992) standards [8], the Australian Building Code (BCA, 2005) [9] and the Japanese Architectural Institute (AIJ, 1997) [10]. However, Eurocode 4, AISC-LRFD and ACI-318 are being widely used around the world for the design of composite structure. Composite columns are widely used in civil and industrial building construction thanks to their efficiency in constructions with large load capacity and their economic advantages. In this regard, shear connectors are the most common solution to ensure the assembly of steel structures with concrete in composite structures.

I.2 Types of Composite Columns

Composite columns sections can be classified into three types, (a) Fully encased composite column, (b) Partially encased composite column, and (c) Concrete filled steel column. A typical cross-section of

these three types of composite columns is shown in Figure I.1. These three types of columns are divided by the position and shape of structural steel. As shown in Figure I.1(a) steel sections are surrounded by concrete while in partially encased composite columns the steel section is partially encased by concrete with or without reinforcement indicated in Figure I.1(b) and Figure I.1(c). On the other hand, in concrete-filled tubular columns, the concrete is fully confined by the surrounding steel section shown in Figure I.1(d) to Figure I.1(f). These composite sections have been developed to make the best out of both materials (concrete and steel).

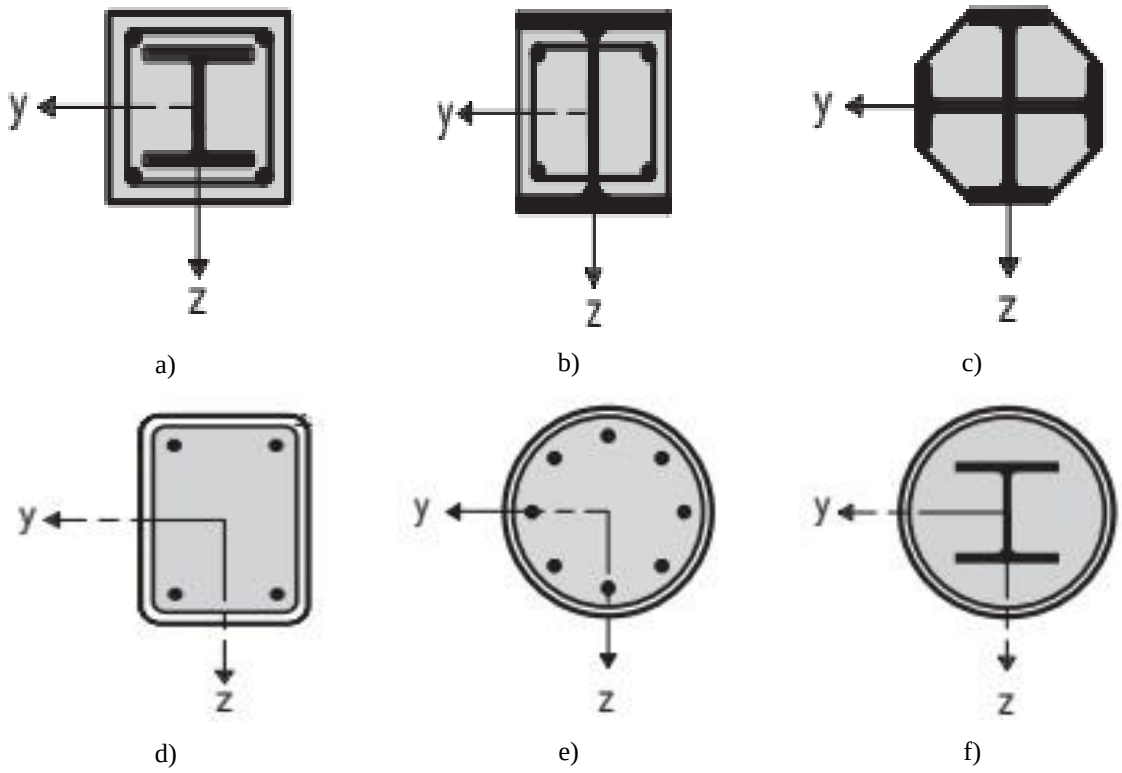

Figure I.1: Typical cross-sections of composite columns [2]**.**

Concrete gives compressive strength, stiffness and stability, while steel gives tensile strength, high speed of construction and ductility. Among these three sections, a fully encased composite column provides the best fire resistance and corrosion protection because the steel section is surrounded by concrete. The cost for fire resistance and corrosion protection is not required for fully encased composite columns as compared to partially encased composite columns and concrete-filled tube columns.

I.3 Types of shear connectors

Many researchers focused on the shear stud connector, combined with the composite beam also combined with the composite column. Headed stud shear connectors are among the most popular types of connection devices used in composite constructions shown in Figure I.2 (a). Additionally, the bolted shear connectors in composite steel-concrete structures are shown in Figure I.2 (b). And other types of

shear connectors have been investigated, as well as perfobond connectors, channel and angle shear connectors, connector made of top-hat profile, omega-shaped connector, transversal connector, angled, V-shaped connector and longitudinal connector as shown in Figure I.2.

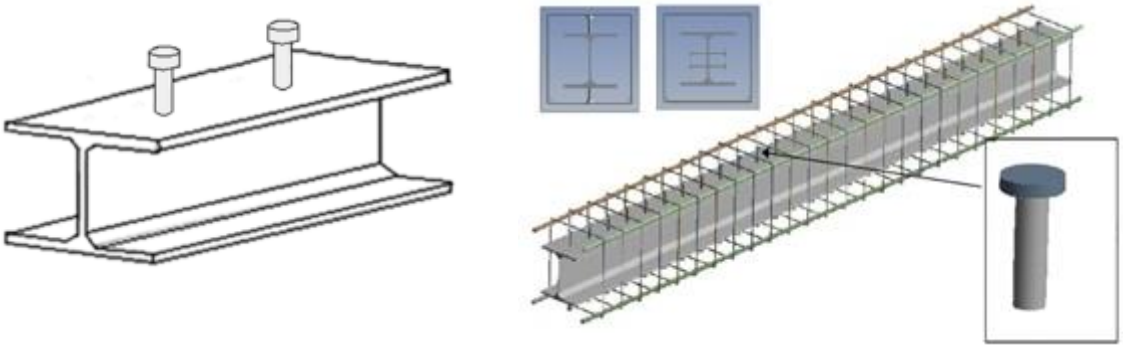

a) Headed stud shear connectors for beam and column

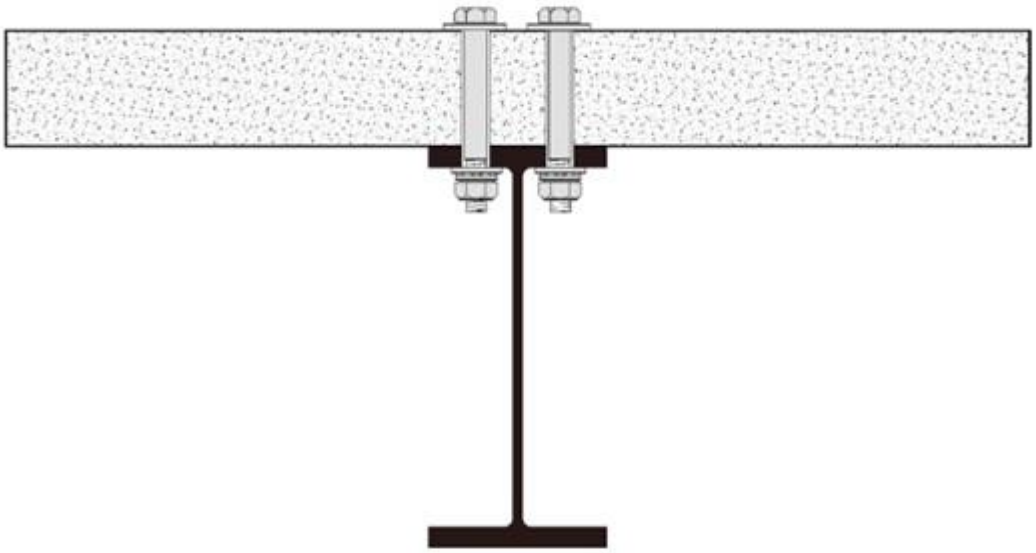

a) Bolted shear connectors [11].

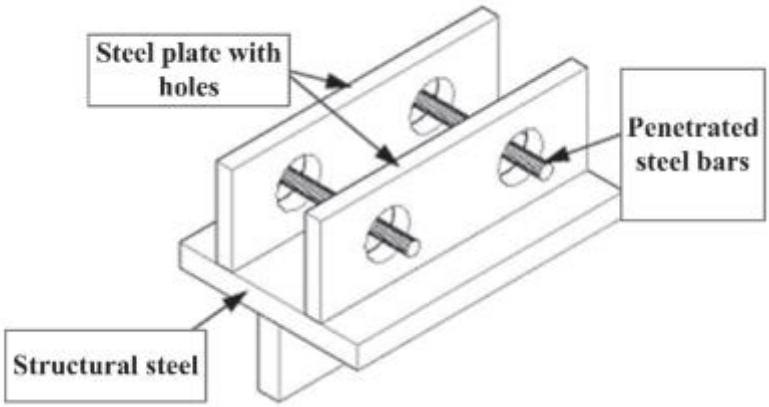

b) Perfobond connectors [12].

c) Channel and angle shear connectors [13].

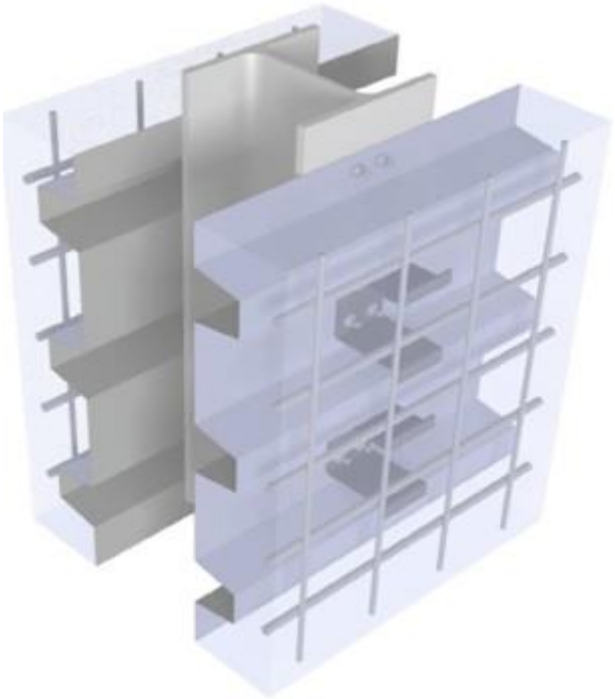

d) Connector made of top-hat profile [14].

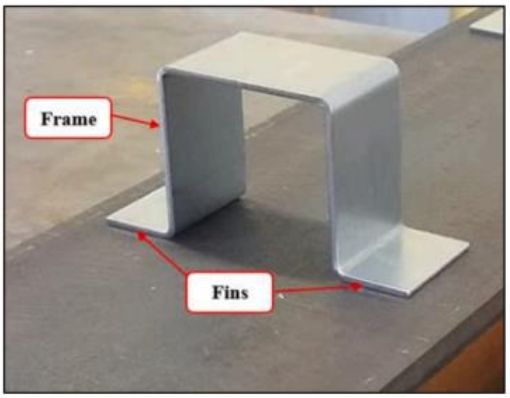

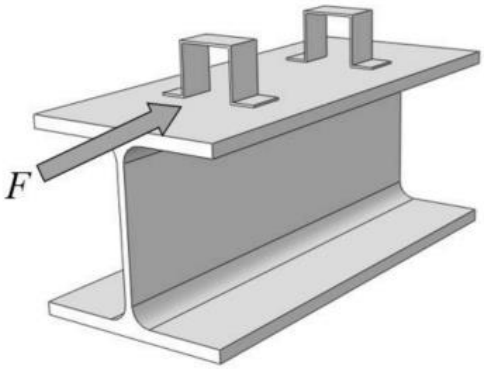

e) Omega shaped connector [15].

f) Transversal connector, angled, V-shaped connector and longitudinal connector [16].

Figure I.2: Some examples of shear connectors.

I.4 Research on composite columns and shear connectors

Several experimental, analytical and a few numerical research works were carried out on a composite column by previous researchers. Experimental study on composite columns started in 1907 for concentric axial load. The investigations of composite columns under cyclic loads started in 1972 [17]. Bridge and Roderick [4] and Eggemann [5] reported that Emperger in 1907 determine the buckling loads of steel columns by tested the columns. Successively, he carried out more than 1500 tests on composite columns in North America and in Europe from 1907 to 1932. Furthermore, he distinguished different types of composite columns. Finally, design formula published by the researchers to determine the ultimate capacity of composite columns. Recently, the numerical models were designed to investigate the behaviour and the strength of fully encased composite column. Some previous researches have been

also carried out on filled steel tube reinforced concrete columns and encased steel concrete composite columns under constant axial load and cyclic load, it was found that both columns exhibit favourable ductility and energy dissipation and are adoptable in areas with strong earthquakes.

I.4.1 Fully encased composite column

Chen et al. [18] carried out on stirrup ratio and embedded depth ratio for steel-concrete composite columns shown in Figure I.3, by testing twenty-six columns under low cyclic loading. By analysing skeleton curve, hysteresis loops, failure patterns, ductility and energy dissipation of each specimen. It was found that the seismic behaviour is better when the stirrup ratio is increased, the composite columns with cross-shaped steel have better seismic performance than those with H-shaped steel, and the minimum value can be 2.5 of the embedded ratio of steel-concrete composite columns.

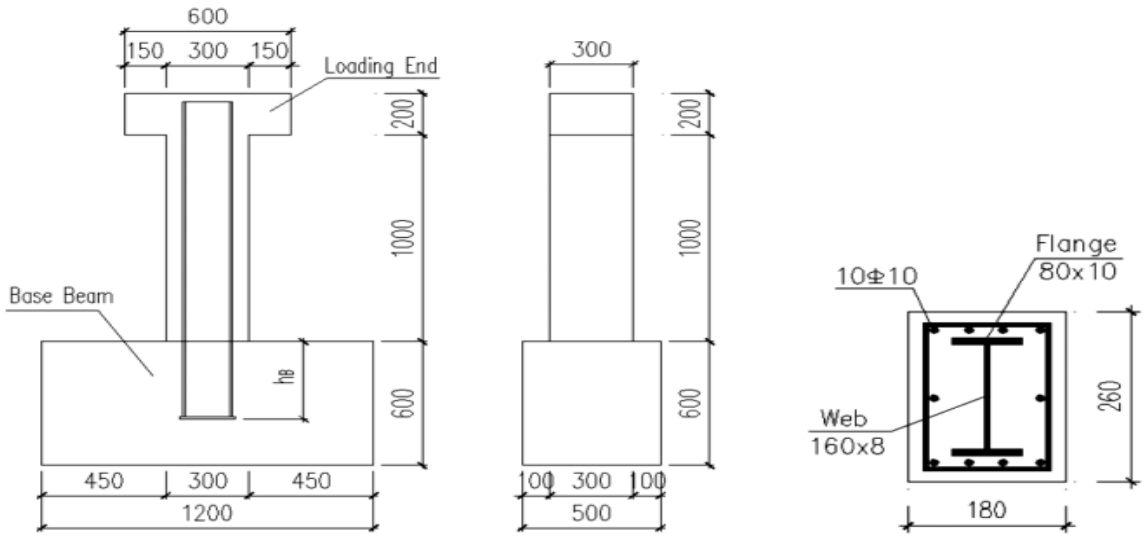

a) Outline and section details of the first batch of specimens

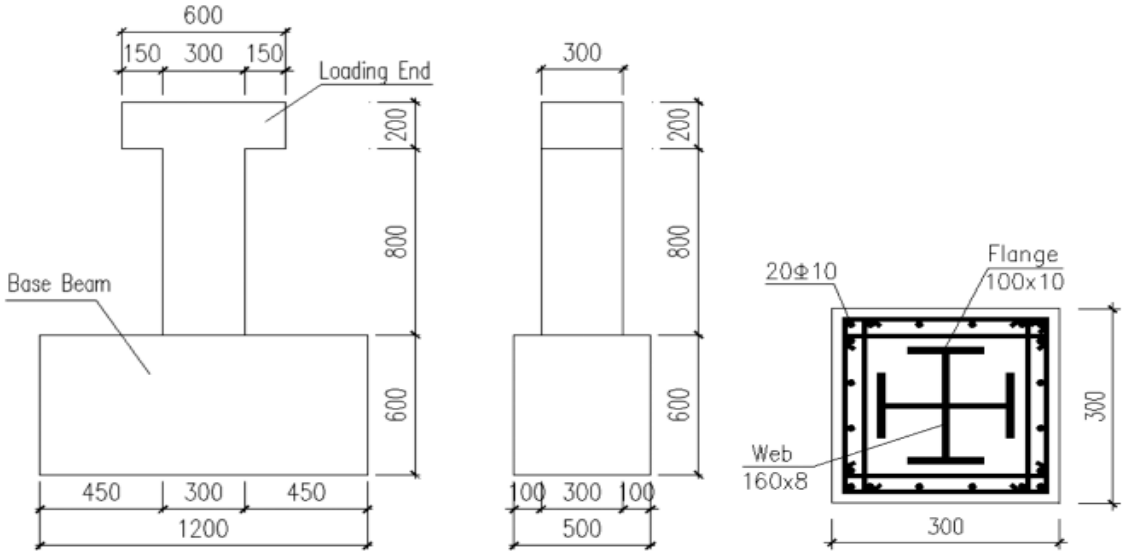

b) Outline and section details of the second batch of specimens

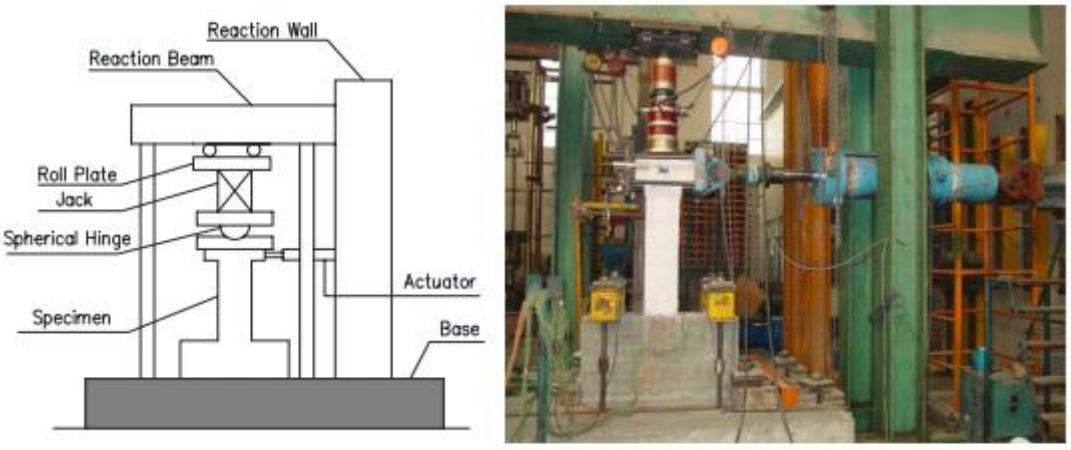

c) Setup of the cyclic test

Figure I.3: Experimental test of Chen et al. [18]**.**

Campian et al. [19] compared the results of composite encased columns made of high strength concrete to those constructed of normal strength concrete. The findings show that high-strength concrete columns are more susceptible to fragile failure than normal-strength concrete columns and that high-strength concrete has a favourable energy absorption capacity

Zhu et al. [20] tested the effects of stirrup arrangement and structural steel details with studs and studied the behaviour of the steel-reinforced high strength concrete columns (SRHC) under cyclic load by experientially testing twenty-one of SRHC columns as shown in Figure I.4. The SRHC which have multiple stirrups exhibit excellent deformation capacity and sufficient energy dissipation. During the early loading stage, the studs hardly affected the performance of SRHC columns. After cover spalling, studs have a positive effect on the seismic behaviour of SRHC columns. Columns with studs have better energy dissipation capacity and deformation, and when the studs are adopted the stiffness degradation of columns becomes less rapid.

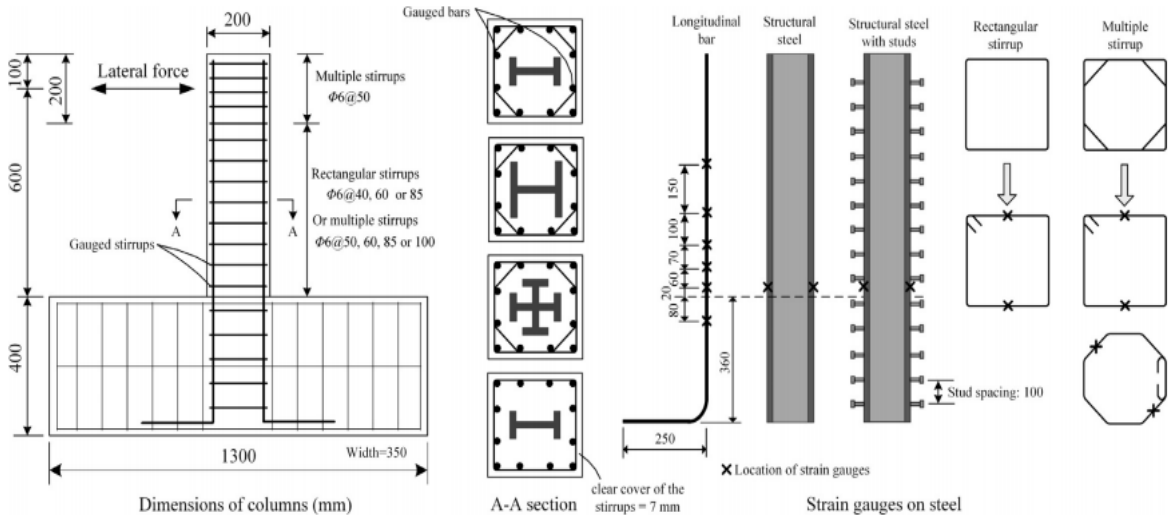

Figure I.4: Details of SRHC column specimens [20]**.**

Fang et al. [21] studied the seismic behaviour of cross-shaped columns, L-shaped section and T-shaped section as shown in Figure I.5, by testing four specimens subjected to combined cyclic load and constant axial load, to measure the effects of the loading angle, the steel ratio, and the axial load ratio on the behaviour of concrete-encased steel cross-shaped columns. It was indicated that with the increase of the axial compression ratio, the maximum lateral load increases simultaneously, while the stiffness degrades and the displacement ductility decreases significantly. The loading angle of 45° gives preferable maximum lateral load than 0° contrary to the displacement ductility in 0° preferable than 45°. Also, the columns show a decent energy dissipation capacity, deformation capacity and ductility.

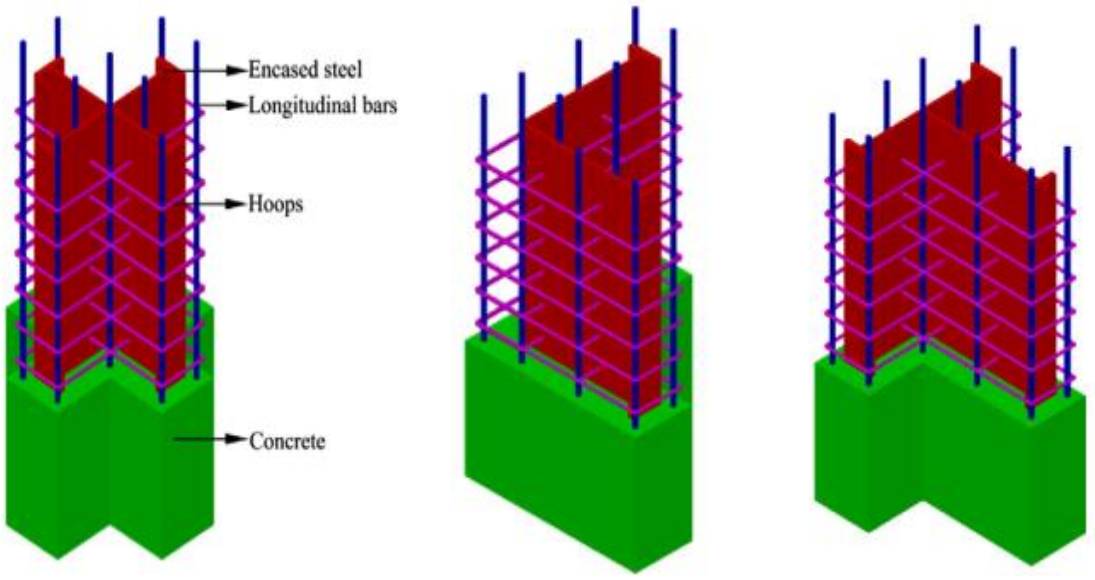

a) Cross-shaped section b) L- shaped section c) T- shaped section

Figure I.5:Schematic view of CESS columns [21]**.**

XU et al. [22] investigated the seismic behaviour of T-shaped steel sections columns shown in Figure I.6, by testing twelve specimens subjected to combined constant axial load and cyclic loading, to study the effects of the presence of cross tie, stirrup ratio, shear span ratio and axial compression level. It was found that the unsymmetrical phenomenon effects the hysteresis curve, with the increase of axial load level the ductility decreases. The cross tie reduces the stiffness degradation and strength attenuation and reinforces the bearing capacity.

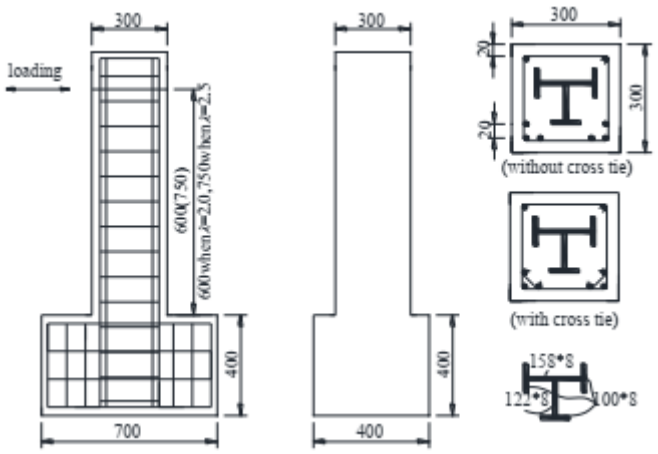

Figure I.6: Specimen dimension and steel details [22].

Shim et al. [23] investigated composite columns with less than 4% of steel, loading pattern and the amount of transverse reinforcement, by testing eight concrete-encased composite columns with various steel ratios, to investigate the seismic performance of composite columns, especially those with less than 4% steel as shown in Figure I.7. Embedded steel members on cyclic performance were evaluated, the effects of transverse reinforcements and the failure modes were carefully observed as illustrated in Figure I.8. Based on test results, design considerations related to the details of transverse reinforcements of composite columns were suggested.

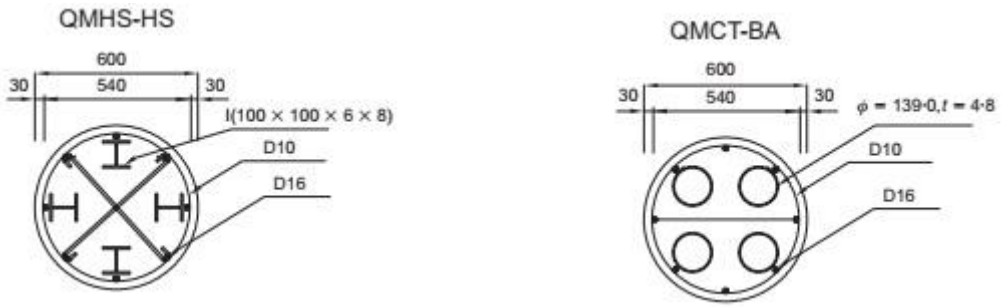

Figure I.7: Examples of test specimens a) Composite column with 4 H-shaped members Cross ties. b) Composite column with 4 steel tubes. [23].

a) Composite column with 4 H-shaped members Cross ties

b) Composite column with 4 steel tubes

Figure I.8: Failure pattern of specimens [23]**.**

Hsu et al. [24] determined member strengths under combined axial load and bi-axial bending, by proposing the interaction coefficients α and β. Through testing series of composite members with different sectional compositions under various axial load and bi-axial bending combinations as shown in Figure I.9. Furthermore, experimental and analytical investigations are proposed on the performance of composite members which are subject to various biaxial loading and composed of steel with different strengths to be conducted to refine the above parameters. The relationships between structural parameters and members' seismic performance, similarly the magnitude of bi-axial bending and the sectional steel strength ratio, were determined in this study as well. From tests, it was found that the rates of strength degradation increased when the strength ratios of the member's steel increased in the weak axis. This study proposed that the ratio of the strong axis and the steel strength ratios of the weak axis was set at approximately 2.2 to improve the element's seismic performance. The test results indicated that the steel strength ratios in the weak and the strong directions of the sections should be adjusted appropriately so that the high performance of the members could be achieved.

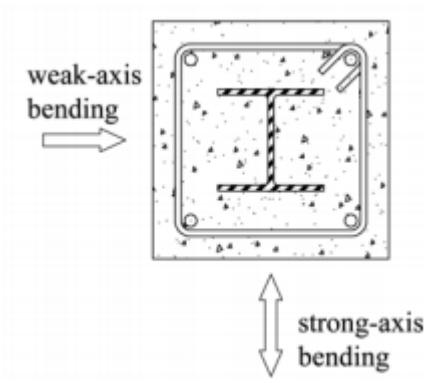

a) Definitions of load directions

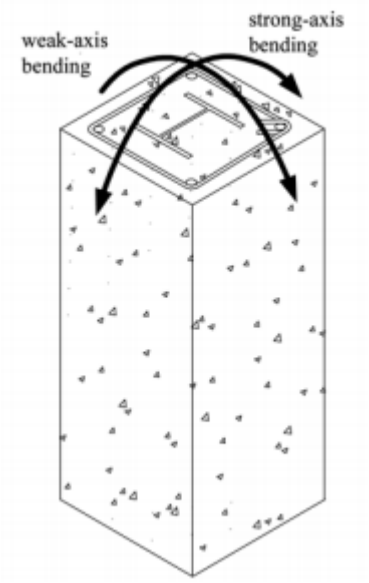

b) 3-D sketch

Figure I.9: Specimen details [24].

Ellobody et al. [25] analysed the effect of concrete confinement as well as the inelastic behaviour of concrete, steel, transverse and longitudinal reinforcement bars, and the interface between the steel section and concrete of the concrete-encased steel composite columns. The authors studied forty-eight specimens to understand modes of failure and structural response of columns and to evaluate the composite column strength against design codes. The primary goal was to validate the finite element (FE) models against current test results and to carry out parametric studies under varying eccentricity. All experimental columns were created with normal strength concrete. It is observed that the composite column strength of the columns with higher slenderness ratios has affected a small effect by the increase of structural steel strength, due to the flexural buckling failure mode. The strengths of the composite column obtained from FE analysis were compared with the design strengths calculated using Eurocode 4 and AISC codes for composite columns.

Taufik et al. [26] determined the fracture patterns, strain, stress, deformation, ductility and capacity of axial load. By analysing serval composite columns under axial load, to analyse the failure behaviour of modelling encased composite steel-concrete columns. The results indicated that the composite column could be analysed using ANSYS software, columns with compressive collapse condition have a higher flexural capacity and less ductile than those columns with tensile collapse, and the analysis of calculation and finite element method determined the behaviour of composite columns.

Naito et al. [27] investigated the ductility of concrete-encased steel piers as a steel-reinforced concrete column under cyclic loading. By testing and analysing nine concrete-encased steel columns to perform an experimental evaluation of the damage process and the ductility of steel-reinforced columns subjected to cyclic lateral loading. To provide a method for calculating ductility of steel-reinforced columns based on instability analysis of H- shaped steel and longitudinal bars, and to determine the maximum condition

of the steel-reinforced columns corresponding to the damage condition. From these tests, the ultimate state and the recoverable boundary state were defined as the local buckling of the H-steel and the spalling of the concrete cover, respectively as shown in Figure I.10. This work proposes a method for estimating the lateral displacement capacity of these two limit states. The lateral displacement at the beginning of spalling can be calculated by integrating the curvature distribution based on the analysis of the bar buckling, taking into account the restraint and the plastic behaviour of the longitudinal bar including the steel ties and the concrete cover. Moreover, the length of the plastic hinge and the bar buckling length can be accurately estimated using the proposed method. The experimental results indicated that the specimens have exceptional cyclic strength and ductility if a sufficient amount of steel is used. In particular, specimens of steel-reinforced concrete columns have a great load-bearing capacity after cracking and buckling of the longitudinal bar. A comparison of theoretical and experimental results showed that the ultimate displacement is estimated by the proposed method and that the experimental results correspond fairly well with the plastic length and flange buckling length. As shown above, the lateral displacement capacity of steel-reinforced concrete bridge piers can be calculated using the proposed method in the ultimate limit states and the restorable.

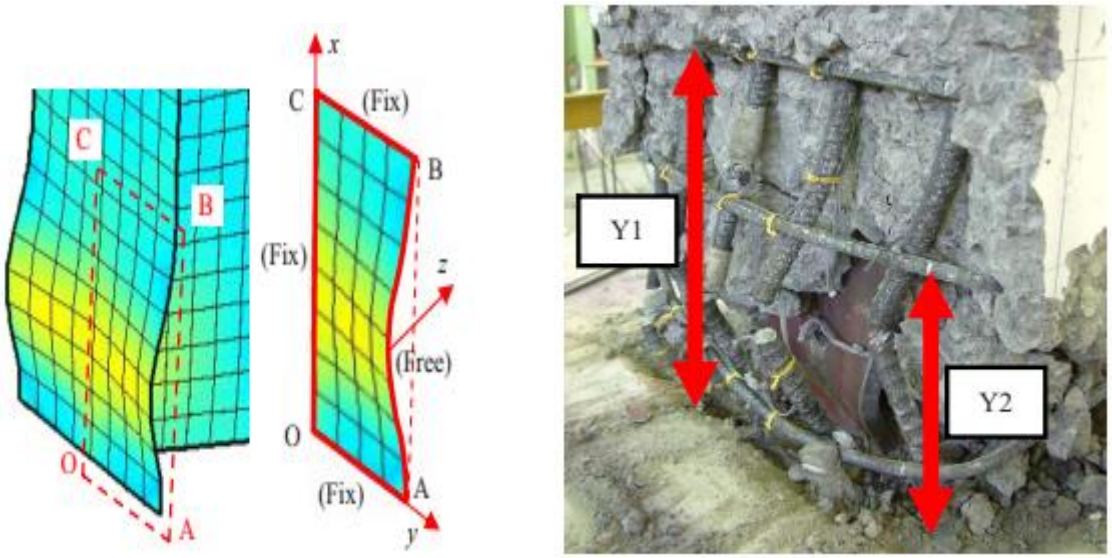

a) Buckling deformation from FE analysis

a) Visible damage to the column specimen. Y1 is the bar buckling length and Y2 is the flange buckling length

Figure I.10: Failure mode of the specimen [27]**.**

Yue et al. [28] tested experimentally two concrete-encased steel columns and numerically 486 concrete encased steel (CES) columns under high axial compressive ratios and low-cyclic lateral loading, to determine damage performances include cover concrete spalling, cover concrete cracking, core concrete crushing, steel flange local buckling, compressive longitudinal reinforcement yielding and longitudinal reinforcement buckling as shown in Figure I.11. CES columns were analysed numerically by the fibre finite element method and evaluated by a modified Park-Ang damage model in each damage performance condition. In conjunction with the results of the statistical damage analysis, five performance

levels were established based on the seismic damage stress and their limit values, namely Serious damage, Minor damage, Collapse, the Basic undamaged and medium damage for the CES columns with a high axial compression ratio. Low-cyclic loading test results indicate that the damage performance states of moment-failure mode of CES columns can be realized as longitudinal reinforcement buckling (I), cover concrete spalling (II), cover concrete cracking (III), core concrete crushing (IV) cover concrete crushing (V1) or steel flange yielding (V2), and longitudinal reinforcement yielding (VI), with stain-base limit values $\varepsilon_s = \varepsilon_{bu}$ for state I, $\varepsilon_{cov} = \varepsilon_{cu}$ for state II, $\varepsilon_{cov} = \varepsilon_{t0}$ for state III, $\varepsilon_{cor} = \varepsilon_{cc0}$ and for state IV, $\varepsilon_{cov} = \varepsilon_{c0}$ for state V1, $\varepsilon_{af} = \varepsilon_{ay}$ for state V2 and $\varepsilon_s = \varepsilon_{sy}$ for state VI.

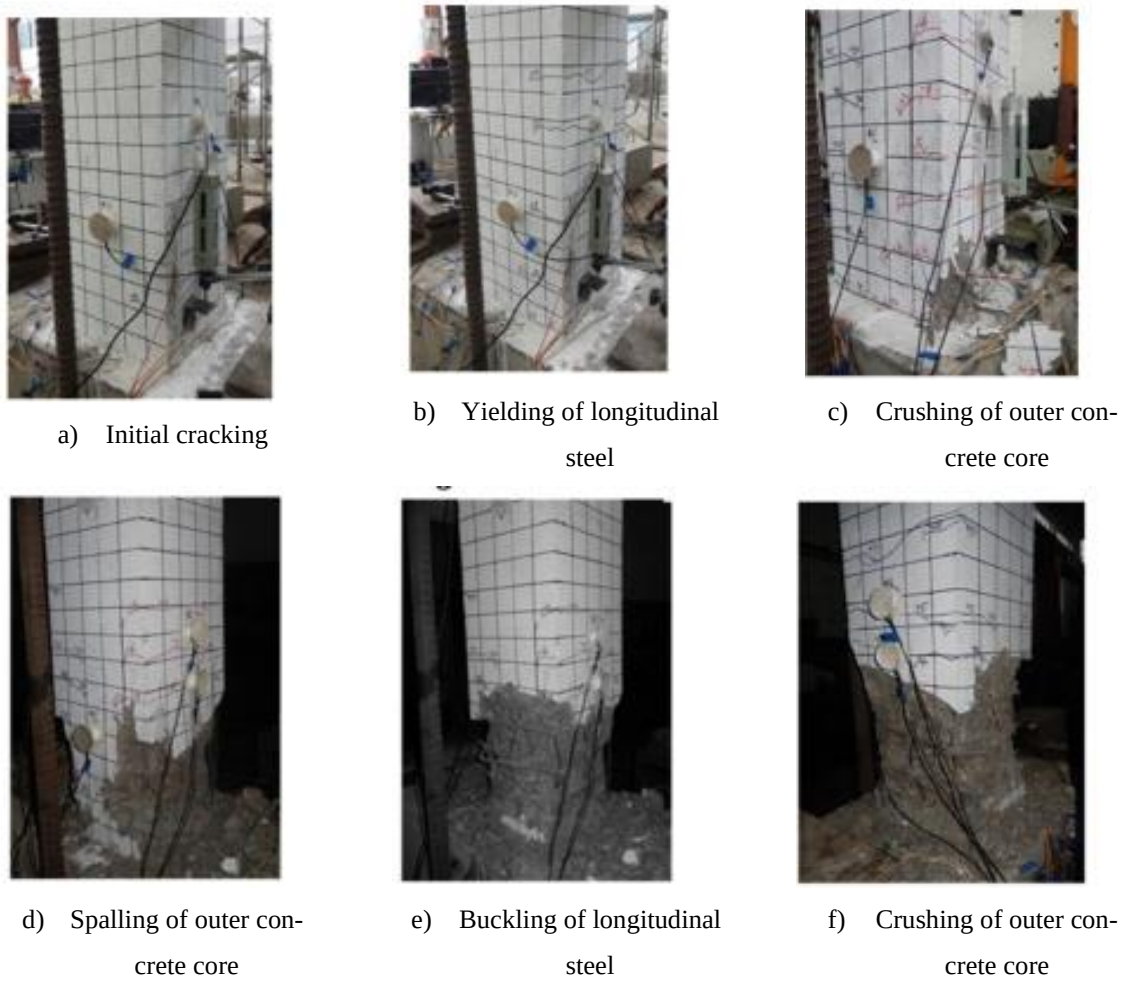

a) Initial cracking

b) Yielding of longitudinal steel

c) Crushing of outer concrete core

d) Spalling of outer concrete core

e) Buckling of longitudinal steel

f) Crushing of outer concrete core

Figure I.11: Damage states of CES [28].

I.4.2 Partially encased composite column

Chen et al. [29] carried out on the rational scope of width-thickness ratio of encased steel flange, benefiting the post-buckling capacity of steel also width-thickness ratio, of partially encased composite (PEC) columns with thin-walled H-shaped steel plates, by testing and numerically analysing six PEC columns under cyclic horizontal loads and constant vertical load. The experimental study detected that relatively favourable energy dissipation capacity and ductile failure mode can be predictable if the axial

compression load does not exceed the encased capacity and the width-thickness ratio does not surpass the limitation by Eurocode 4. By this recherche followed, it is clear that the transverse links and the H steel are a relatively more important role in ductility and resistance of PEC members than stirrups and longitudinal rebars. The comparison of the test results and the numerical analysis indicate the validity of the model. A simple numerical model is suggested, featured with function decomposition springs for concrete, which can reflect main functions of steel and concrete, while avoid the complicated simulation for the uncertain interface behaviours of two materials. A simple numerical model has been suggested, featuring functional decomposition springs for concrete, which can replicate main functions of concrete and steel, while avoiding complex simulations of the indefinite interface behaviours of the two materials.

I.4.3 Concrete filled steel column

Han et al. [30]investigated the influence of energy dissipation, stiffness, ductility, and strength on axial load level and cross-sectional type by testing nine concrete filled steel tube reinforced concrete (CFSTRC) columns under constant axial load and cyclically increasing flexural loading. Figure I.12 shows a general view of the nine CFSTRC columns after tests. Results show that the CFSTRC columns exhibit favourable ductility and energy dissipation. In general, with increasing axial load level the energy dissipation ability and the ductility of the columns decrease. The rigidity degradation for specimens with a higher axial load level was less significant than that with a lower axial load level as shown in Figure I.13. The concrete filled steel tube reinforced concrete column shows a good seismic performance, it is expected that this type of composite column will be adaptable in practical building structures in regions of high seismicity.

Figure I.12: CFSTRC columns after tests [30]**.**

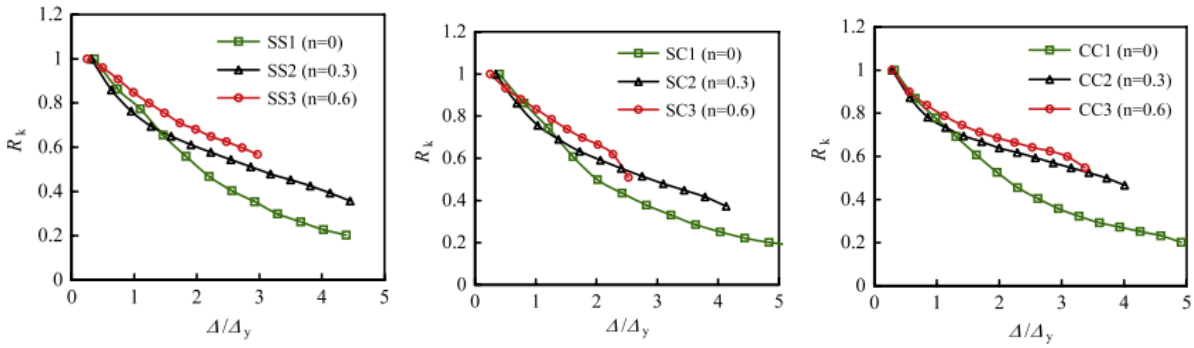

a) Series I b) Series II c) Series III

Figure I.13: Rigidity degradation of the CFSTRC columns [30]**.**

Gajalakshmi et al. [31] studied the diameter thickness ratio of the steel tube, steel fibre reinforced concrete and two types of in-fills namely Plain cement concrete, by testing several concrete-filled steel (CFT) columns and steel fibre reinforced concrete in-filled steel tube (SCFT) columns under constant and variable amplitude loading combined with constant axial load. The test consisted of cyclic loading with constant capacity focused on the effects of number of cycles and amplitude on the accumulation of damage to the in-filled columns. Also, consisting of benchmark tests to determine the hysteresis behaviour under variable amplitude cyclic loading. It was found that CFT columns show about 1.5 to 2 times less enhanced ductility, reduced damage index and energy absorption capacity compared to SCFT columns as shown in Figure I.14. Thus, it can be preferred in seismic regions.

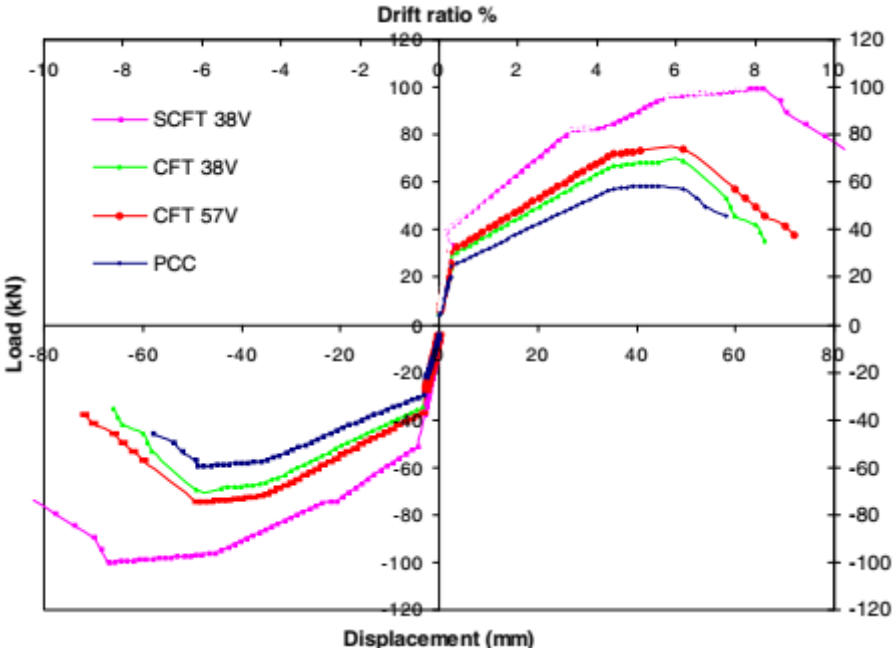

Figure I.14: Load displacement of the SCET and CFT columns [31]**.**

Han et al. [32] suggested simplified models for the lateral load-lateral displacement relationship and the moment-curvature response, as well as ductility coefficient for the composite columns. By studying

analytically serval concrete-filled double skin steel tubular columns subjected to axial load and cyclically increasing flexural loading. A mechanical model was constructed to predict the behaviours of concrete-filled double skin steel beam-columns subjected to a constant axial load and cyclically increasing flexural load, the test results are in good agreement with the predicted cyclic responses of the composite columns. To approximate the ductility of concrete-filled double skin steel beam-columns, the formula suggested in this paper may be suitable for inclusion in building codes.

Qian et al. [33] conducted the interaction between concrete and steel as well as the cumulative damage of concrete by analysing seventeen concrete-filled steel tube (CFST) columns as shown in Figure I.15. The aim was to investigate the behaviour of concrete-encased CFST columns under cyclic lateral loading, to present analytical results of CFST columns under cyclic lateral loading including the contact stress between steel tube and concrete and the axial load distribution among inner CFST and outer reinforced concrete components and the load–displacement relationships. The results indicate that the axial load level affects the distribution of the axial load between the components. The proportion of the axial load resisted by the outer reinforced concrete increases initially, then decreases with the increase in the displacement level when it is under a low axial load level (n = 0.2) as shown in Figure I.16.

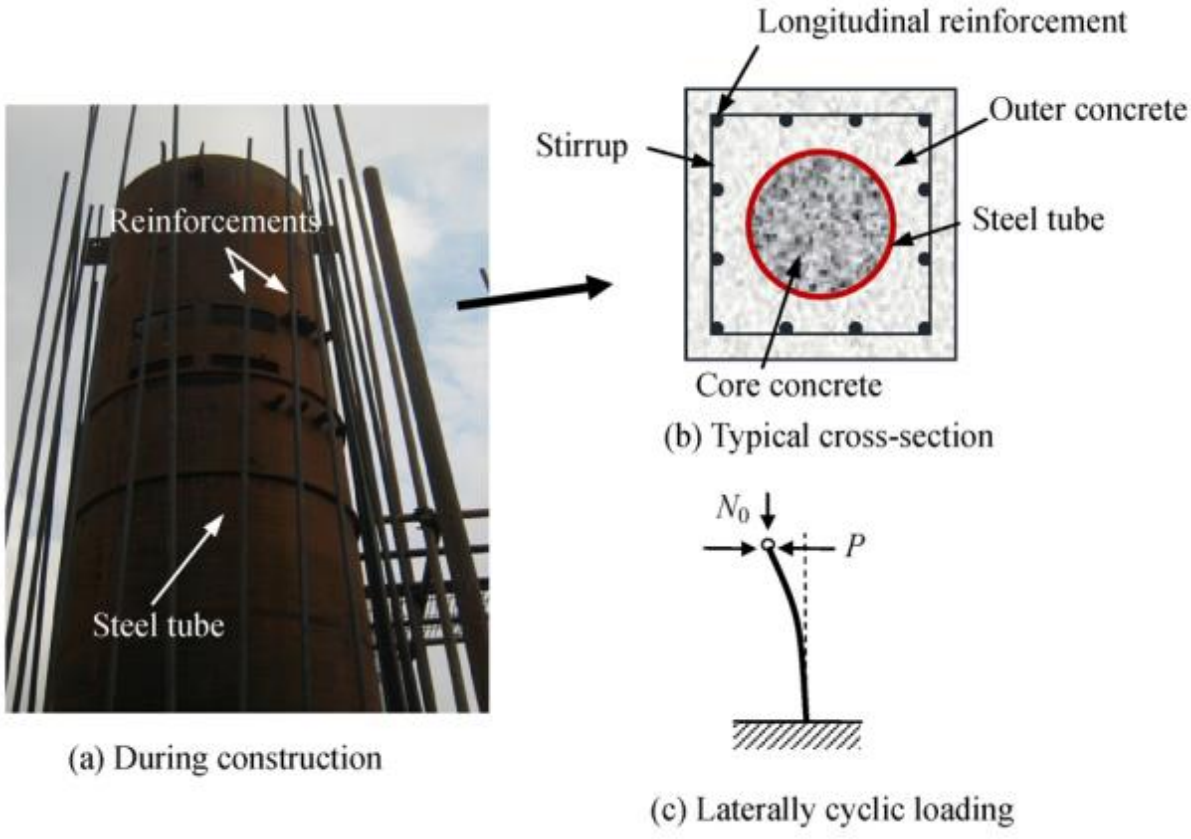

Figure I.15: Concrete-filled steel tube columns [33].

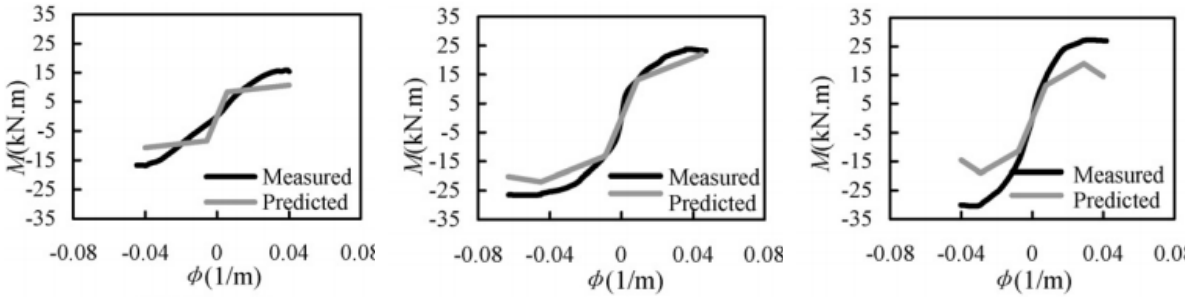

a) n=0 b) n=0.3 c) n=0.6

Figure I.16: Predicted and Measured M-ϕ skeleton cures [33].

I.4.4 Shear connectors

Shear connectors are the most common solution to ensure the assembly of steel structures with concrete in composite structures. Many researchers focused on the shear stud connector, combined with the composite beam [34]–[37] also combined with the composite column [12], [38]–[40]. Shear stud connector has been investigated by many parametric studies, including the shear stud geometry, various material, surface treatment, the difficulty of the reinforcement application, shear-span ratio, the type of structural steel, steel-plate hooping ratio and axial compression ratio. It was concluded that results show that the capacity of shear stud reduced almost 40% of cyclic loading test compared to static test [34]. The ultimate shear strengths under the tensile stress become 27%–49% of those under the compressive stress [35]. With the increase in the number of cycles in the cyclic loading test, the capacity of the beam increased against longitudinal splitting and did not lead to early failure of the composite beam [36]. The shear resistance of the stud connectors could be underestimated in some cases and in other cases overestimated by EC-4 and AISC-LRFD [37]. The use of connectors enhanced the axial capacity load of thin-walled short concrete-filled steel tubes increased the load transferred to the steel tube by 13-15% [38]. The shear capacity is increased when the length of the composite area increased [39]. Additionally, the bolted shear connectors in composite steel-concrete structures have been studied with numerical analysis and experimentally tests by several researchers[11], [41]–[47]. Other types of shear connectors have been investigated, as well as perfobond connectors[12], channel and angle shear connectors [13], [40], [48], [49], connectors made of top-hat profile [14], [50], omega-shaped connector [15], transversal connector, angled, V-shaped connector and longitudinal connector [16]. These research results have confirmed that the perfobond connectors provided a larger shear strength than the stud shear connectors under the same axial compression ratio [12]. The angle connector is more efficient than the stud bolts, reducing the slip and increasing the load capacity at maximum load applied [40]. Channel connectors showed up to 18.5% more shear strength than those of angle under cyclic loading, and 6.8–30.1% more subjected to monotonic loading [13], [48], [49]. For the connector made of top-hat profile, Lacki et al. [14] demonstrated that the load-bearing capacity of the connector is affected by the sheet fold length of the connector, the load-bearing capacity increases by increasing the sheet length. Odenbreit et al. [16]

compared between, transversal connector, angled, V-shaped connector and longitudinal connector, transversal connector, angled, V-shaped connector and longitudinal connector and concluded that the specimen with shear transversal connector exhibited the best load-bearing properties but also showed the most brittle type of failure, the specimen with angled V-shaped connector showed a high load-bearing capacity and good ductility properties at the same time, and the specimen with longitudinal connector exhibited the poorest performance in terms of the load-bearing capacity.

I.5 Conclusions

Through a review of the literature presented in this chapter, it became apparent that extensive experimental investigations have been undertaken into patterns of strength and failure modes of composite columns with different parametric: normal and high strength of concrete, the effects of stirrups ratio, effects of axial loads under cyclic loads and biaxial loads condition, composite columns with various percentages of structural steel ratio and also carried out on different types of connectors. In previous studies, studying the effect of reinforcement and connectors in the static and also cyclic behaviour of composite columns is still not yet sufficient to fully understand the behaviour of composite columns under cyclic or seismic loads. Therefore, the code specified design equations and guidelines for composite columns need to be extended to incorporate the behaviour of composite columns under cyclic loads. However, it is not possible to obtain a complete understanding of the effects of the different components from experimental investigations only due to the time requirements and the high cost of large-scale testing. Thus, finite element models that can accurately predict the behaviour of fully encased composite columns under various combinations of engineering and material properties are also needed. From the above works, it can be seen that investigations on the behaviour of composite columns are still not yet sufficient, in order to understand the cyclic behaviour of composite columns. It is necessary to focus on the effects of the cover concrete, the coefficient of friction and the connection between steel concrete interface.

Chapter II
FINITE ELEMENT MODELLING OF THE FEC COLUMNS

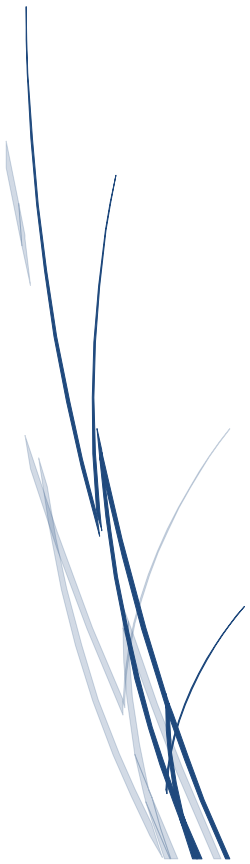

CHAPTER II
FINITE ELEMENT MODELLING OF THE FEC COLUMNS

II.1 Introduction

Composite columns are composed of two or more longitudinal elements which are limited in their longitudinal displacements with respect to the interface between the steel and the concrete by means of the coefficient of friction and the shear connectors between these elements. The shape of a shear connector and the number of the shear connectors used have a decisive influence on the behaviour of composite columns, which increases the degree of connection of the columns. A series of composite columns with varying effects subjected to a cyclic load are studied as part of the FEC column investigation. As a consequence, the authors were able to get the curve of the cyclic load against the lateral displacement of the column. Nonlinear finite elements and digital modelling software ANSYS are used for the numerical simulation. Nonlinearities were also present, including nonlinear material behaviour and nonlinear geometry, since the specimen underwent large displacements under lateral loads. Moreover, the contact between the steel section and concrete inside of the columns also contributed to the complexity of the model.

II.2 Model properties of the FEM

All of the 3D finite element models were designed in this study to understand the strength and the behaviour of FEC columns under cyclic loads encompassing a variety of geometry. ANSYS [51] finite element code was used to investigate the nonlinear FE model of FEC columns in this study. Descriptions of elements type and the mesh used in the finite element models of the analysed specimens, along with the boundary conditions including the interaction between steel and concrete are presented in the next sections.

II.2.1 Geometric properties

The geometric dimension of the proposed composite columns was divided into five series as shown in Table II.1, based on the difference of cover concrete, coefficient of friction, the connection between steel and concrete, longitudinal and transverse reinforcement and boundary conditions. The first series (I.1-I.8), have the same section of steel HEA240 and same reinforcing bars (longitudinal and transversal) 4ϕ20, 26ϕ8 respectively but the cross-section of the composite column is variable as shown in Figure II.1(a-b). The second series (II.1-II.11) have the same cross-section 450x450 mm, same steel section HEA240, same reinforcing bars (longitudinal and transversal) 4ϕ20, 26ϕ8 respectively as shown in Figure II.1(c). The third series (III.100-III.200) have the same section of steel HEA240 and the same cross-section but the reinforcing bars (longitudinal) and the spacing between the transversal bars are variable as shown in Figure II.1(d). The fourth series (IV.1-IV.3) have the same section of steel HEA240, the same cross-section and the same reinforcing bars (longitudinal and transversal) 4ϕ20, 26ϕ8 respectively

but the boundary condition is different, as shown in Figure II.1(j). However, the fifth series (FES.150, FEC.C1-FEC.C4) have the same section of steel HEA240, the same cross-section and the same reinforcing bars (longitudinal and transversal) 4ϕ20, 26ϕ8 respectively but the connection between steel and concrete is different as shown in Figure II.1(e-i).

Table II.1: Characteristics of the columns

Specimens	coeff.	c (mm)	Section	Longitudinal reinforcement bars	Transversal reinforcement bars	$N= P/N_{Pl,Rk}$	Connector	Connector spacing (mm)	Boundary conditions
I.1	-	10	370x370	4ϕ20	26ϕ8	0.2	-	-	Fixed-Free
I.2		20	390x390						
I.3		30	410x410						
I.4		40	430x430						
I.5		50	450x450						
I.6		60	470x470						
I.7		70	490x490						
I.8		80	510x510						
II.1	0.2	50	450x450	4ϕ20	26ϕ8	0.2	-	-	Fixed-Free
II.2	0.25								
II.3	0.3								
II.4	0.35								
II.5	0.4								
II.6	0.45								
II.7	0.5								
II.8	0.55								
II.9	0.6								
II.10	0.65								
II.11	0.7								
III.100. I.1	-	50	450x450	4ϕ16	39ϕ8	0.1	-	-	Fixed-Free
III.100. I.2				4ϕ16	39ϕ8	0.3			
III.100. I.3				4ϕ16	39ϕ8	0.5			
III.100.II.1				4ϕ20	39ϕ8	0.1			
III.100.II.2				4ϕ20	39ϕ8	0.3			
III.100.II.3				4ϕ20	39ϕ8	0.5			
III.100.III.1				8ϕ16	39ϕ8	0.1			
III.100.III.2				8ϕ16	39ϕ8	0.3			
III.100.III.3				8ϕ16	39ϕ8	0.5			

III.100.IV.1				8ϕ20	39ϕ8	0.1			
III.100.IV.2				8ϕ20	39ϕ8	0.3			
III.100.IV.3				8ϕ20	39ϕ8	0.5			
III.150. I.1				4ϕ16	26ϕ8	0.1			
III.150. I.2				4ϕ16	26ϕ8	0.3			
III.150. I.3				4ϕ16	26ϕ8	0.5			
III.150.II.1				4ϕ20	26ϕ8	0.1			
III.150.II.2				4ϕ20	26ϕ8	0.3			
III.150.II.3				4ϕ20	26ϕ8	0.5			
III.150.III.1				8ϕ16	26ϕ8	0.1			
III.150.III.2				8ϕ16	26ϕ8	0.3			
III.150.III.3				8ϕ16	26ϕ8	0.5			
III.150.IV.1				8ϕ20	26ϕ8	0.1			
III.150.IV.2				8ϕ20	26ϕ8	0.3			
III.150.IV.3				8ϕ20	26ϕ8	0.5			
III.200. I.1				4ϕ16	19ϕ8	0.1			
III.200. I.2				4ϕ16	19ϕ8	0.3			
III.200. I.3				4ϕ16	19ϕ8	0.5			
III.200.II.1				4ϕ20	19ϕ8	0.1			
III.200.II.2				4ϕ20	19ϕ8	0.3			
III.200.II.3				4ϕ20	19ϕ8	0.5			
III.200.III.1				8ϕ16	19ϕ8	0.1			
III.200.III.2				8ϕ16	19ϕ8	0.3			
III.200.III.3				8ϕ16	19ϕ8	0.5			
III.200.IV.1				8ϕ20	19ϕ8	0.1			
III.200.IV.2				8ϕ20	19ϕ8	0.3			
III.200.IV.3				8ϕ20	19ϕ8	0.5			
IV.1	-	50	450x450	4ϕ20	26ϕ8	0.2	-	-	Fixed-Fixed
IV.2		70	470x470						Fixed-Fixed
IV.3	0.6	50	450x450						Fixed-Fixed
FEC.S.150	-	50	450x450	4ϕ20	26ϕ8	0.2	Stud	150	Fixed-Free
FEC.C1.100							Flange	100	
FEC.C1.150								150	
FEC.C1.200								200	
FEC.C1.250								250	
FEC.C2.100							Web	100	

FEC.C2.150								150	
FEC.C2.200								200	
FEC.C2.250								250	
FEC.C3.100							Welded	100	
FEC.C3.150							to the	150	
FEC.C3.200							side of	200	
FEC.C3.250							steel's flange	250	
FEC.C4.100							Welded	100	
FEC.C4.150							to the	150	
FEC.C4.200							side of	200	
FEC.C4.250							steel's flange	250	

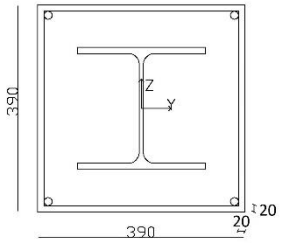

a) Specimen I.2

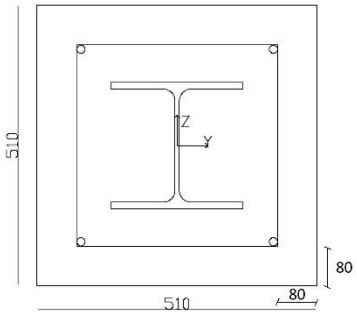

b) Specimen I.8

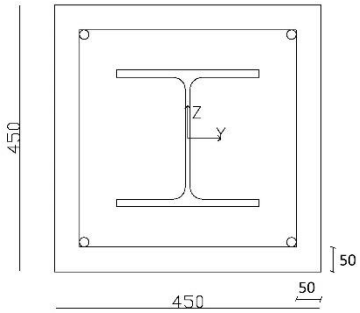

c) Specimen II.1-II.11

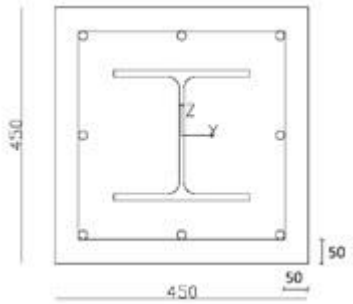

d) Specimen III.100.III

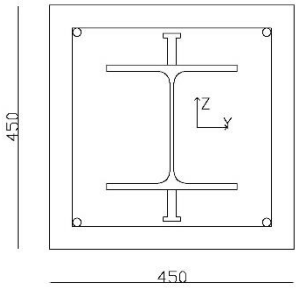

e) Specimen FEC.S.150

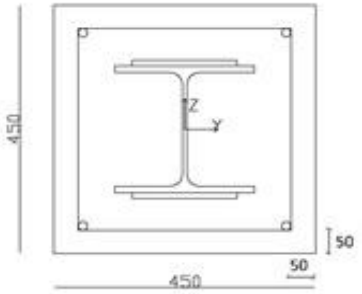

f) Specimen FEC.C1

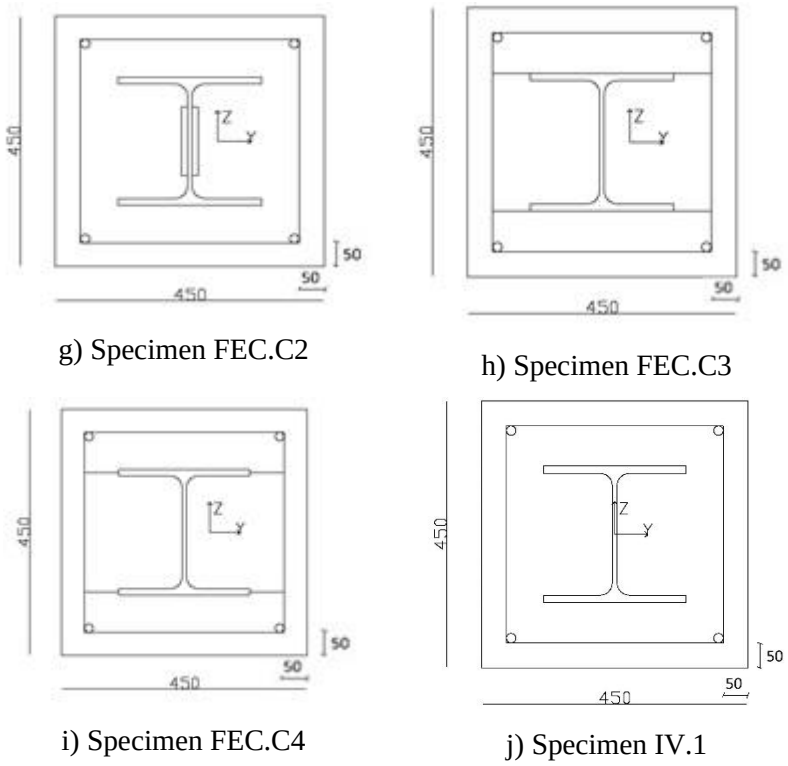

g) Specimen FEC.C2 h) Specimen FEC.C3

i) Specimen FEC.C4 j) Specimen IV.1

Figure II.1: Dimensions of some designed composite columns.

II.2.2 Finite element selection

The fully encased composite columns analysed in this study consisted of four components, such as concrete, structural steel section, longitudinal reinforcement and stirrups indicated in Figure II.2. Considering several studies described in the literature [26], [52], [61], [53]–[60], it was decided to choose the used finite element model Solid185, Link8 and Solid65 finite elements of the ANSYS software [51]. In 3-D model of solid structures with eight nodes and three degrees of freedom at each node as shown in Figure II.3(a), structural steel section is defined as Solid185. Stress stiffening, plasticity, large strain capabilities, significant deflection, and also creep all are properties of this element. The ANSYS software defines concrete as Solid65 in 3-D modelling of solids with reinforcing bars because of its potential to crush in compression and crack in tension. The element is made up of eight nodes as shown in Figure II.3(b), each with three degrees of freedom. Concrete has the ability to crack, crush, and deform plastically. Rebar is capable of compression and tension, as well as plastic deformation. The failure criterion for concrete due to multiaxial stress condition used in the study was the Willam- Warnke five parameter model [62], the failure surface could be defined by two constants, f_{cm} and f_t. There are several properties that should be entered into ANSYS to define the concrete material including (the Poisson's ratio (v), elastic modulus (E_{cm}), compressive uniaxial stress-strain relationship for concrete, ultimate uniaxial compressive strength (f_{cm}), ultimate uniaxial tensile strength (f_t), and shear transfer coefficient) which represents the conditions of the crack plane. The shear transfer coefficient value ranges from 0.0 to 1.0, with 0.0 representing a smooth crack (no shear transfer at a crack section) and 1.0 representing a rough

crack (full shear transfer). In this study, a shear transfer is 0.75 and 0.9 for open cracks β_t and closed cracks β_c, respectively [58]. Link8, a uniaxial compression-tension element with two nodes and three degrees of freedom at each node as shown in Figure II.3(c) [51], is used to design the reinforcing bars [51]. Their flexural rigidity is neglected.

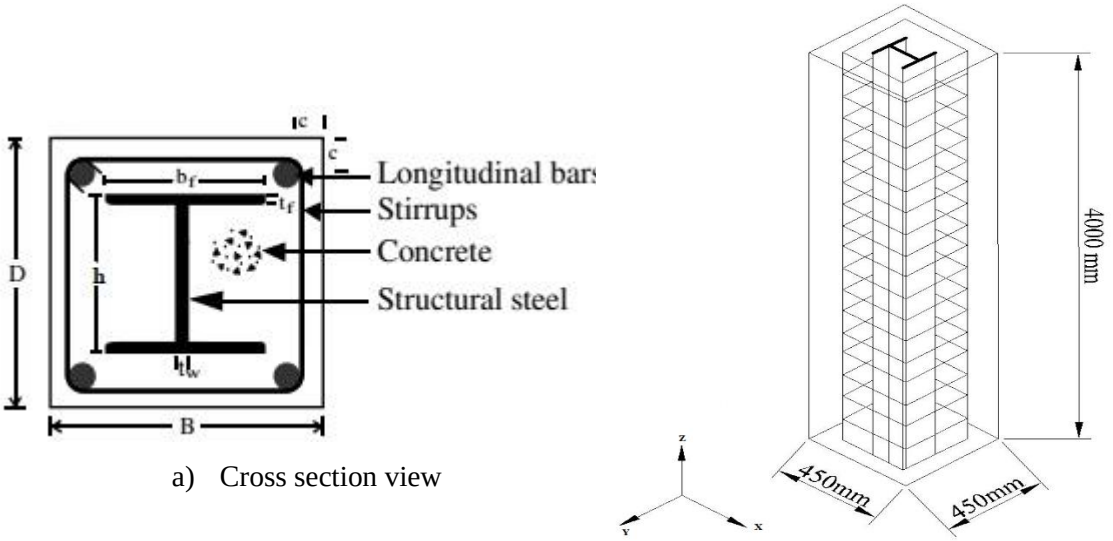

a) Cross section view

b) 3d view

Figure II.2: Geometry of fully encased composite columns

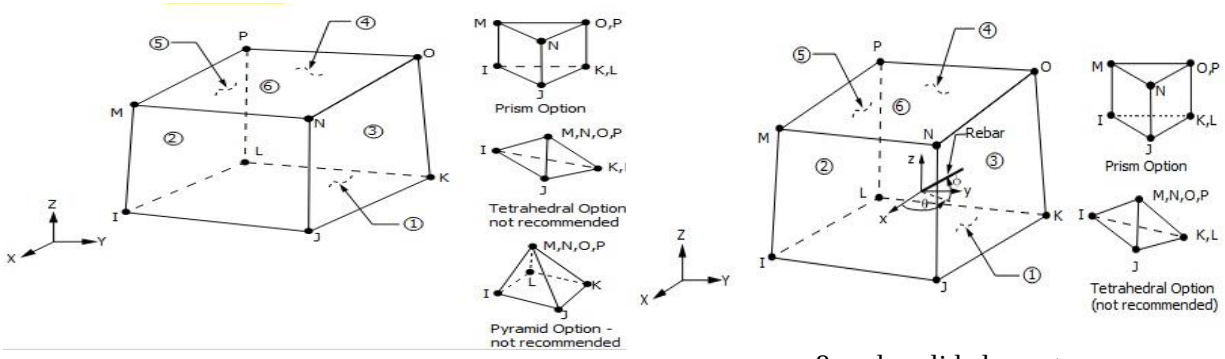

8-node solid element

a) Solid185 element

8-node solid element

b) Solid65 element

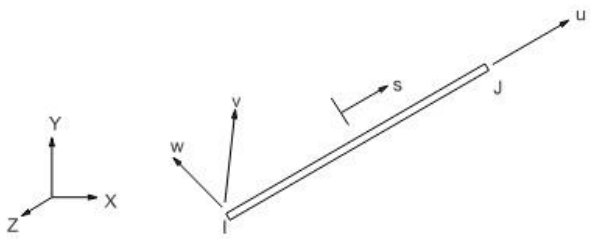

2-node solid element

c) Link180 element

Figure II.3:Numerical model of composite Columns. [51]

II.2.3 Mesh description

A sensitivity analysis was performed on the FE model to optimize the mesh size in order to produce the accurate behaviour of FEC column with less computational time. The FEC column was modelled using different mesh size (90, 60, 30, 15) mm as shown in Figure II.4. The comparison of the different mesh results for FEC column with the selected mesh sizes are shown in Figure II.5 . It was found that a mesh size of 30 mm was the appropriate one for the composite columns.

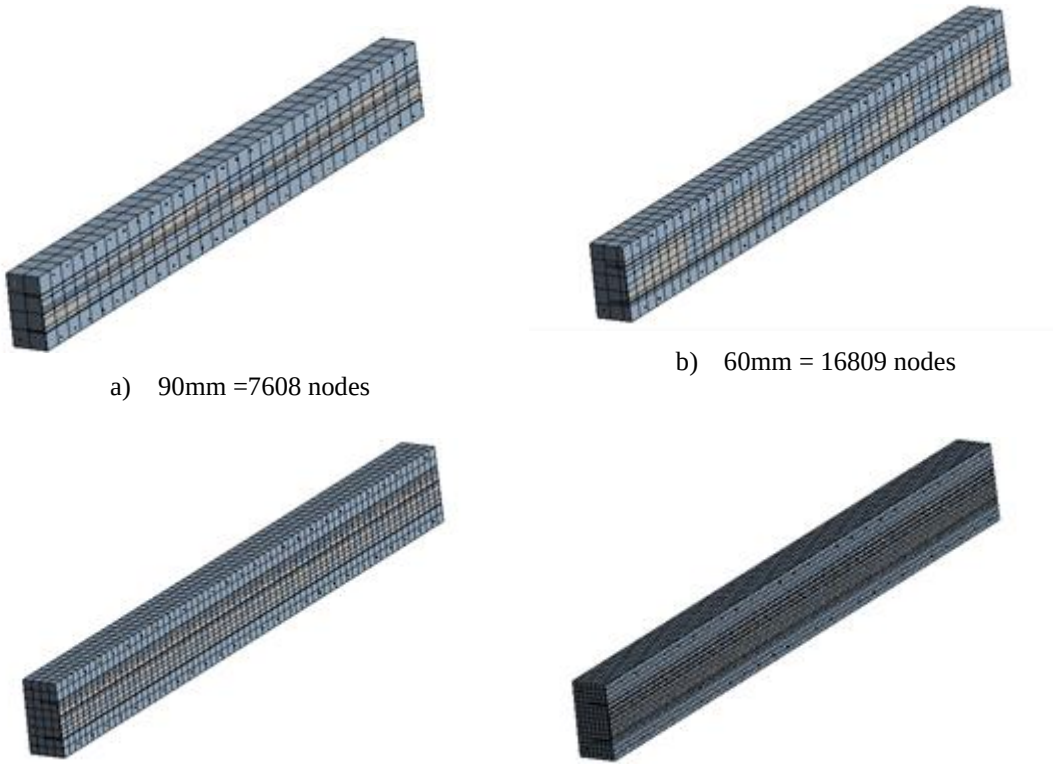

a) 90mm =7608 nodes

b) 60mm = 16809 nodes

c) 30mm = 45495 nodes

d) 15mm = 124608 nodes

Figure II.4: Finite element mesh for FEC columns.

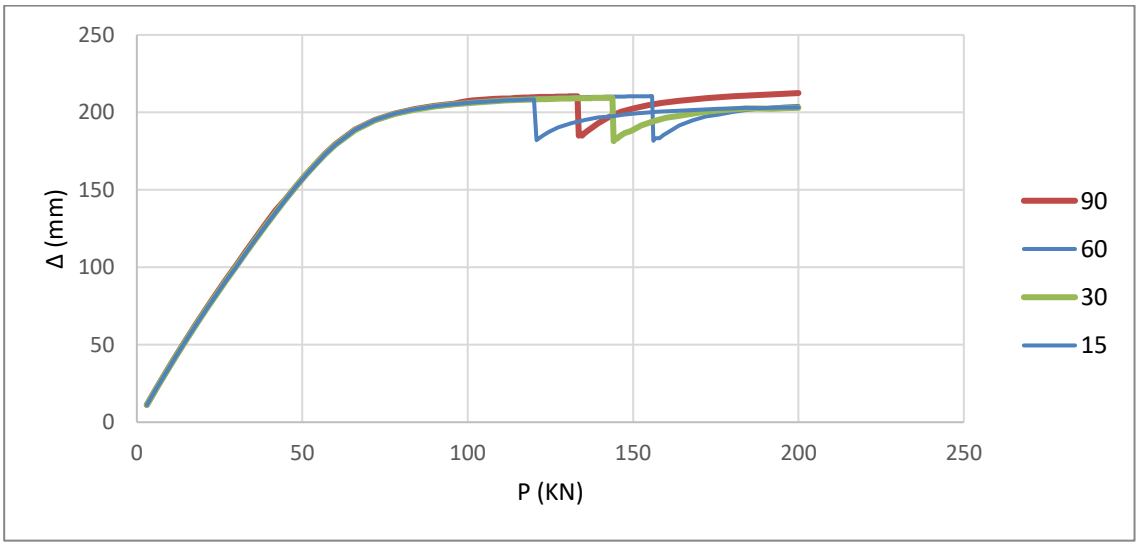

Figure II.5: Results of finite element mesh for FEC columns.

II.2.4 End boundary conditions

The end boundary condition was defined in the finite element model in such a way as to comply with that applied in the experimental test. The boundary conditions applied in the finite element model to simulate the conditions for cyclically loaded specimens are shown in Figure II.6. The first three series are fixed at the bottom end of the column and supposed free at the top end of the column as indicated in Figure II.6(a). Firstly, the axial force was applied at the middle of the composite columns and the horizontal load is applied with displacement using boundary condition under different increment steps. For the fourth series, the boundary conditions are fixed at the bottom end of the column also fixed at the top end of the column indicated in Figure II.6(b). Firstly, the top end of the column was fixed by remote displacement then the axial force was applied at the middle of the composite columns and the horizontal load is applied with displacement using boundary condition under different increment steps.

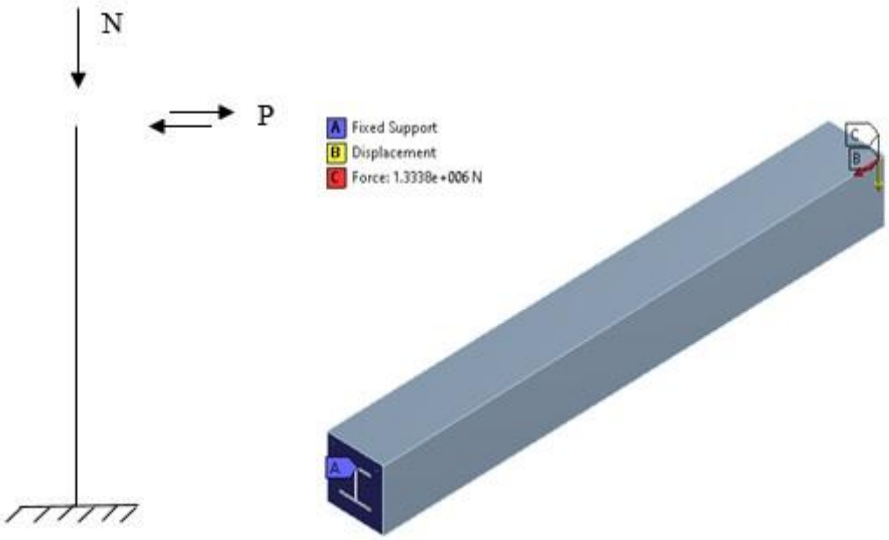

a) fixed-free

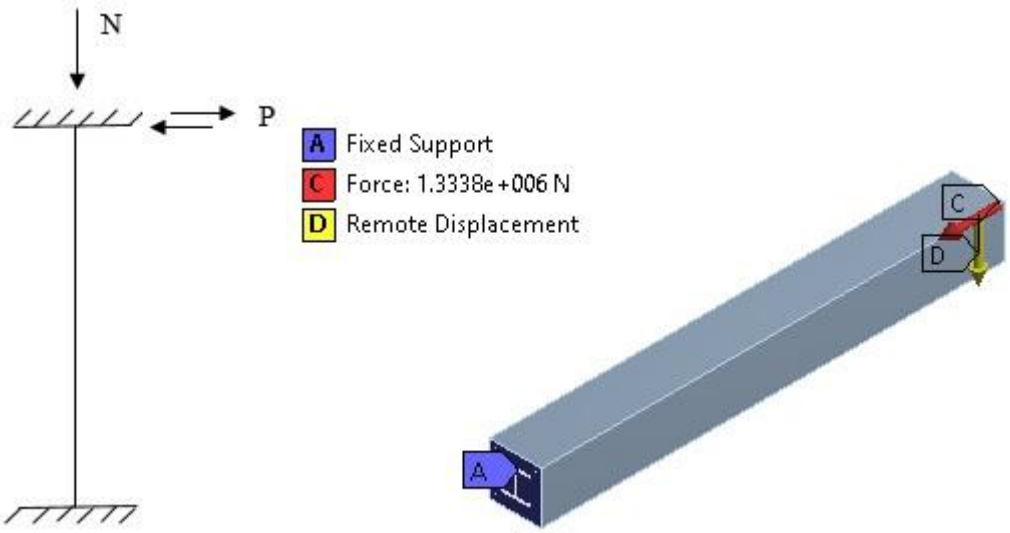

b) fixed-fixed

Figure II.6: Boundary conditions of fully encased composite columns

II.2.5 Modelling of steel-concrete contact

The physics preference used in the analysis is explicit. A surface-to-surface contact is defined to model the interaction between steel and concrete, CONTA174 is used for the mesh of the concrete interface to contact with the steel interface and TARGE170 is used for the mesh of the concrete interface to contact with the concrete interface [63]–[65]. The contact between structural steel section and concrete is used as frictional. In this thesis, different friction coefficients ranging from 0.2 to 0.7 was selected to explore their effects on fully encased composite column behaviour. Therefore, a friction coefficient of 0.6 was suggested to achieve a quick convergence.

II.3 Material properties

Concrete and steel are the main materials used in construction of FEC columns. The nonlinear behaviour of these two materials were incorporated in the FE model using the appropriate material models for concrete and steel available in the ANSYS [51] finite element software. The description of the material models for concrete and steel along with their mechanical properties (stress versus strain relationship) used in the FE model is described in the following sections.

II.3.1 Steel

The steel material properties for the H-shaped structural steel and reinforcements bars (longitudinal and transverse) were modelled with an elastoplastic model. The behaviour of steel under cyclic loading is defined as a linear kinematic hardening model adopted to simplify the modelling of the composite columns. Steel properties specified in ANSYS contain a yield strength, modulus of elasticity and Poisson's ratio. In this numerical modelling, modulus of elasticity is E_s=210 000 MPa and Poisson's ratio of steel is taken as 0.3, according to Eurocode3 [66], also the steel grade is S275 (f_y=275 MPa) and S500 (f_{sk}=500 MPa), for structural steel section and reinforcing bars respectively, described as elastic perfectly plastic as Figure II.7:

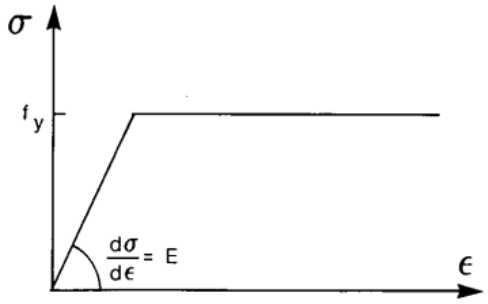

Figure II.7: Bi-linear stress-strain relationship of steel material [66]**.**

II.3.2 Concrete

The concrete used in the proposed model is for non-linear stress-strain relation. The equivalent stress-strain relationship of concrete is shown in Figure II.8, recommended by Eurocode 4 [2] is used in eq.II.1.

Modulus of elasticity as E_{cm}=31000 MPa and Poisson's ratio of concrete is taken as 0.2, according to Eurocode 2 [67]. The following equation mentions concrete's stress-strain relation.

$$\frac{\sigma c}{f_{cm}} = \frac{K.\eta - \eta^2}{1+(K-2)\eta} \quad \text{(II.1)}$$

where:

$K= 1{,}05\ E_{cm} \times |\varepsilon_{c1}| / f_{cm}$

$\eta= \varepsilon_c / \varepsilon_{c1}$

ε_{c1}=0.2% is the strain at reaching the maximum strength.

ε_{cu1}=0.35% is the ultimate strain.

f_{cm}=33MPa is mean value of concrete cylinder compressive strength.

f_t =1.2MPa is the value of the design tensile strength.

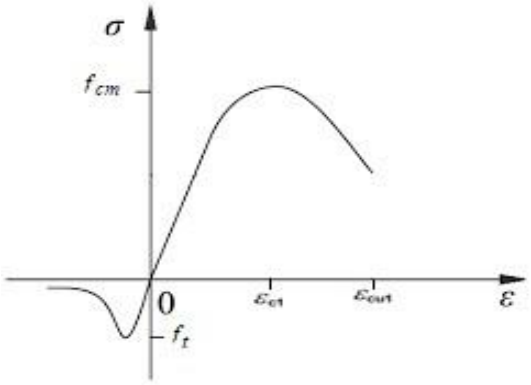

Figure II.8: Parabola-rectangle diagram for concrete under compression of concrete material [67]**.**

II.4 Load application

In this study, the horizontal load was applied using the displacement control technique on the free top surface of the column. The nodes at the top and bottom surfaces of columns were made rigid. The displacement was applied at the rigid body reference node. The base of the column is fixed in all directions during concentric axial load. The columns were subjected to a prescribed horizontal-displacement history under a chosen constant axial load of P=1333.8kN selected as 20% of the plastic resistance of the composite cross-section to compressive axial force $N_{pl,Rk}$, with $N_{pl,Rk} = A_a.F_y + 0.85A_c.F_{ck} + A_s.F_{sk}$,according to Eurocode 4 [2]. It is interesting subsequently to study the effect of the applied axial load P. The horizontal displacement history consists of sequences of fully reversed displacement cycles as indicated in Figure II.9.

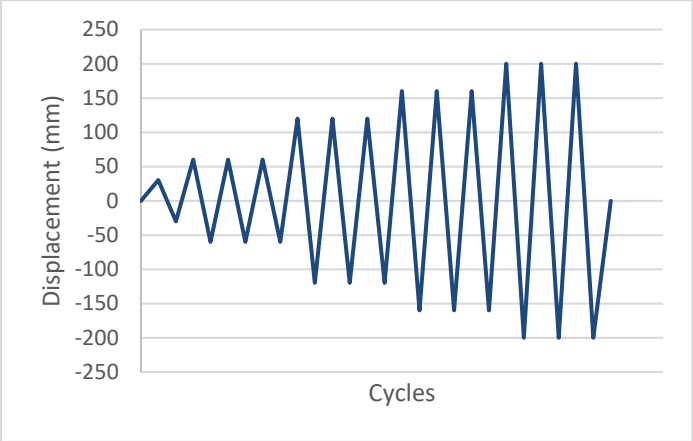

Figure II.9: Cyclic applied horizontal displacement history.

II.5 Validation of the numerical results

To validate the accuracy of the numerical model for the composite columns described in the previous section, four previously published test specimens by Aribert et al. [1] shown in Figure II.10 were used for comparison purpose. The materials used in the elements were S235 for the steel structural section, S550 for the reinforcing steel and for the concrete used C25 concrete class, as defined in Eurocode. The material parameters and the geometrical properties are shown in Table II.2.To satisfy the plastic rotation demand at the column base and to compensate for possible loss of resistance due to spalling of cover concrete, a transverse reinforcement for efficient concrete confinement was ensured by closed rectangular stirrups of 10 mm diameter with a spacing of 10 cm along the whole column length. The comparison between experimental and numerical failure mode is shown in Figure II.11. The comparison of computed cyclic load (P) versus lateral displacement (v) curves with the experimental ones is shown in Figure II.12. The difference between numerical and experimental values is +1.51%, +0.66%, -0.48% and +0.74% respectively for SI-1, S1-2, SIV-1 and SIV-2 specimens, as shown in Table II.3. Generally, good agreement is obtained between the numerical and the tested curves. This confirms that the present numerical model can be used with good confidence to simulate the behaviours of the FEC columns under cyclic loading.

Figure II.10: Experimental equipment of the test [1].

Table II.2: The material parameters and the geometrical properties of experimental test.[1]

Specimen	Length (m)	Concrete class	f_{ck} (28 days on cylinder) (N/mm2)	E_{cm} (N/mm2)	f_y (N/mm2)	f_{sk} (N/mm2)	E_a, E_{s2} (N/mm2)
SI	2.00	C25	25.4	29000	302	560	207000
SIV	3.00	C25	24.5	29000	302	560	207000

Table II.3: Values for experimental lateral force and FEM lateral force

Specimen	Length (m)	Loads	P_{exp} (KN)	P_{FEM} (KN)	Difference (%)
SI-1	2.00	Monotonic	28.1	28.53	+1.51
SI-2	2.00	Cyclic	25.7	25.87	+0.66
SIV-1	3.00	Monotonic	16.9	16.82	-0.48
SIV-2	3.00	Cyclic	17.4	17.53	+0.74

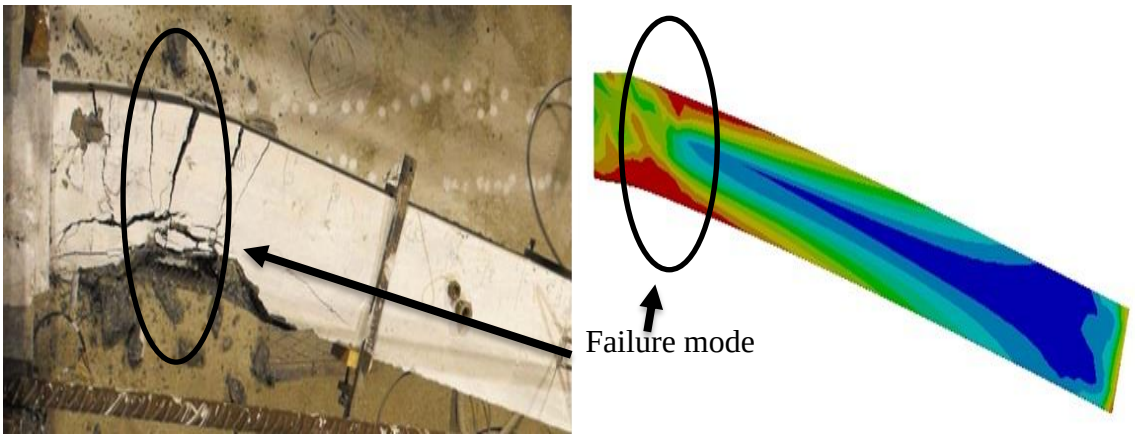

Figure II.11: Comparison of failure mode of numerical and experimental specimen [19].

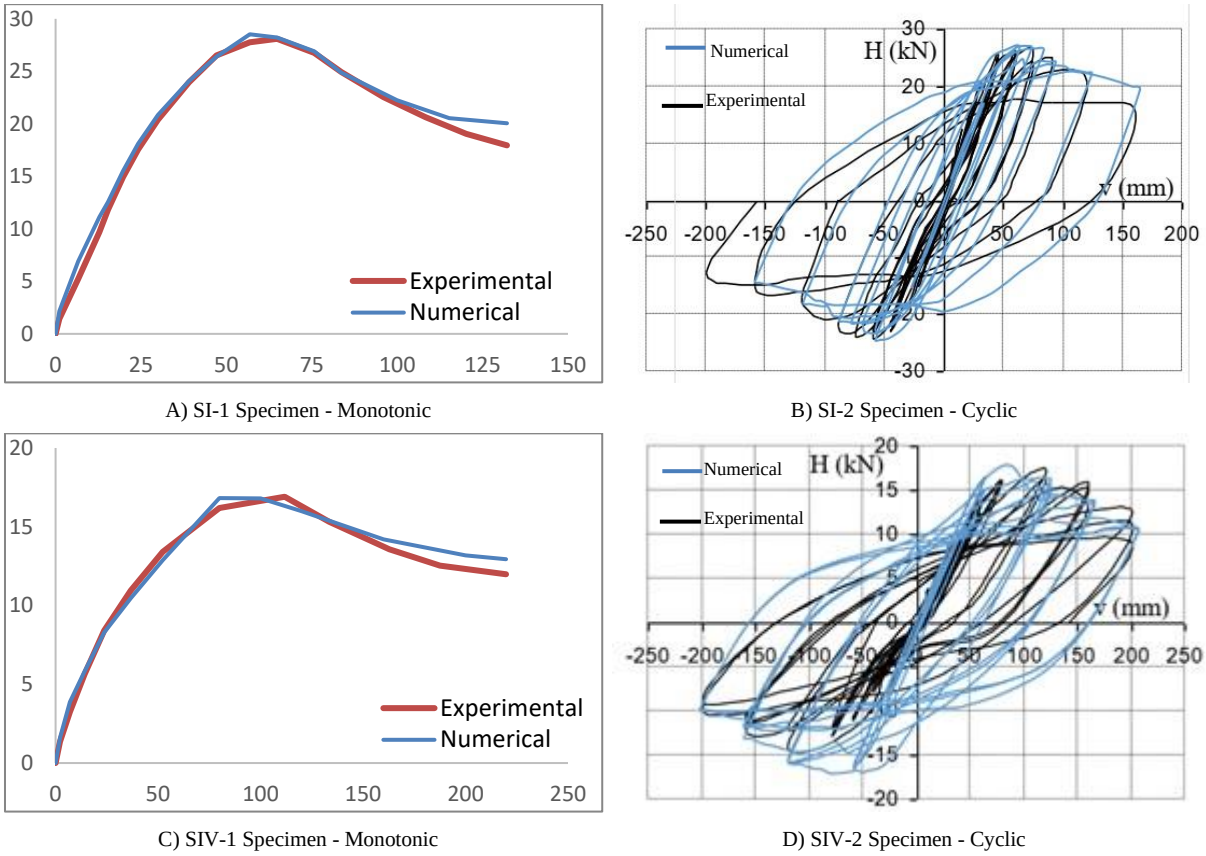

A) SI-1 Specimen - Monotonic

B) SI-2 Specimen - Cyclic

C) SIV-1 Specimen - Monotonic

D) SIV-2 Specimen - Cyclic

Figure II.12: Lateral force-displacement curves of numerical and experimental test.

II.6 Conclusion

A finite element model was proposed using the finite element software ANSYS to simulate the cyclic behaviour of FEC columns. Two-steps of analysis procedure was used in the model. Firstly, the proposed finite element model has been verified by the results of the cyclic tests and monotonic tests presented in this chapter. Then, a sensitivity analysis was performed on the FE model to optimize the mesh size in order to produce the accurate behaviour of the FEC column with less computational time. The choice of a model report on the precision research and that the modelling must be as close as possible to the real behaviour of the composite columns.

In the next chapiter, a parametric study is developed for detailed knowledge of the cyclic behaviour of the FEC column.

Chapter III
PARAMETRIC STUDY OF THE GEOMETRIC AND MECHANIC EFFECTS TO THE CYCLIC COMPOUND OF THE FEC COLUMNS

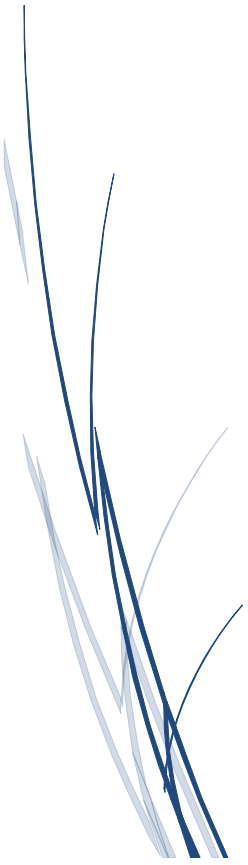

CHAPTER III
PARAMETRIC STUDY OF THE GEOMETRIC AND MECHANIC EFFECTS TO THE CYCLIC COMPOUND OF THE FEC COLUMNS

III.1 Introduction

During the past few decades, steel-concrete composite structural systems have been used in many tall buildings all over the world. Most of the early research on FEC columns investigated the behaviour of these columns for axial load and cyclic loads with different steel ratios, concrete strength, shape and size of the core steel section and slenderness ratios. These studies were mainly carried out on FEC columns constructed with normal to the high strength of concrete up to 70 MPa and structural steel yield strength up to 415 MPa. Studies on numerical simulations of FEC columns are limited. As experimental studies are costly and time-consuming, a numerical study on varying different parameters of FEC columns can be a good alternative. The FE models developed as stated in Chapter 2 were used to assess the influence of important geometric and material parameters on the behaviour of FEC columns. The efficiency and accuracy of the model were demonstrated through comparisons between the experimental and numerical results of a large number of FEC column tests. The model was found to be capable of tracing a stable load-displacement history up to failure with good accuracy for FEC columns, constructed with variant cover concrete, coefficient of friction and boundary conditions properties of the composite columns. This finite element model was used to simulate the parametric columns to explore the behaviour and strength of FEC columns under axial load and cyclic loading.

III.2 Design of parametric study

For the parametric study, a square column with outer dimensions of 450 mm × 450 mm was selected. The typical cross-section and elevation of the FEC column used in the parametric study are shown in Figure III.1. This is a moderate size for composite columns and might be suitable in the construction of mid-rise buildings. These columns were designed and analysed during the parametric study to incorporate the effects of several parameters geometric, mechanic and boundary conditions that can significantly affect the FEC column behaviour. The geometric variable is the percentage of cover concrete. The coefficient of friction and boundary conditions were variables as described in the sections below.

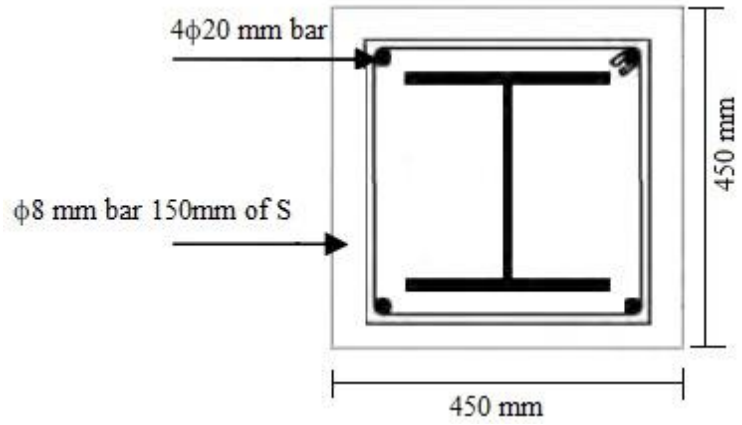

a) Cross section

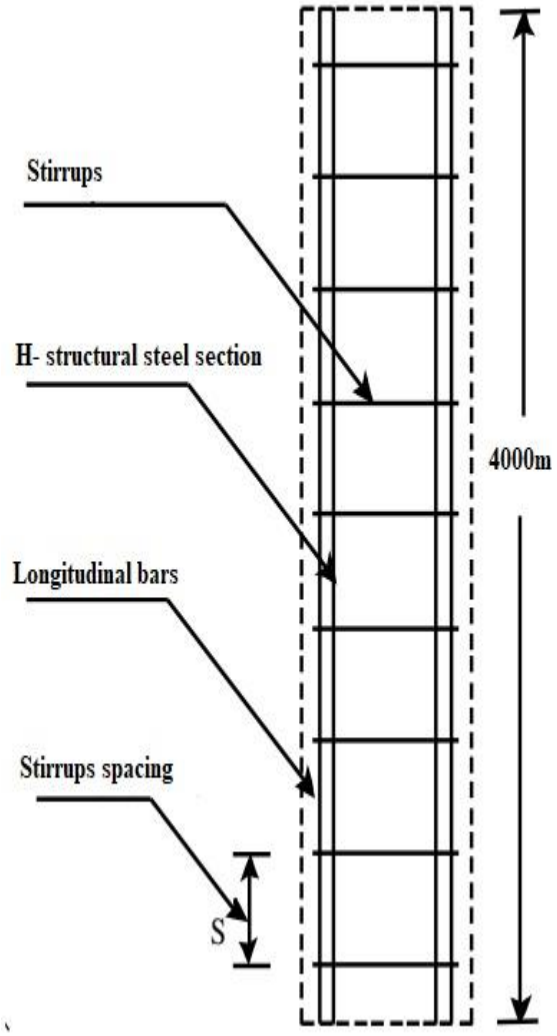

b) FEC column

Figure III.1: Typical cross section of parametric FEC column.

III.2.1 Coefficient of friction

The coefficient of friction provides a beneficial residual strength to the FEC columns with the adhesion

between steel and concrete that leads to improved ductility. Hence, eleven FEC columns were built with various coefficients of friction starting with 0.2 until 0.7 as described in Table II.3 to investigate the perfect coefficient of friction on the FEC columns under cyclic loads. The cover concrete, boundary conditions, the reinforcement bars ratio and the transverse reinforcement spacing of the FEC columns were kept constant in all cases. The load was applied cyclically in these columns.

III.2.2 Cover concrete

Cover concrete provides local buckling resistance and fire resistance for the steel section. However, when the transverse bars are not closely spaced, the FEC columns are vulnerable to premature spalling of the cover concrete. In particular, when the columns are subjected to high axial compression force, the load-carrying capacity and deformation capacity of the FEC columns can be degraded by early spalling of the cover concrete. Moreover, under cyclic lateral loading, the FEC columns are expected to be more susceptible to such damages as the ductility demand increases. Hence, eight FEC columns were built with various cover concrete starting with 10mm until 80mm as indicated in Figure III.2 to understand the effect of the cover concrete on the FEC columns under cyclic loads.

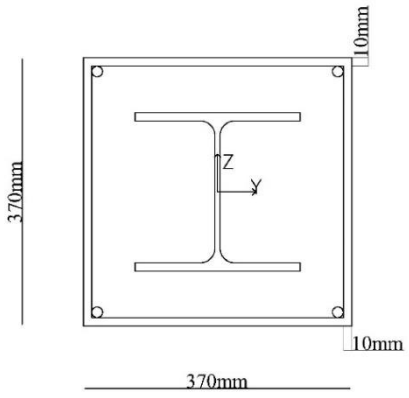

a) FEC column 370x370

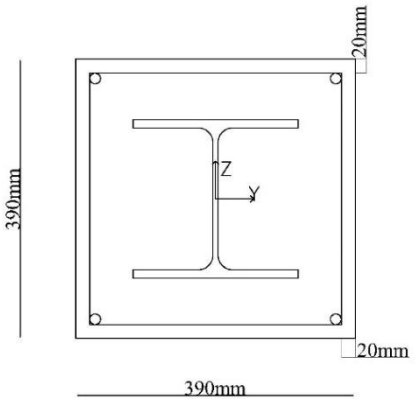

b) FEC column 390x390

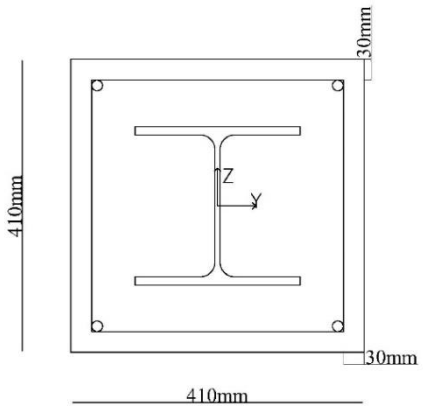

c) FEC column 410x410

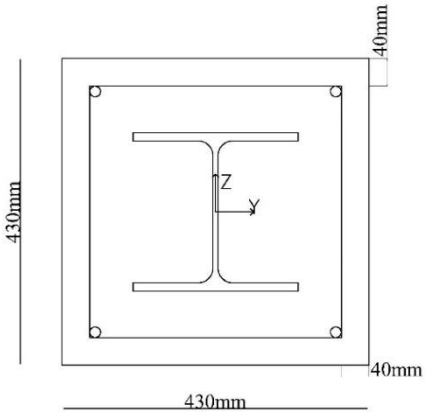

d) FEC column 430x430

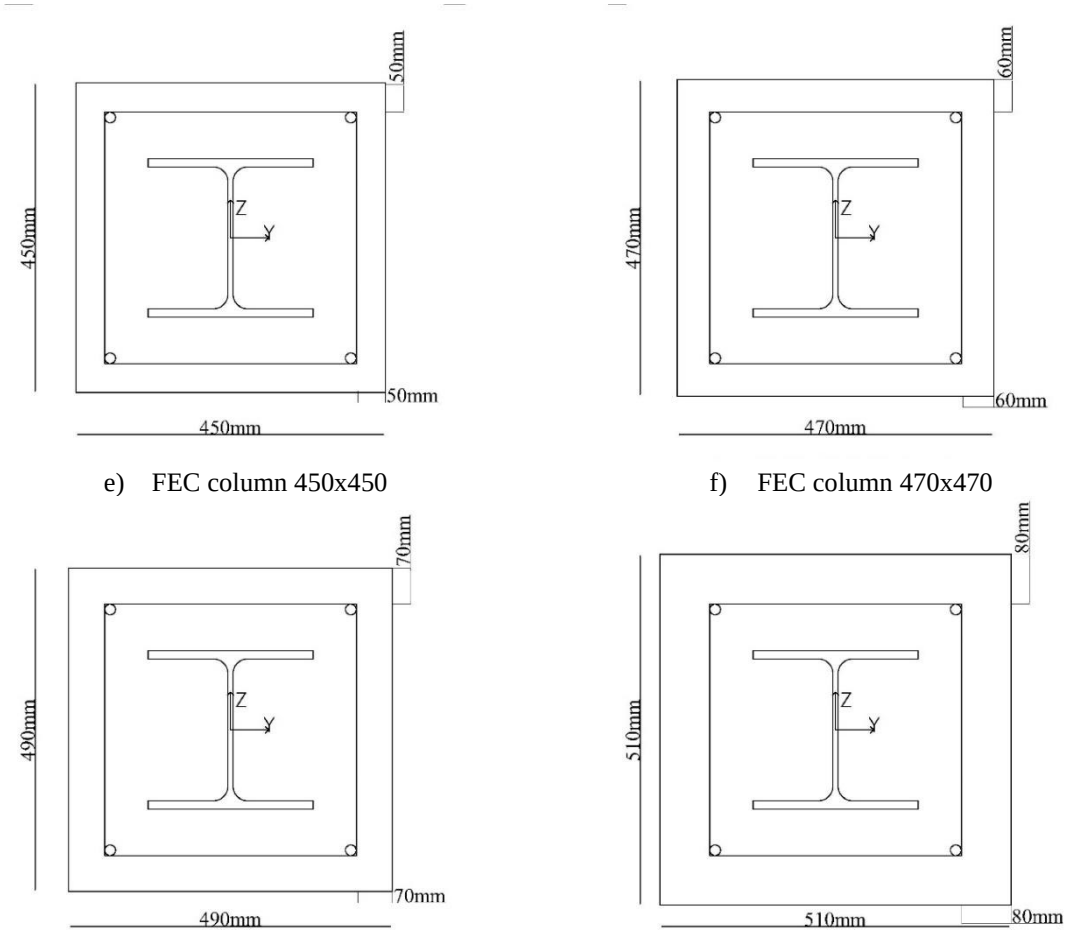

e) FEC column 450x450 f) FEC column 470x470

g) FEC column 490x490 h) FEC column 510x510

Figure III.2: Designed FEC columns with deference Cover concrete.

III.2.3 Effect of boundary condition

The behaviour of FEC columns under bending induced by the applied axial load and cyclic loads is greatly affected by the boundary conditions. It is obtained by applying different boundaries conditions (fixed-free and fixed-fixed) as shown in Figure III.3. It reduced the load-carrying capacity of the column as compared to a fixed-free column.

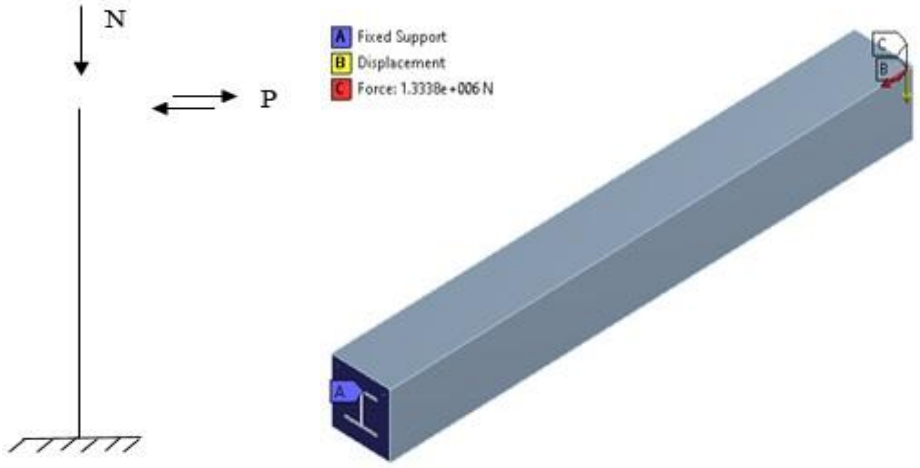

c) fixed-free

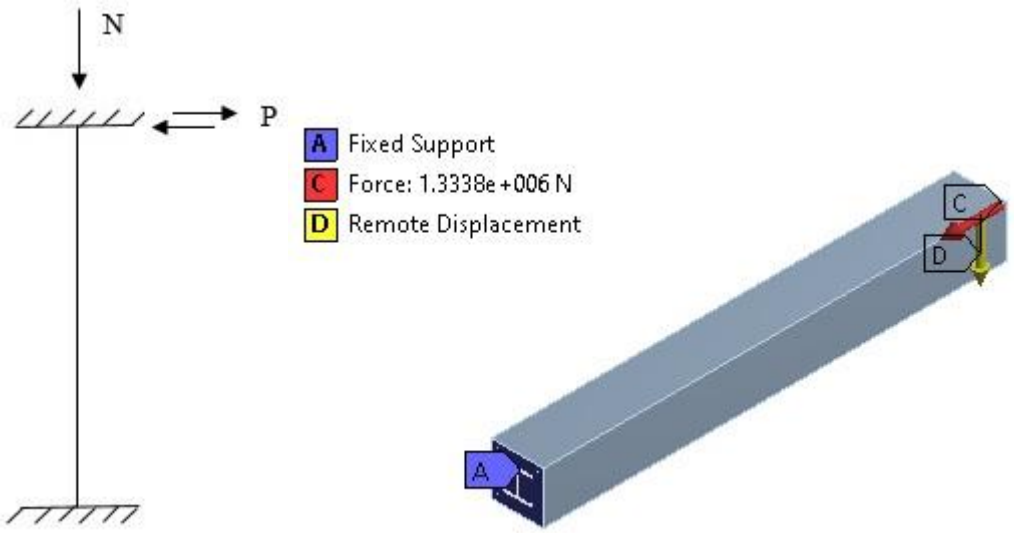

d) fixed-fixed

Figure III.3: Boundary conditions of fully encased composite columns

III.3 Results and discussion

To understand the rigidity of this element before failure, the parameters of the cyclic response of the composite columns, as shown in Table III.1 and Table III.2, were investigated including (hysteresis curves, skeleton curves, ductility coefficient, dissipation energy, and initial stiffness). Figure III.4 shows an example of the stress equivalent (Von-Mises) distribution of composite columns, it can be found that the columns reach the plastic mode at the bottom counter to the top of the columns still in the elastic mode. As illustrated in Figure III.5, the deformed shape of the composite column at failure mode is also recorded. The finite element model predicted a steel yielding and concrete crushing as the failure mode. The compressive yield strength of concrete and yield stress of structural steel were both exceeded. The compressive stress was found to be highest near of the composite column bottom. The failure modes of the concrete and structural steel elements can be clearly identified by comparing the stresses of the elements to the strengths of the materials. Both modes of failure happen simultaneously, with the steel flange yielding initially accompanied by concrete crushing. The concrete fails in tension before the steel reaches its yield stress, while the concrete fails in compression before the concrete reinforcement reaches its yield stress.

Table III.1: Summary of the numerical results of boundary condition's effect

Specimens	Pm (KN)	Δy (mm)	Py (KN)	Δu (mm)	Pu (KN)	μ	E (KN.m)	Ky (KN/m)
I.5	198.65	64.2	194.24	200	164.34	3.12	378.45	3025.545
IV.1	195.21	48	167.01	200	153.52	4.17	367.24	3479.375
I.6	231.57	61.45	210.2	200	179.33	3.25	419.55	3420.667
IV.2	213.06	30	144.23	200	170.34	6.67	395.39	4807.667
II.9	172.84	48.5	148.65	200	86.55	4.12	347.26	3064.948
IV.3	172.5	40	145.47	200	84.01	5.00	341.53	3636.75

Table III.2: Summary of the numerical results of cover concrete effect.

specimens	Coeff.	c (mm)	Section	$N_{pl,Rk}$ (KN)	P_m (KN)	Δ_y (mm)	P_y (KN)	Δ_u (mm)	P_u (KN)	μ	E (KN.m)	K_y (KN/m)
I.1		10	370x370	5459.24	136.37	68	122.5	200	131.77	2.94	341.81	1801.471
I.2		20	390x390	5782.24	150.67	66	138.35	200	142.66	3.03	343.03	2096.212
I.3		30	410x410	6122.24	171.34	65	154.42	200	137.92	3.08	379.91	2375.692
I.4		40	430x430	6479.24	181.09	64.8	173.47	200	151.1	3.09	374.72	2677.006
I.5	-	50	450x450	6853.24	198.65	64.2	194.28	200	164.34	3.12	378.45	3026.168
I.6		60	470x470	7244.24	231.57	61.45	210.2	200	179.33	3.25	419.55	3420.667
I.7		70	490x490	7652.24	237.11	60	218.43	200	193.52	3.33	421.64	3640.5
I.8		80	510x510	8077.24	282.4	66	269.19	160	212.93	2.42	316.37	4078.636
II.1	0.2			6853.24	160.37	48.5	148.78	80	165.58	1.65	37.54	3067.63
II.2	0.25			6853.24	160.64	48.5	148.71	80	165.65	1.65	37.95	3066.19
II.3	0.3			6853.24	161.57	62.5	171.93	150	107.4	2.40	163.34	2750.88
II.4	0.35			6853.24	163.54	55.5	158.01	200	99.53	3.60	320.09	2847.03
II.5	0.4			6853.24	165.49	55.5	163.97	200	87.23	3.60	327.08	2954.41
II.6	0.45	-	450x450	6853.24	167.84	55.5	163.99	200	107.64	3.60	324.13	2954.77
II.7	0.5			6853.24	169.45	55.5	164.01	200	99.69	3.60	321.5	2955.14
II.8	0.55			6853.24	170.33	48.5	145.65	200	85.92	4.12	334.57	3003.09
II.9	0.6			6853.24	172.84	48.5	148.65	200	86.55	4.12	347.26	3064.95
II.10	0.65			6853.24	173.28	48.5	149.96	200	91.43	4.12	339.97	3091.96
II.11	0.7			6853.24	176.27	48	153.51	200	100.75	4.17	331.75	3198.13

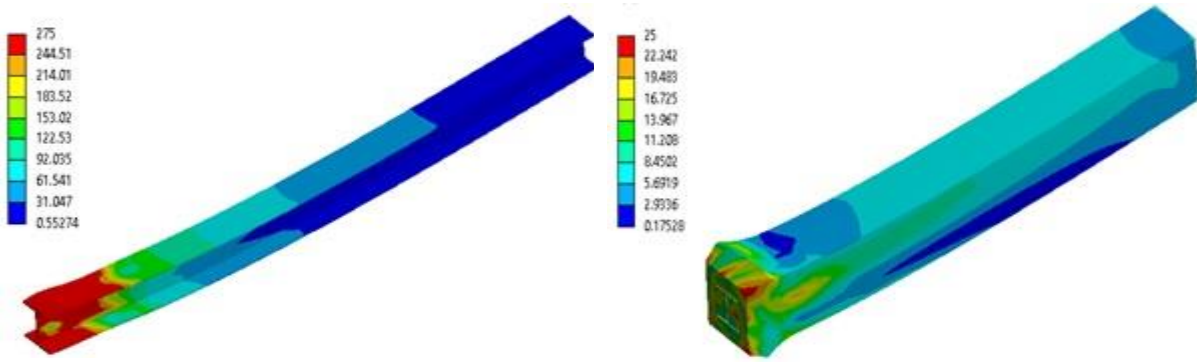

a) The stress of the structural steel section. b) The stress of the concrete.

Figure III.4: Von-Mises Stresses of composite column specimen FEC.CF.9 (steel and concrete).

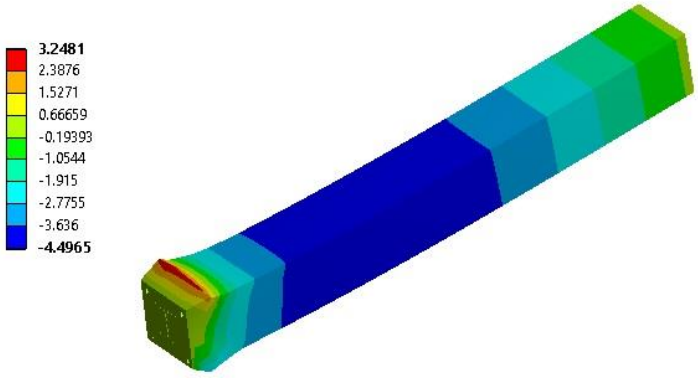

Figure III.5: The deformed shape of composite column specimen FEC.CF.9.

III.3.1 Hysteresis Curves

The load-lateral displacement curves of the structures contribute to a very important role to understand the inelastic behaviour in developing a seismic design methodology for these structures.

III.3.1.1 Cover Concrete

As shown in Figure III.6 among all specimens, the test of specimen I.8 failed to complete all the cycles, because the concrete cover is too high and the outer concrete is without reinforcement, all the hysteresis curves show high energy dissipation except the last one. It is observed that all specimens have some common hysteretic characteristics. The specimens have an elastic stage and a linear relationship between load and displacement at the early stages of loading, the hysteretic curves are symmetrical. After the cracking of the concrete, the specimens show an elastic-plastic response. As the lateral displacement increases, the hysteretic loops slowly approach the displacement axis. However, after the seventh cycle, the lateral load decreases under each displacement loading level, and loading and unloading gradually decrease stiffness for all specimens, due to spalling of the outer concrete and increasing loading displacement. On the other hand, the hysteresis curve gets plumper after the load reaches the ultimate load

which explain a good energy dissipation capacity. All the specimens exhibit that has good cyclic behaviour except the last one.

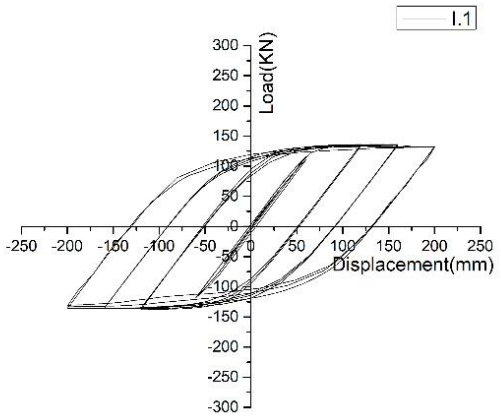

a) I.1

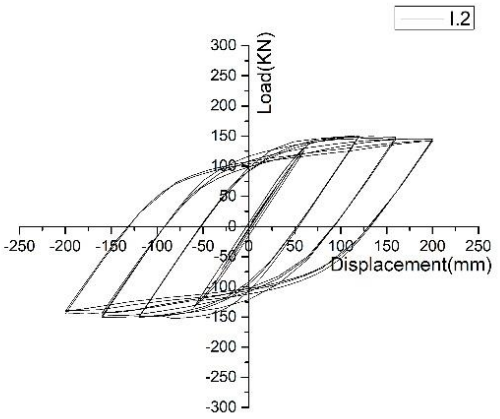

b) I.2

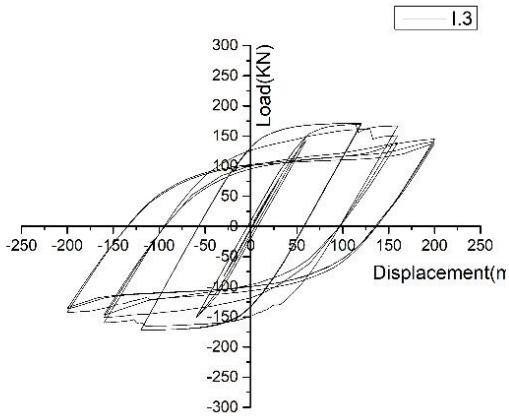

c) I.3

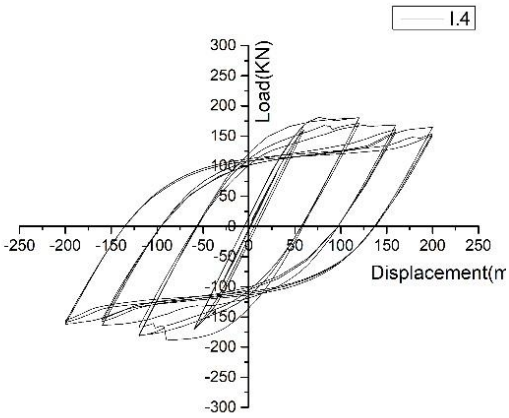

d) I.4

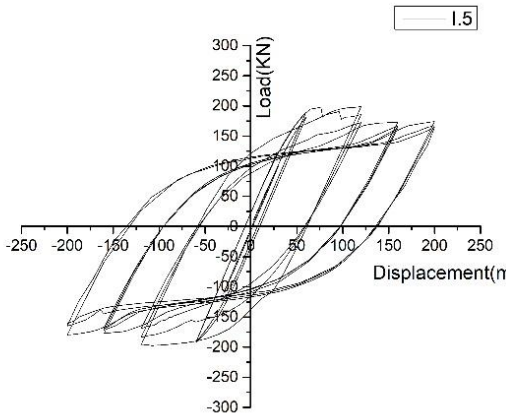

e) I.5

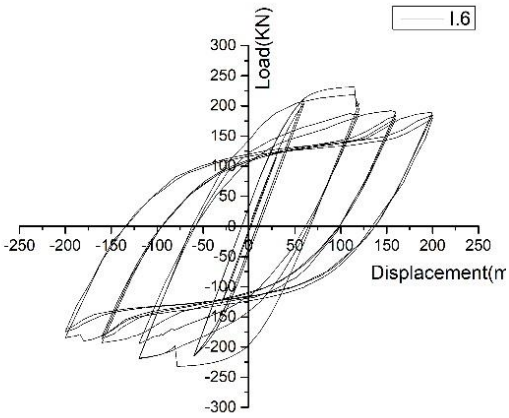

f) I.6

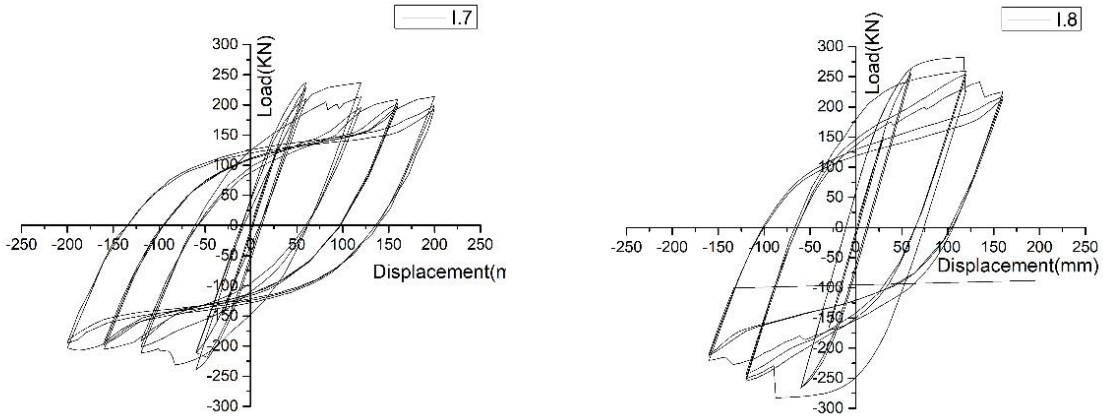

g) I.7 h) I.8

Figure III.6: Hysteresis curves of the effect of cover concrete

III.3.1.2 Coefficient of friction

As shown in Figure III.7, the test of the specimen (II.1- II.3) failed to complete all the cycles because the coefficient of friction is too low, and the friction between structural steel and concrete prevent the ductility. All the hysteresis curves show high energy dissipation except the first three curves.

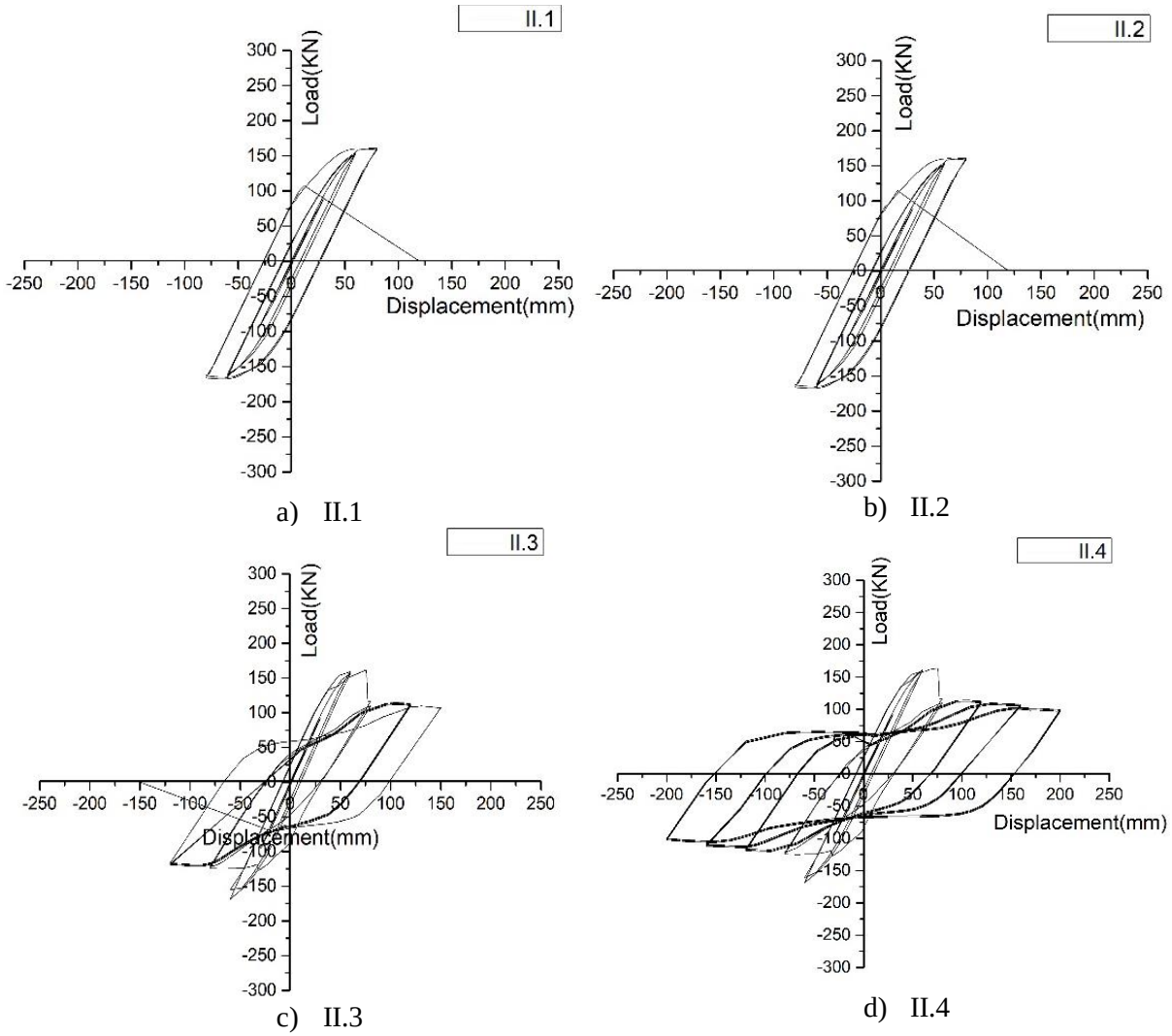

a) II.1 b) II.2

c) II.3 d) II.4

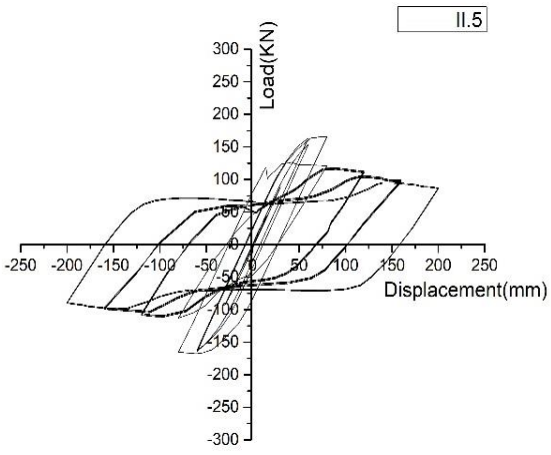

e) II.5

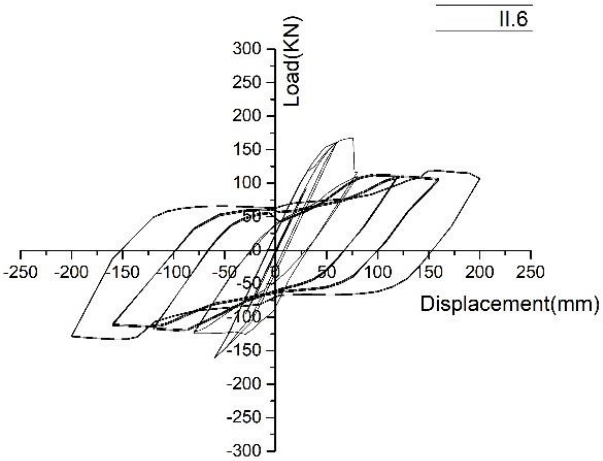

f) II.6

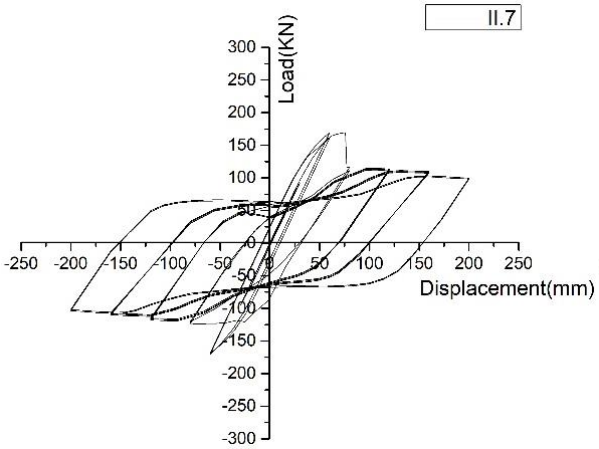

g) II.7

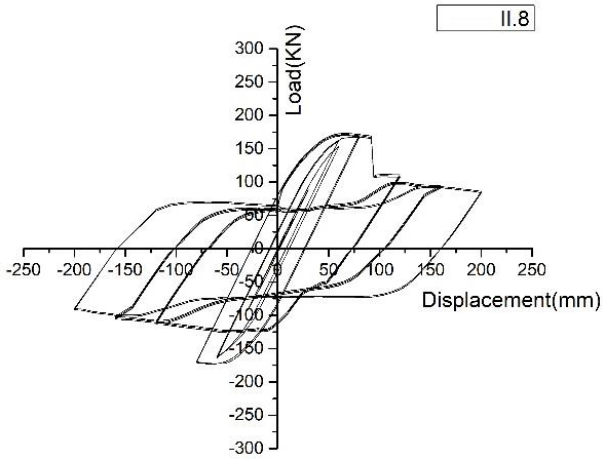

h) II.8

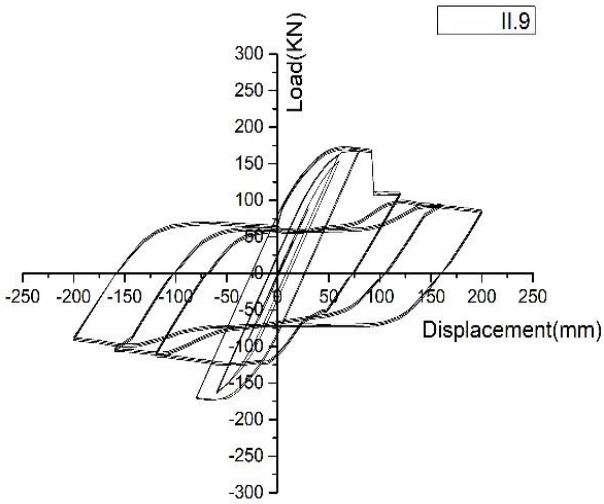

i) II.9

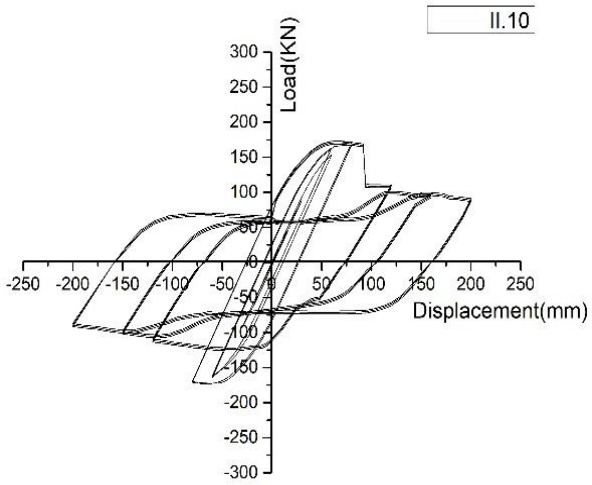

j) II.10

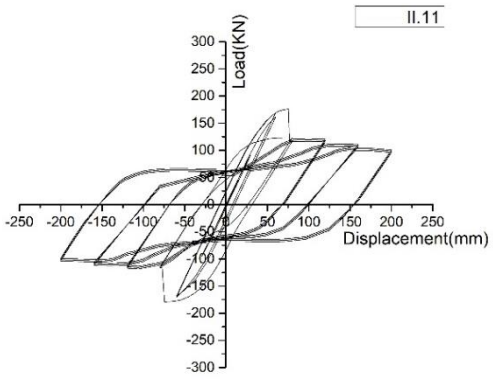

II.11

Figure III.7: Hysteresis curves of the effect of Coefficient of friction

III.3.3.1 Effect of boundary condition

The hysteretic curves for the three specimens are shown in Figure III.8. It can be found that the hysteretic curves are stable without an obvious pinching effect. The performance of the boundary conditions was initially linear, the horizontal load gradually increased with the growth of horizontal displacement. Then the slope of the curve started to decrease, which demonstrated the inelastic performance with reducing stiffness. It could be noted that the sudden drop of the curve in specimen IV.3 is caused by the spalling of the cover concrete [20]. The first yield in the steel section was recorded at 167.01 KN during the push cycle at the composite column (IV.1) at a displacement of 48 mm. For the specimen with a fixed-free boundary of condition, the first yield in the steel section was recorded at 194.24 KN during the push cycle at composite column (I.5) at a displacement of 64.2 mm as shown in Table III.2. It can be found that the boundary of conditions affects the FEC columns. A more detailed analysis of the differences among the three specimens will be given in the following sections.

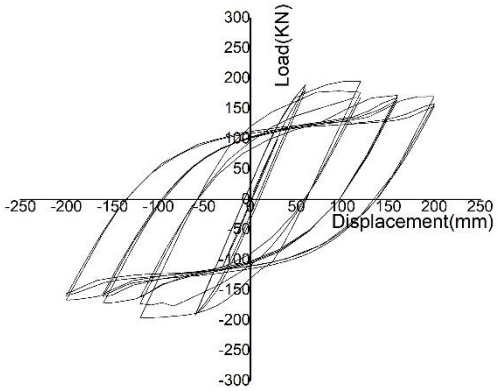

a) IV.1

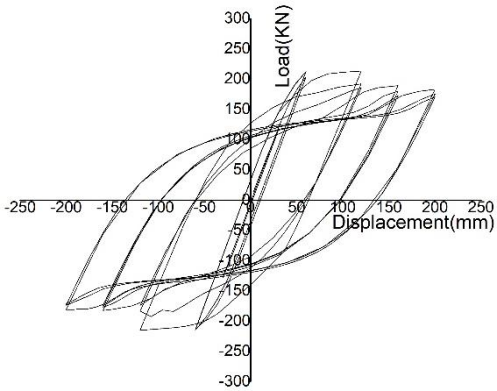

b) IV.2

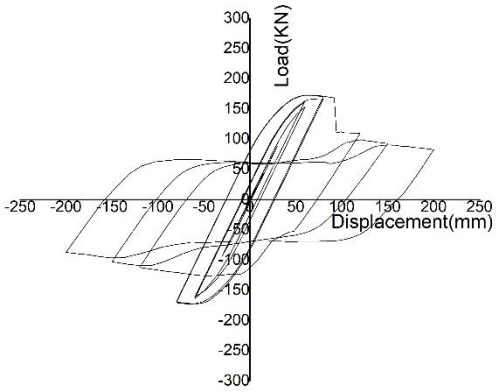

c) IV.3

Figure III.8:Hysteresis curves of the effect of boundary condition

III.3.2 Skeleton Curves

A skeleton curve is generated by connecting the peak points of each cycle lateral load-displacement curves. A skeleton curve is an important parameter since it is used to measure ductility, strength, deformation capacity of specimens and for studying inelastic cyclic or seismic response. In an analysis of the skeleton curve, when the wider flange of inner structural steel is subjected to compression, the negative loading direction is defined, while the positive loading direction is defined when subjected to tension [68].

III.3.2.1 Cover Concrete

For convenient comparison of the specimens, the skeleton curves are compared in Figure III.9. It is shown with increasing concrete cover the lateral load increases, the figure exhibit the discontinuity in the curves due to the spalling of the concrete cover [20].

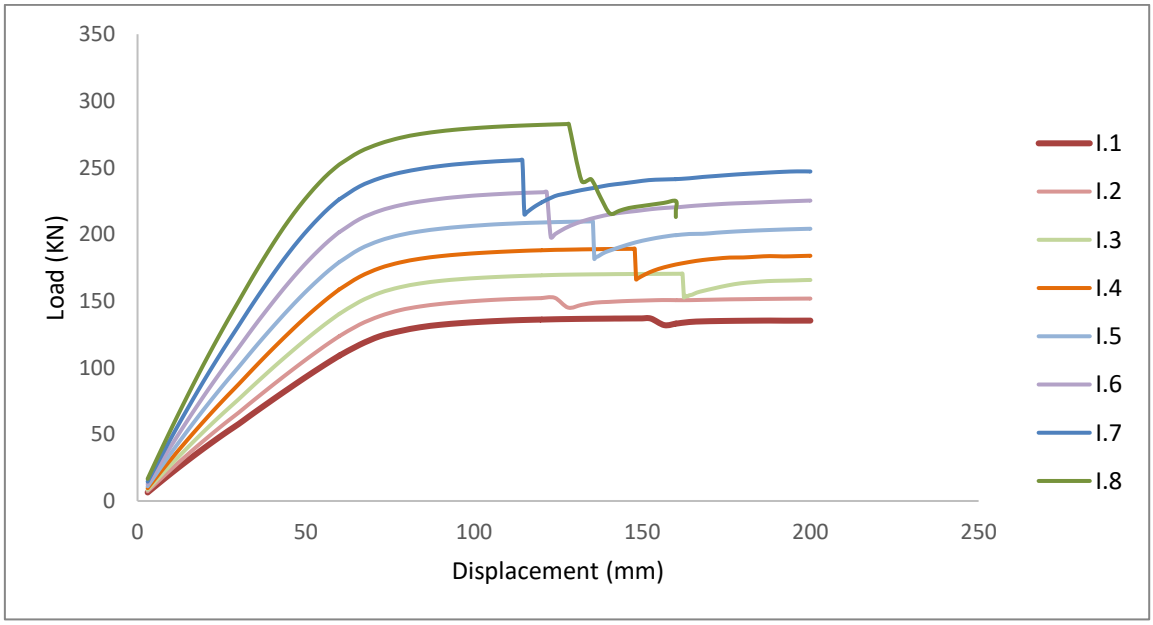

Figure III.9: Comparison of skeleton curves of the effect of cover concrete.

III.3.3 Dissipated energy

The amount of energy dissipated by a structural element is an important factor in determining its seismic performance. The area contained by the hysteretic hoops is used to determine dissipated energy from the lateral load-displacement curve. In general, specimens with a lower concrete cover level had less dissipated energy than higher cover levels.

III.3.3.1 Cover Concrete

The energy dissipation is shown in Table III.2, with specimen I.1 having a 341.81 KN.m dissipated energy according to the column's lower durability than the others, while I.7 has a 421.64 KN.m dissipated energy, and specimen I.8 reaching the failure mode at the end of the 10th cycle. However, with an increase of the concrete cover, the energy of a specimen tends to increase until it reaches 70 mm (c/h=0.0175), it begins to decrease sharply, shown in Figure III.10 indicates that the energy of the first specimen is 341.81 KN.m and the peak point is 421.64 KN.m.

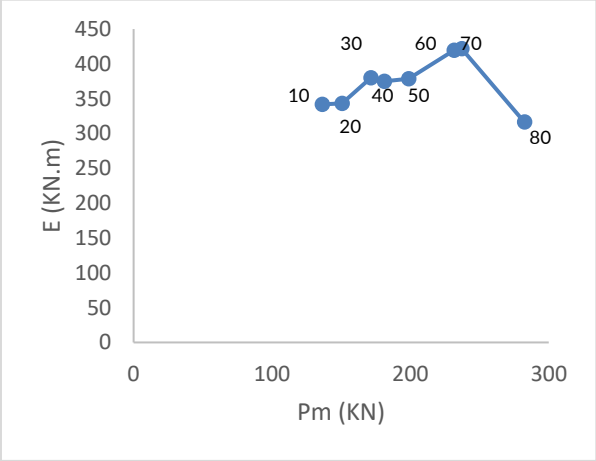

Figure III.10: Dissipated energy of the effect of the cover concrete *(c=10mm to 80mm)*

III.3.3.2 Coefficient of friction

The energy dissipation in the second series (II.1-II.11) at the begging is low, and as the coefficient of friction increases also the energy increases until it reaches 0.6 then the energy degrades gradually. Figure III.11 shows that the energy of the first specimen, with 0.20 of friction coefficient is 37.54 KN.m and it increases and stabilized than the friction coefficient of 0.35. The peak point is 347.26 KN.m, which means that the coefficient of friction has an obvious effect over the cover concrete. But its effect is almost negligible from 0.35.

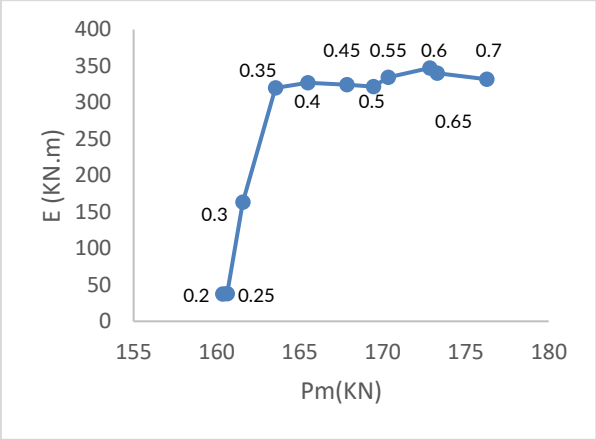

Figure III.11: Dissipated energy of the effect of the coefficient of friction *(Coeff. =0.2 to 0.7)*

III.3.3.2 Effect of boundary condition

A comparison between energy dissipation of boundary condition specimens is presented in Figure III.12. As shown in this figure, specimens (fixed-free), attained the highest energy dissipation capacity as compared to other specimens. This can be attributed to the degree of freedom at the top of the FEC columns. It can be found that there is an obvious difference between the specimens 450x450 and 470x470 compared with the specimens with a 0.6 coefficient of friction.

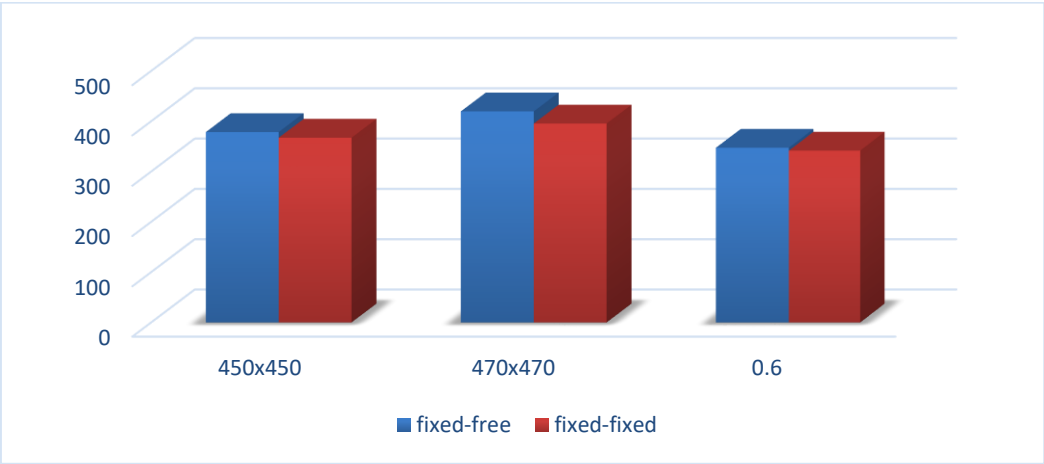

Figure III.12: Energy dissipation of boundary condition effects.

III.3.4 Ductility Factor

The ductility coefficient μ is used to estimate the cyclic behaviour and deformation capacity of test specimens, which is defined as the ratio of ultimate displacement to yield displacement as given in Eq. (III.1) [69].

$$\mu = \frac{\Delta u}{\Delta y} \qquad \text{(III.1)}$$

Where, Δ_y is the yielding of the structural steel section displacement corresponding to yield load P_y and Δ_u is the ultimate displacement corresponding to ultimate load P_u.

III.3.4.1 Cover Concrete

For the first series (I.1-I.8), it is shown that the cover concrete thickness improves the ductility of the column. For a thick cover concrete, as 80mm (c/h=0.02) the column ductility decreases by 27.33%. Results in Table III.2 indicate that I.6 and I.7 columns have better ductility than the others by +11.71% as shown in Figure III.13.

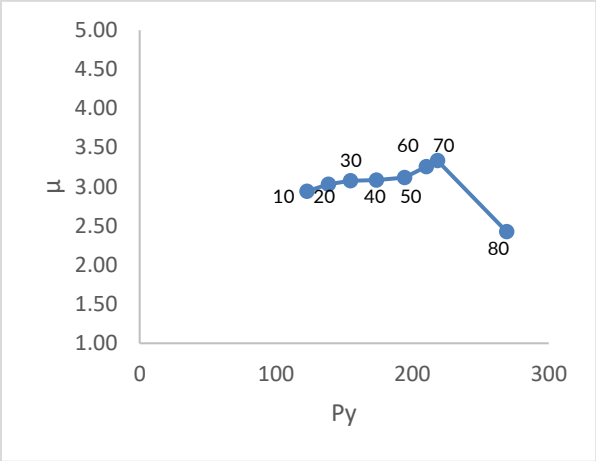

Figure III.13: Ductility Factor of the effect of cover concrete *(c=10mm to 80mm)*

III.3.4.2 Coefficient of friction

For the second series (II.1-II.11) varying coefficient of steel-concrete friction, ductility generally increases proportionally. The first two columns have a low ductility, with the increase of the coefficient of friction the ductility increases, specimen II.4-II.7 have constant ductility, but at specimen II.8 it increases again, improving it by +12.62% as shown in Figure III.14.

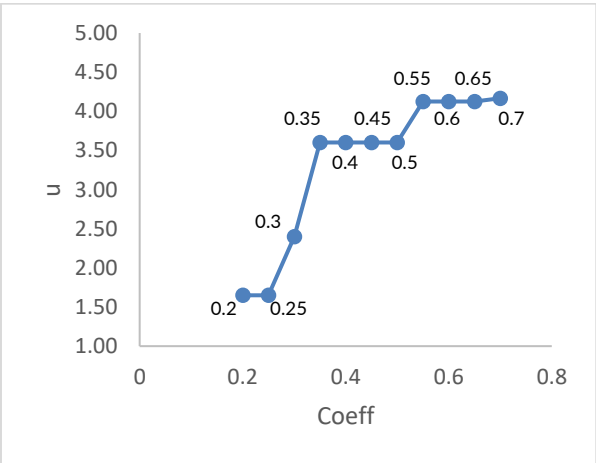

Figure III.14:Ductility Factor of the effect of coefficient of friction *(Coeff. =0.2 to 0.7)*

III.3.3.3 Effect of boundary condition

A comparison between different boundary conditions (fixed-free and fixed-fixed) is shown in Figure III.15. Specimens IV.2 have higher ductility than the other two specimens. Table III.1 summarizes the

yield displacement, the ultimate displacement as well as the ductility coefficients of the numerical results. It can be found that the specimens with fixed-free improved the ductility by 25.18%,51.27% and 17.6% for the 450x450, 470x470 and 0.6 FEC columns respectively.

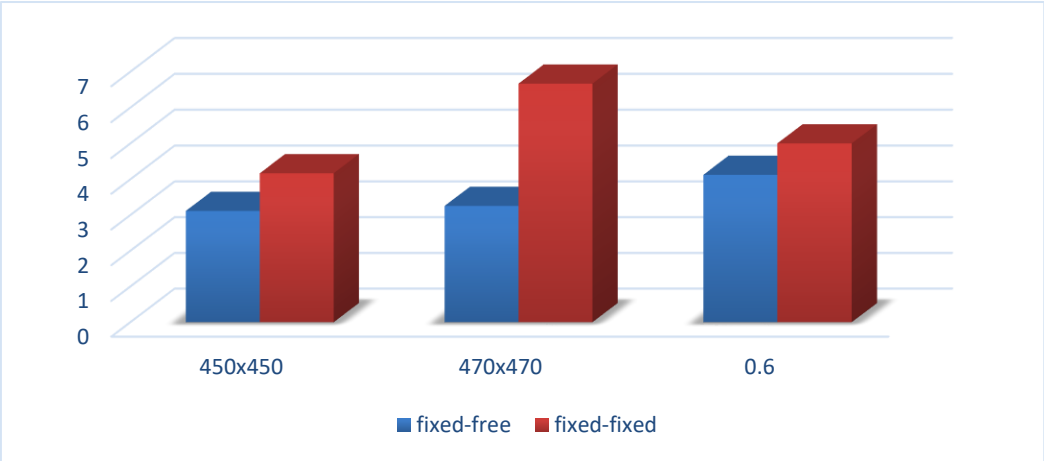

Figure III.15:Ductility of boundary condition.

III.3.5 Structural stiffness

Determined by the numerical results, stiffness degradation reflects the degree of cumulative damage to the structure during repeated loading. the stiffness degradation is evaluated by Eq. (III.2):

$$K_i = \frac{|+P_i|+|-P_i|}{|+\Delta_i|+|-\Delta_i|} \quad \text{(III.2)}$$

Where $+P_i$ and $-P_i$ are the peak loads of the i^{th} lateral displacement level in two reversal directions respectively, $+\Delta_i$ and $-\Delta_i$ are the peak corresponding displacements corresponding to the peak loads respectively [43].

III.3.5.1 Cover Concrete

Figure III.16 describes the stiffness degradation curves of the specimens with the displacement, which K_y is the initial loop stiffness listed in Table III.2. As exhibited in the curve, for the first series (I.1-I.8) the specimens with higher cover concrete experienced stiffness degradation at an early stage of loading. This is mostly attributable to the restriction of the concrete crack. However, stiffness degradation is more obvious in the specimens with higher cover concrete. The stiffness gradually degrades as the lateral displacement increases, but it degrades significantly when the cover concrete thickness gets bigger.

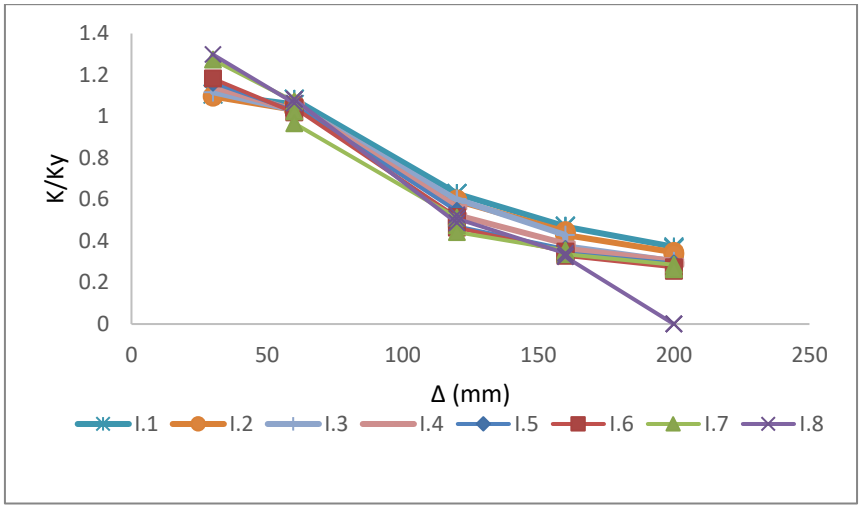

Figure III.16: Structural stiffness of the effects of the cover concrete (c=10mm to 80mm)

III.3.5.2 Coefficient of friction

For the second series (II.1-II.11), with increases in the coefficient of friction, the stiffness at the 3rd cycle degrades seriously as shown in Figure III.17, until it reaches 0.6 then it degrades gradually.

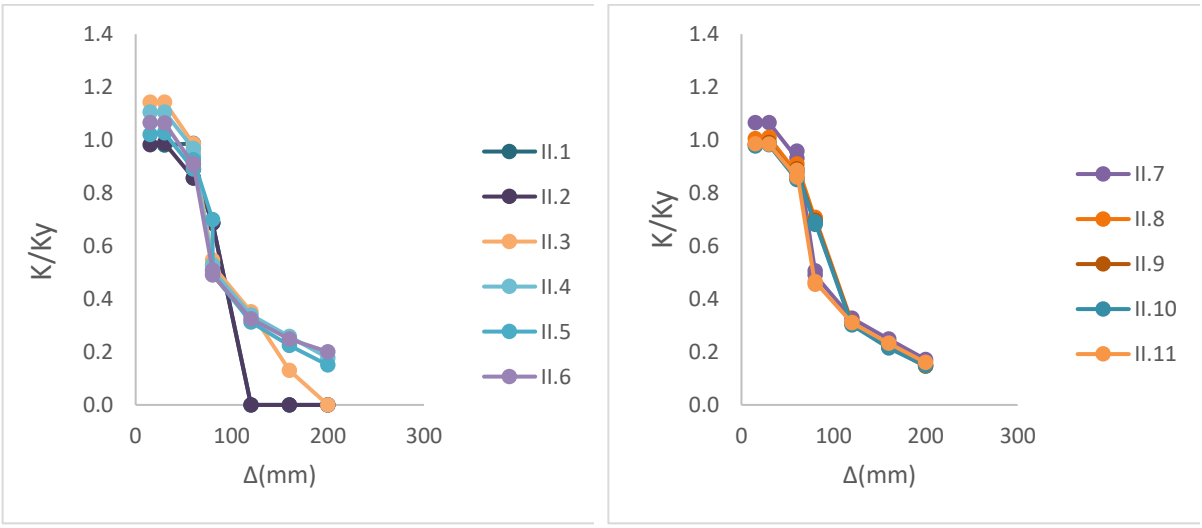

Figure III.17: Structural stiffness of the effects of the coefficient of friction (Coeff. =0.2 to 0.7)

III.3.3.4 Effect of boundary condition

The relationship between stiffness and loading level is shown in Figure III.18. It can be seen that all specimens showed similar responses with different boundary condition.

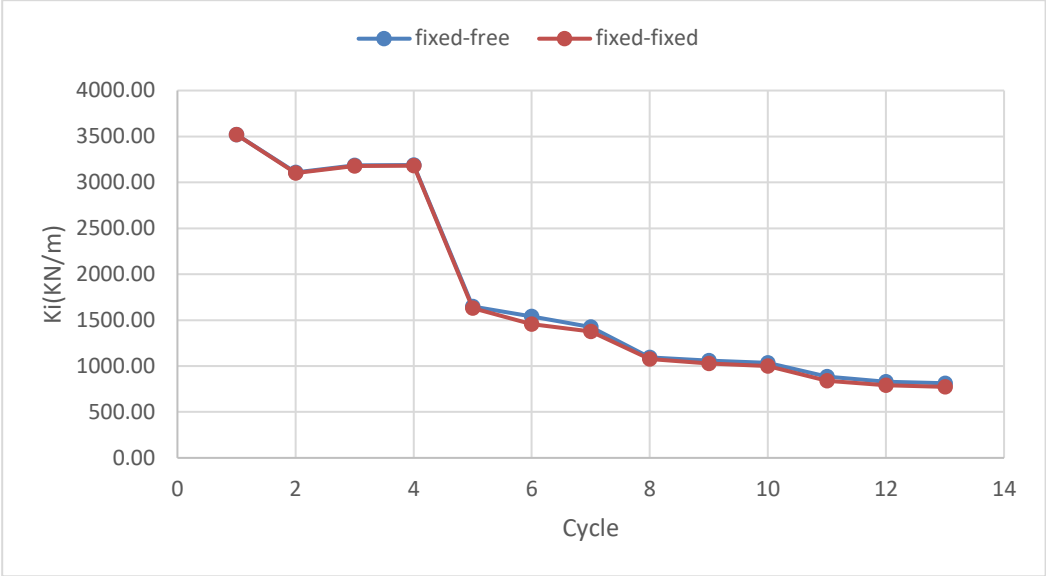

a) 450x450 FEC column

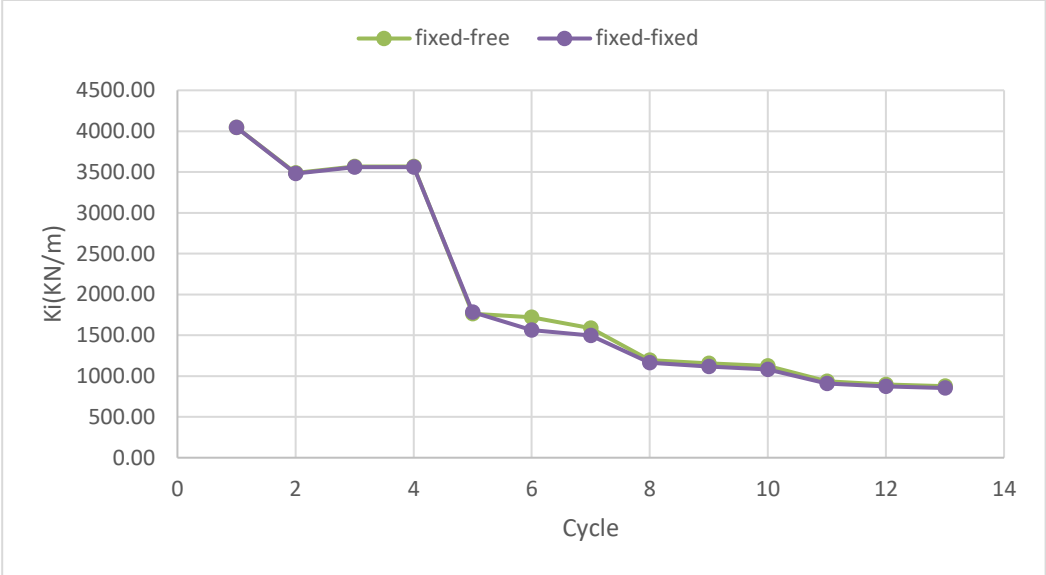

b) 470x470 FEC column

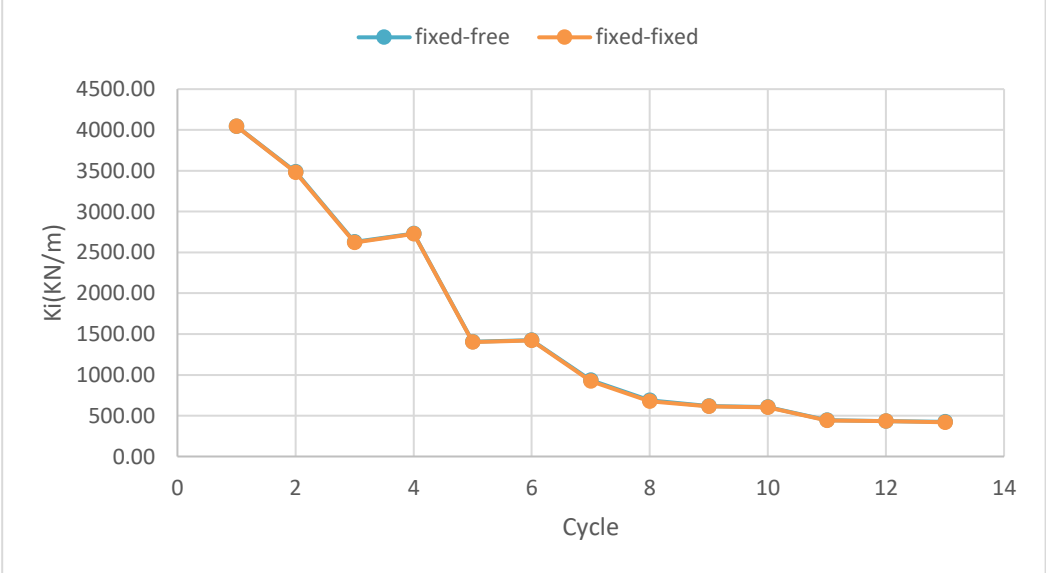

c) 0.6 coefficient of friction

Figure III.18: Structural stiffness of the effects of boundary condition.

III.4 Conclusion

To understand the cyclic behaviour of composite columns, the effects of the cover concrete were numerically investigated, as well as the steel-concrete coefficient of friction by testing the columns under a combined cyclically increasing lateral load and constant axial load. Based on this study the following conclusions can be drawn:

- With an increase of the cover concrete, the displacement ductility, the energy dissipation and the stiffness increase by 11.71%, 18.93% and 50.52% receptively compared with specimen I.1. With an increase of the concrete cover, the ductility and the energy dissipation of a specimen tends to increase until it reaches 70 mm (c/h=0.0175). However, when the cover concrete is so large reaches 80mm (c/h=0.02) in the analysed specimens, the displacement ductility and the energy dissipation decrease by 27.33%, 24.97% receptively, and the stiffness decreases seriously due to the absence of the reinforcement bars in cover concrete.

- After the load reaches the ultimate load, the hysteretic curves of the columns are plumped and affected by the spalling of cover concrete. Specimens (I.1-I.7) exhibit good ductility, energy dissipation capacity and good rigidity, counter to specimen I.8 that failed to complete the test, it reached the failure mode at the end of the 10th cycle because the concrete cover is too high and the outer concrete is without reinforcement.

- With an increase of the coefficient of friction between steel and concrete, the ductility, the energy dissipation and the stiffness increase by 12.62%, 7.82% and 7.11% receptively. However, when the coefficient of friction reaches 0.6, it gives a better energy dissipation. It proves that the columns with a 0.6 coefficient of friction exhibit favourable cyclic behaviour.

- The coefficient of friction has an important effect on the cyclic behaviour of composite columns. The cyclic behaviour worsens when the coefficient of friction is decreased and it improves when the coefficient is increased, especially under 0.6.

- Stiffness degradation showed similar responses with different boundary conditions.

- The boundary condition has a significant effect on the FEC columns, boundary condition (fixed-free) has the highest peak load, ductility, energy dissipation and higher initial stiffness much better than fixed-fixed.

The results show that the cover concrete has a slight impact on the composite columns, counter to the effects of the coefficient of friction owing that to the composite work between the steel section and the concrete. The sandblasting method of the steel in the composite column is necessary to improve the friction and to increase the dynamic dissipative capacity.

Chapter IV
CONCRETE REINFORCEMENT BARS EFFECTS UNDER CYCLIC LOADS OF THE FEC COLUMNS

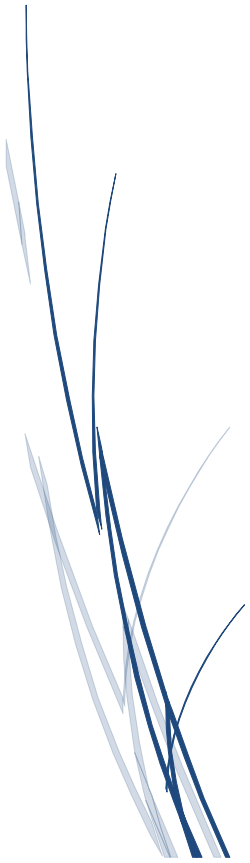

CHAPTER IV
CONCRETE REINFORCEMENT BARS EFFECTS UNDER CYCLIC LOADS OF THE FEC COLUMNS

IV.1 Introduction

A numerical investigation to determine the full failure modes and the load capacity behaviour of FEC columns are presented in this chapter. The main variables considered in the test program were the applied axial load ratio, longitudinal reinforming bars and transversal reinforming bars. The applied loads were axial and cyclic positioned on top of the columns. Numerical results were obtained from 3D nonlinear finite element analysis using ANSYS finite element code. The numerical simulations were performed on a wide variety of FEC columns with different geometric properties. The finite element analysis was conducted on thirty-six FEC columns. The descriptions of the geometric and material properties of these test specimens were presented in Chapter 2.

IV.2 Design of parametric study

For the parametric study, a square column with outer dimensions of 450 mm × 450 mm was selected. Typical cross-section and elevation of FEC column was used in the parametric study. These columns were designed and analysed during the parametric study to incorporate the effects of several geometric parameters that can significantly affect the FEC column behaviour. The geometric variables are the percentage ratio of reinforcement bars and various ratio of axial load.

The presence of reinforcement bars provides a beneficial residual strength following concrete crushing that leads to improved ductility. Four different percentages of longitudinal bars 4ϕ16, 8ϕ16, 4ϕ20 and 8ϕ20 (as shown in Figure IV.1) were used in the parametric study with 100mm, 150mm and 200mm of spacing between transversal bars as shown in Figure IV.2. The primary purpose of transverse reinforcement in FEC columns is to provide concrete confinement to prevent spalling around the structural steel section and to properly support longitudinal reinforcement to prevent buckling of the bars. These columns are divided into three groups (Table II. 3) depending on the spacing between transversal bars. The cover concrete, coefficient of friction and boundary conditions of the FEC columns were kept constant in all cases. The loads were applied axially and cyclically in these columns.

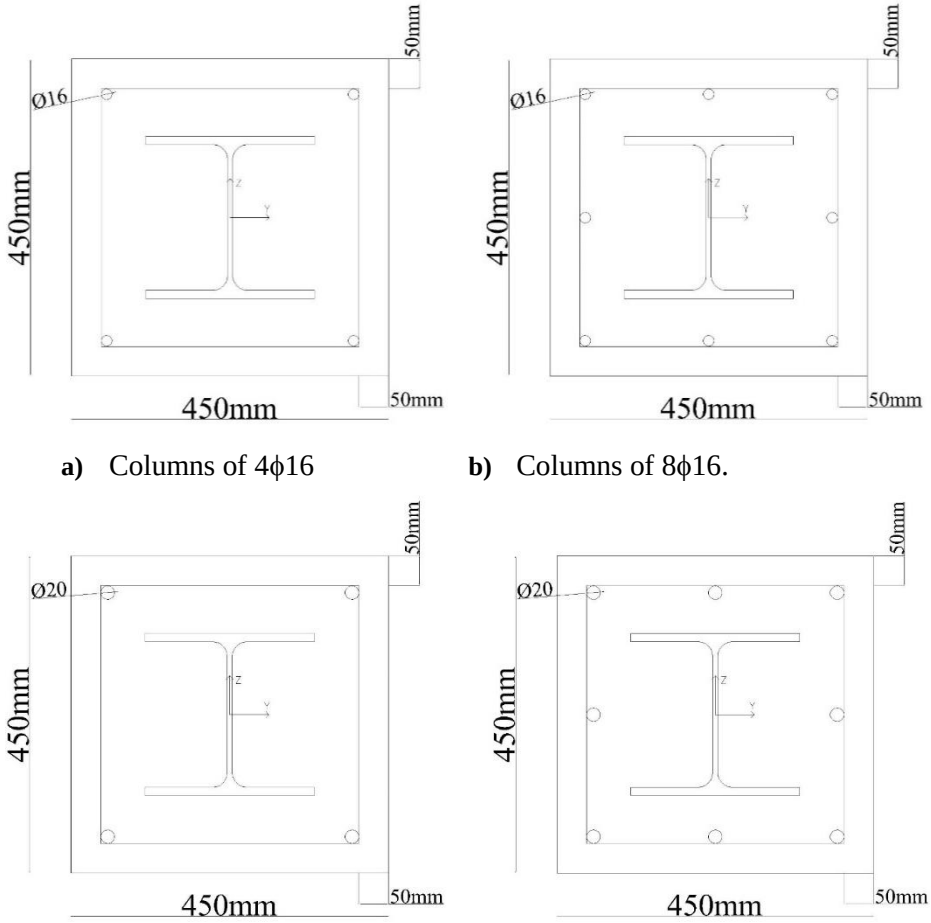

a) Columns of 4ϕ16 **b)** Columns of 8ϕ16.

c) Columns of 4ϕ20 d) Columns of 8ϕ20.

Figure IV.1: Dimensions of the FEC columns with different longitudinal bars.

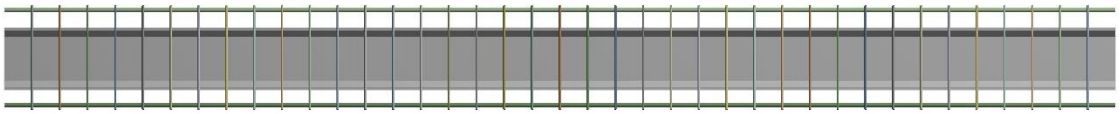

a) **Spacing of 100mm**

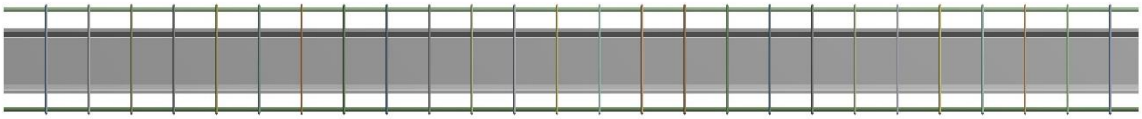

b) **Spacing of 150mm**

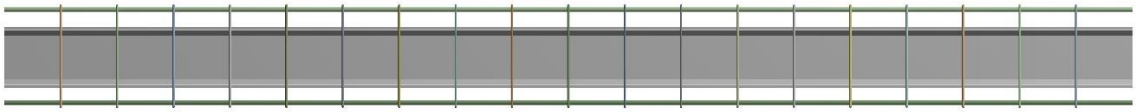

c) **Spacing of 200mm**

Figure IV.2: FEC columns with different transversal bars.

IV.3 Results and discussion.

The columns designed for the parametric study was simulated and analysed using the FE model developed in the current study (as presented in Chapter 2). The output parameters extracted from the analysis results were: P_m maximum lateral load that can be supported by the composite columns, Δ_y the yielding of the structural steel section displacement corresponding to yield load P_y and Δ_u is the ultimate displacement corresponding to ultimate load P_u. The cyclic load versus lateral displacement curves were also generated from the numerical analysis for parametric columns. The stiffness, energy dissipation and ductility index were also determined to observe the effect of reinforcement bars as shown in Table IV.1. All the results obtained from the parametric analyses were organized and presented to highlight the individual effect of each parameter in the following sections.

Table IV.1: Summary of the numerical results of concrete reinforcement bar's effect.

Specimens	spacing	Bars	Load	P_m (KN)	Δ_{max} (mm)	Δ_y (mm)	P_y (KN)	Δ_u (mm)	P_u (KN)	μ	E (KN.m)	K_y (KN/m)
III.100. I.1	**100**	**4ϕ16**	**n=0.1**	194.92	120	71.20	182.15	273.36	179.71	3.839	380.48	2558.29
III.100. I.2			**n=0.3**	179.12	80	65.00	163.59	185.50	152.25	2.854	130.08	2516.77
III.100. I.3			**n=0.5**	152.60	60	58.50	129.44	114.40	129.71	1.956	87.63	2212.65
III.100. II.1		**4ϕ20**	**n=0.1**	195.23	120	71.20	192.33	273.64	179.89	3.843	382.65	2701.26
III.100. II.2			**n=0.3**	179.30	80	65.00	163.75	185.87	152.41	2.860	130.66	2519.23
III.100. II.3			**n=0.5**	152.77	60	58.50	129.59	114.80	129.85	1.962	87.82	2215.21
III.100. III.1		**8ϕ16**	**n=0.1**	195.42	120	71.20	192.50	274.00	180.16	3.848	382.90	2703.65
III.100. III.2			**n=0.3**	179.59	80	65.00	163.93	186.20	152.65	2.865	131.59	2522.00
III.100. III.3			**n=0.5**	153.02	60	58.50	129.77	115.20	130.07	1.969	88.24	2218.29
III.100. IV.1		**8ϕ20**	**n=0.1**	195.70	120	71.20	192.76	275.60	179.93	3.871	384.45	2707.30
III.100. IV.2			**n=0.3**	179.86	80	65.00	164.17	186.55	152.88	2.870	131.94	2525.69
III.100. IV.3			**n=0.5**	153.26	60	58.50	130.00	115.60	130.27	1.976	88.82	2222.22
III.150. I.1	**150**	**4ϕ16**	**n=0.1**	194.91	120	71.00	192.64	273.75	179.28	3.86	380.23	2713.24
III.150. I.2			**n=0.3**	179.03	80	65.00	161.99	185.10	152.18	2.848	129.35	2492.15
III.150. I.3			**n=0.5**	152.64	60	58.50	129.39	114.00	129.74	1.949	87.79	2211.79
III.150. II.1		**4ϕ20**	**n=0.1**	195.10	120	71.00	192.81	273.96	179.57	3.86	382.64	2715.63
III.150. II.2			**n=0.3**	179.21	80	65.00	162.14	185.49	152.33	2.854	129.80	2494.46
III.150. II.3			**n=0.5**	152.79	60	58.50	129.54	114.40	129.87	1.956	88.17	2214.36
III.150. III.1		**8ϕ16**	**n=0.1**	195.30	120	71.00	192.99	277.24	179.84	3.90	382.77	2718.17
III.150. III.2			**n=0.3**	179.41	80	65.00	162.32	185.68	152.50	2.857	130.03	2497.23
III.150. III.3			**n=0.5**	153.08	60	58.50	129.72	114.60	130.12	1.959	88.76	2217.44

III.150. IV.1			**n=0.1**	195.56	120	71.00	193.25	274.20	180.23	3.86	384.13	2721.83
III.150. IV.2		**8ϕ20**	**n=0.3**	179.69	80	65.00	162.56	185.86	152.74	2.859	130.65	2500.92
III.150. IV.3			**n=0.5**	153.32	60	58.50	129.96	114.80	130.32	1.962	89.34	2221.54
III.200. I.1	**200**		**n=0.1**	194.85	120	71.00	192.61	273.83	179.32	3.857	380.18	2712.82
III.200. I.2		**4ϕ16**	**n=0.3**	178.98	80	65.00	161.96	185.00	152.13	2.846	129.14	2491.69
III.200. I.3			**n=0.5**	152.60	60	58.50	129.37	113.90	129.71	1.947	87.26	2211.45
III.200. II.1			**n=0.1**	195.04	120	71.00	192.78	274.08	179.53	3.860	382.41	2715.21
III.200. II.2		**4ϕ20**	**n=0.3**	179.16	80	65.00	162.12	185.15	152.29	2.848	129.33	2494.15
III.200. II.3			**n=0.5**	152.77	60	58.50	129.52	114.00	129.85	1.949	87.73	2214.02
III.200. III.1			**n=0.1**	195.22	120	71.00	192.96	280.40	179.82	3.949	383.39	2717.75
III.200. III.2		**8ϕ16**	**n=0.3**	179.36	80`	65.00	162.29	185.40	152.46	2.852	129.78	2496.77
III.200. III.3			**n=0.5**	153.00	60	58.50	129.70	114.40	130.05	1.956	88.19	2217.09
III.200. IV.1			**n=0.1**	195.49	120	71.00	193.22	281.80	181.51	3.969	383.98	2721.41
III.200. IV.2		**8ϕ20**	**n=0.3**	179.64	80	65.00	162.53	184.70	152.69	2.842	130.18	2500.46
III.200. IV.3			**n=0.5**	153.25	60	58.50	129.93	114.80	130.26	1.962	88.75	2221.03

IV.3.1 Hysteresis Curves

The cyclic response of the reinforcement bars is of essential importance to the performance of the composite columns and is greatly relied on the hysteretic curves. Hysteretic curves were plotted based on the relationship between the horizontal load applied to the composite column and the corresponding horizontal displacement. The specimens draw the slip hysteresis loop under fully reversed cyclic loading. Overall, the reinforcement bars show almost symmetrical hysteresis curves as shown in Figure IV.3. The hysteresis curves indicated by this series of investigations that the axial load has a serious effect on the FEC columns under cyclic loads. The specimens behave approximately elastic before the horizontal load increases to the yield load. The rigidity of the specimens decreases slowly from the yield load to the ultimate load and the plastic deformation is small. The axial compression ratio has a significant effect on the hysteresis curves of the specimens. In accordance with the decrease of the axial compression ratio, the loops become larger and more stable. The transversal reinforcement bars have a slight effect on the FEC columns. As the spacing between transversal bars increases, the FEC columns become strong and rigid.

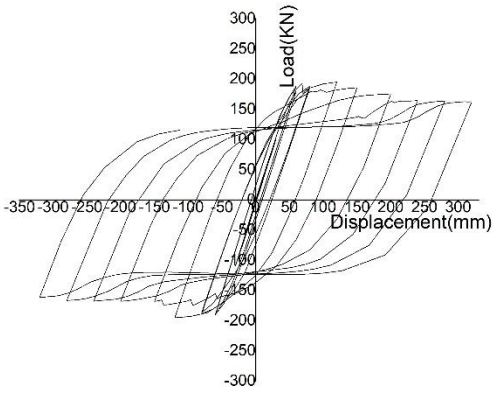

a) III.100. I.1

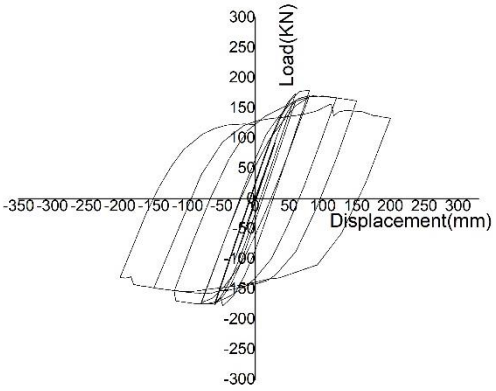

b) III.100. I.2

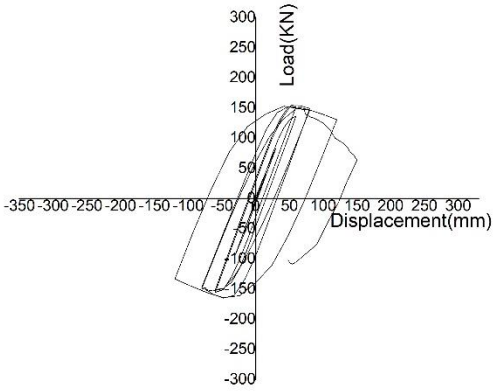

c) III.100. I.3

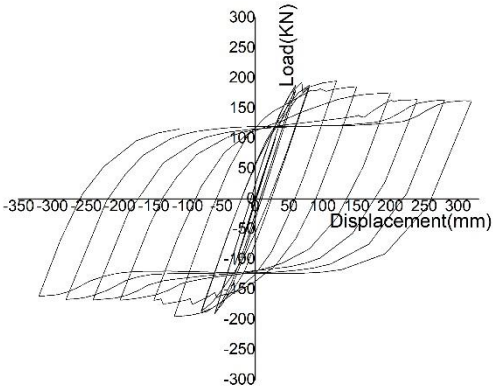

d) III.100.II.1

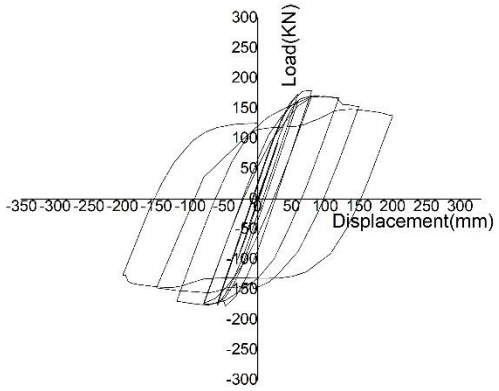

e) III.100.II.2

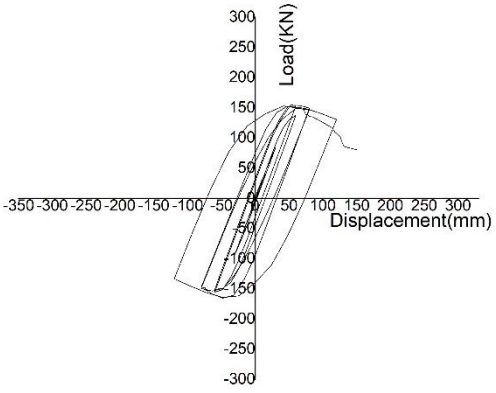

f) III.100.II.3

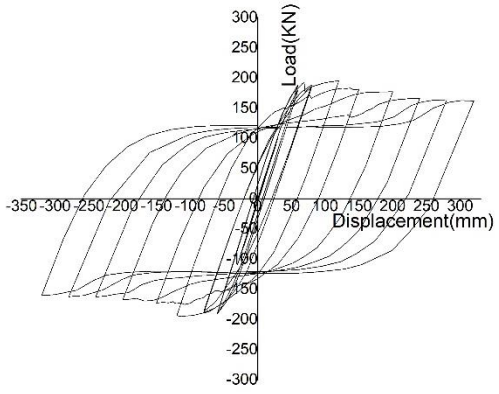

g) III.100.III.1

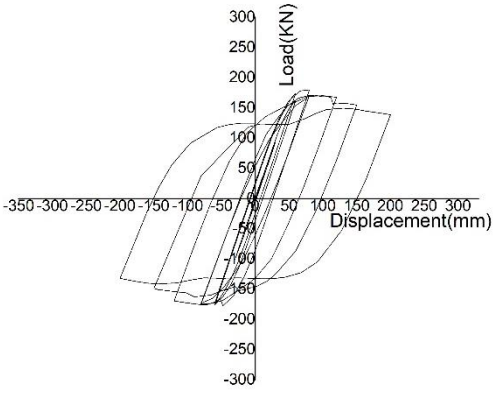

h) III.100.III.2

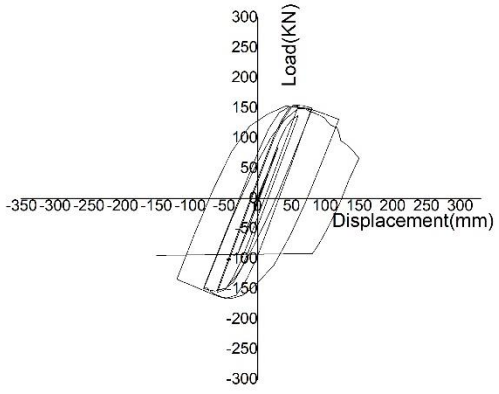

i) III.100.III.3

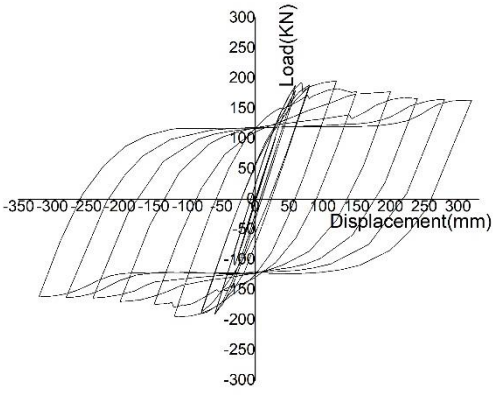

j) III.100.IV.1

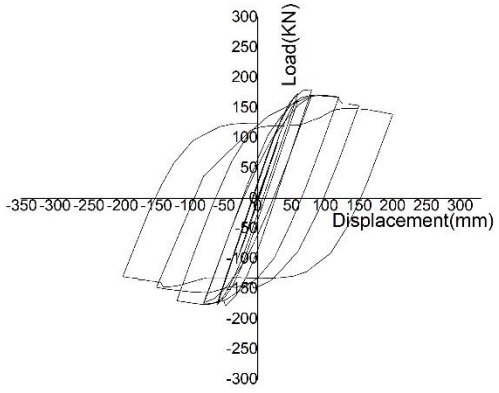

k) III.100.IV.2

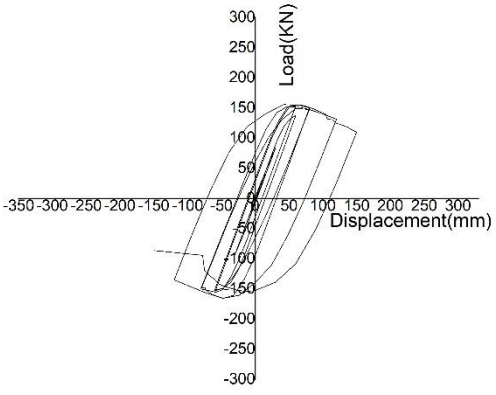

l) III.100.IV.3

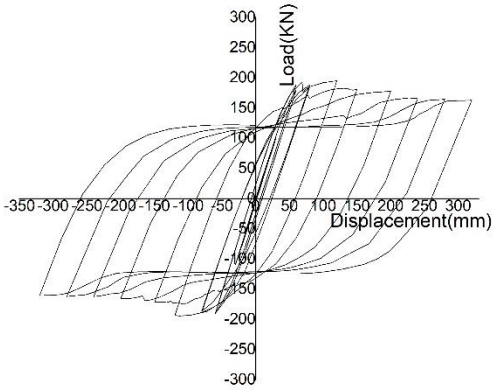

m) III.150. I.1

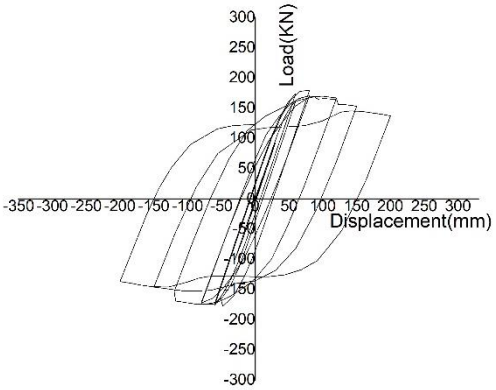

n) III.150. I.2

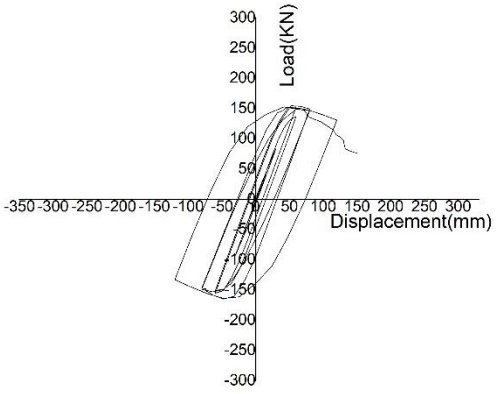

o) III.150. I.3

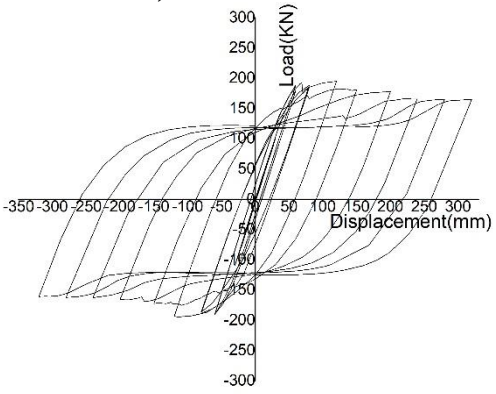

p) III.150.II.1

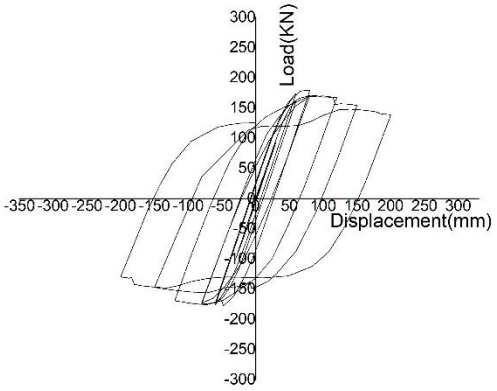

q) III.150.II.2

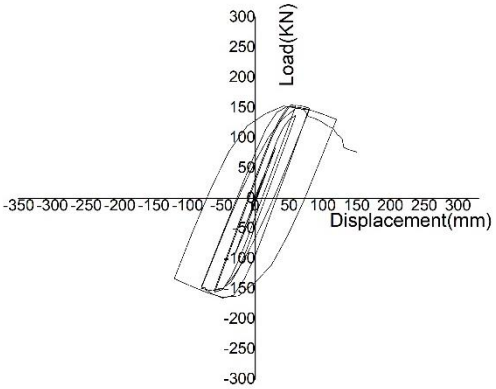

r) III.150.II.3

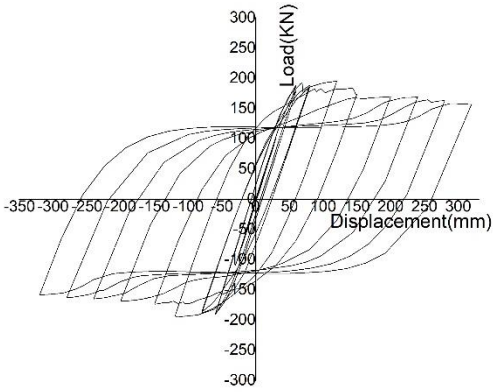

s) III.150.III.1

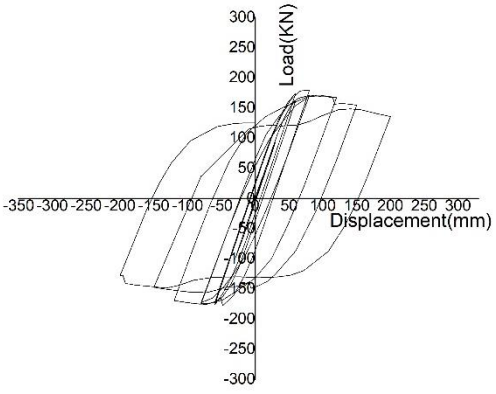

t) III.150.III.2

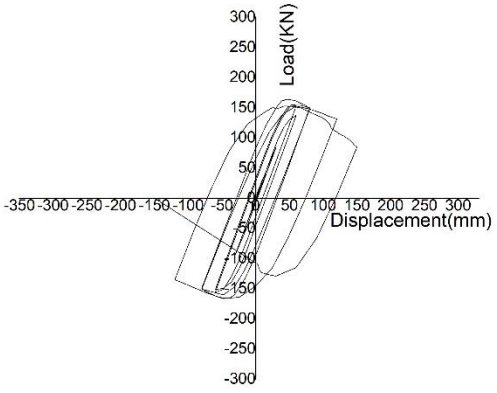

u) III.150.III.3

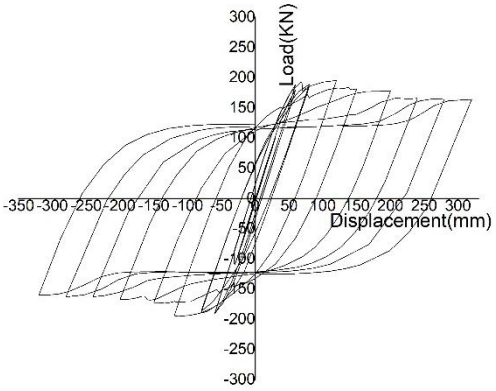

v) III.150.IV.1

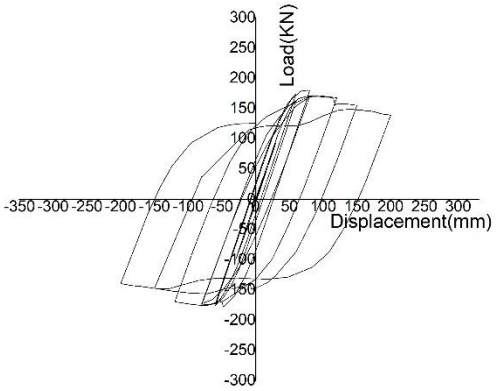

w) III.150.IV.2

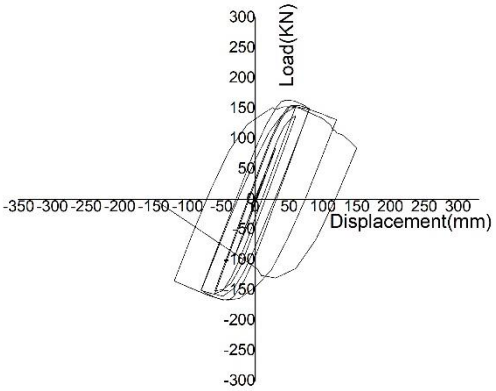

x) III.150.IV.3

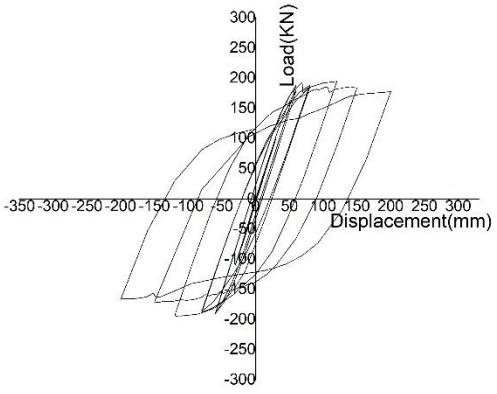

y) III.200. I.1

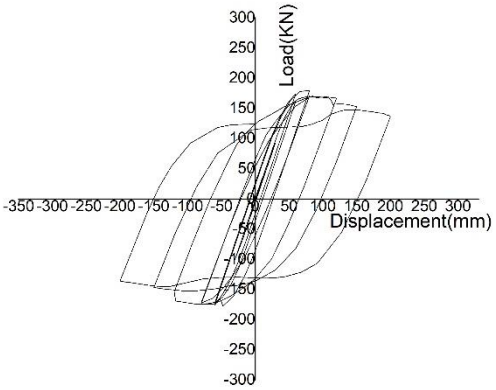

z) III.200. I.2

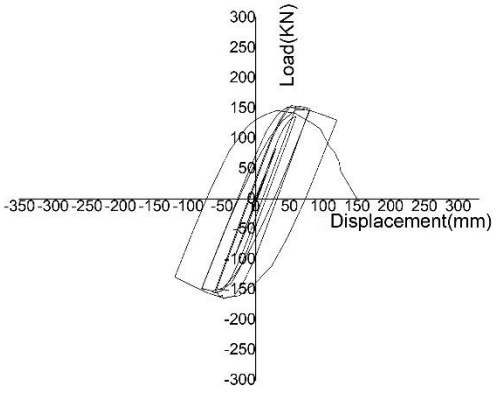

aa) III.200. I.3

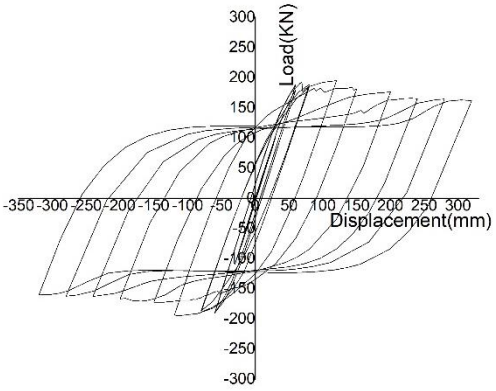

bb) III.200.II.1

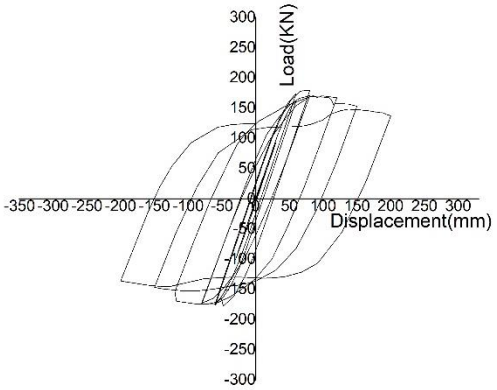

cc) III.200.II.2

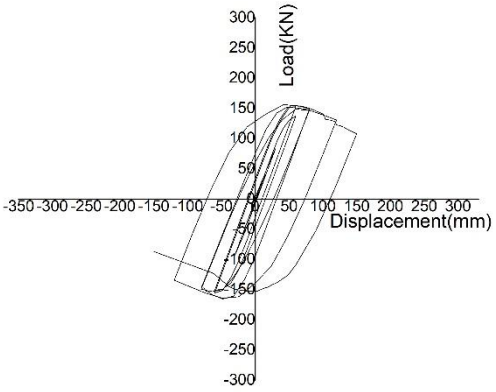

dd) III.200.II.3

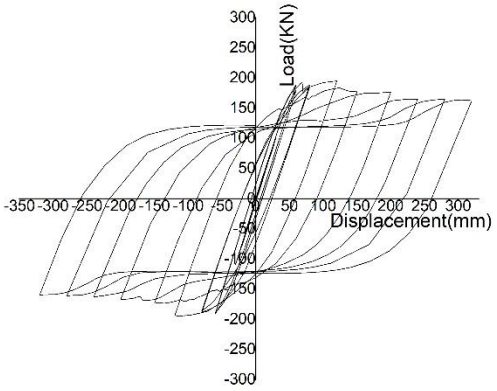

ee) III.200.III.1

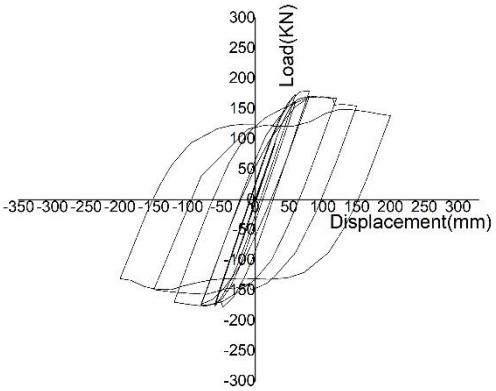

ff) III.200.III.2

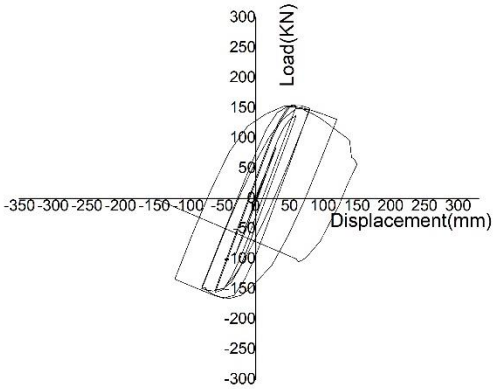

gg) III.200.III.3

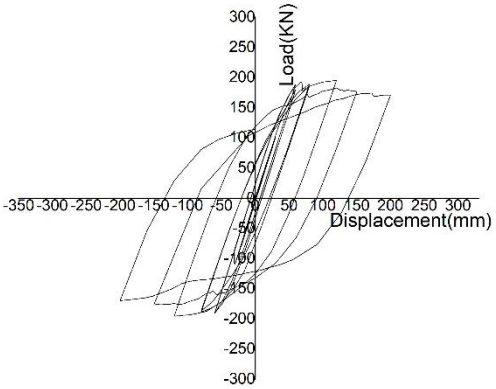

hh) III.200.IV.1

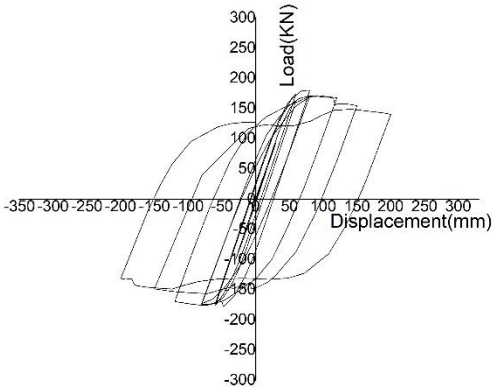

ii) III.200.IV.2

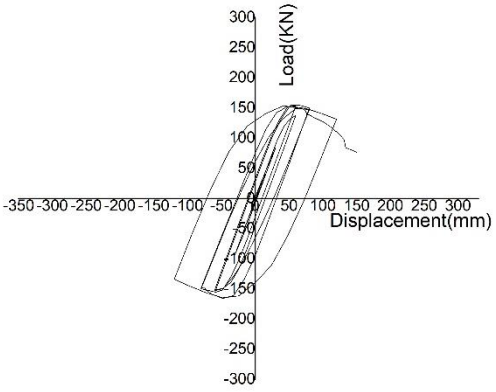

jj) III.200.IV.3

Figure IV.3: Hysteresis curves of the effect of longitudinal and transversal bars

IV.3.2 Skeleton Curves

To compare models, skeleton curves were constructed by connecting the peak points lateral load and the corresponding horizontal displacement from the first cycle of each loading level. The peak load P_m, the corresponding horizontal displacement Δ_{max}, and the initial stiffness K_y of each specimen are listed in Table IV.1. As expected, (see Figure IV.4) specimens with 0.5 ratio of axial load have the lowest peak load and initial stiffness, while the other two specimens exhibit a 10.35%-27.73% increase in peak load, 50.31%-95.92% increase in initial stiffness and 13.74%-15.62% increase in ductility. It can be found that the improvement in reinforcement bars does not significantly affect the peak load. This is because the capacity of the reinforcement bars is dominated by the load-bearing ability of the steel section.

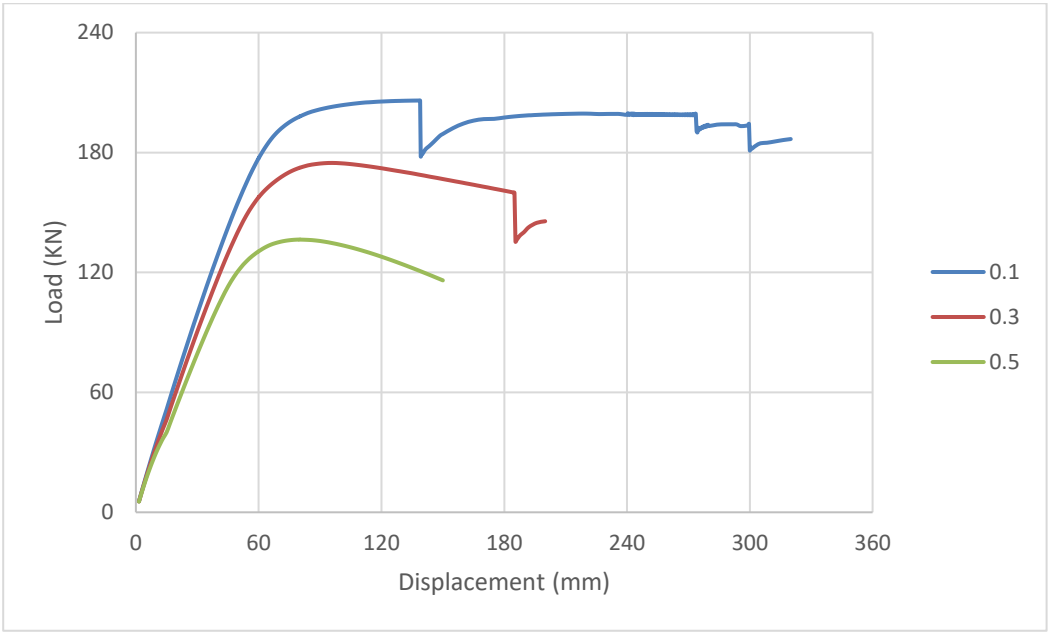

a) III.100.I

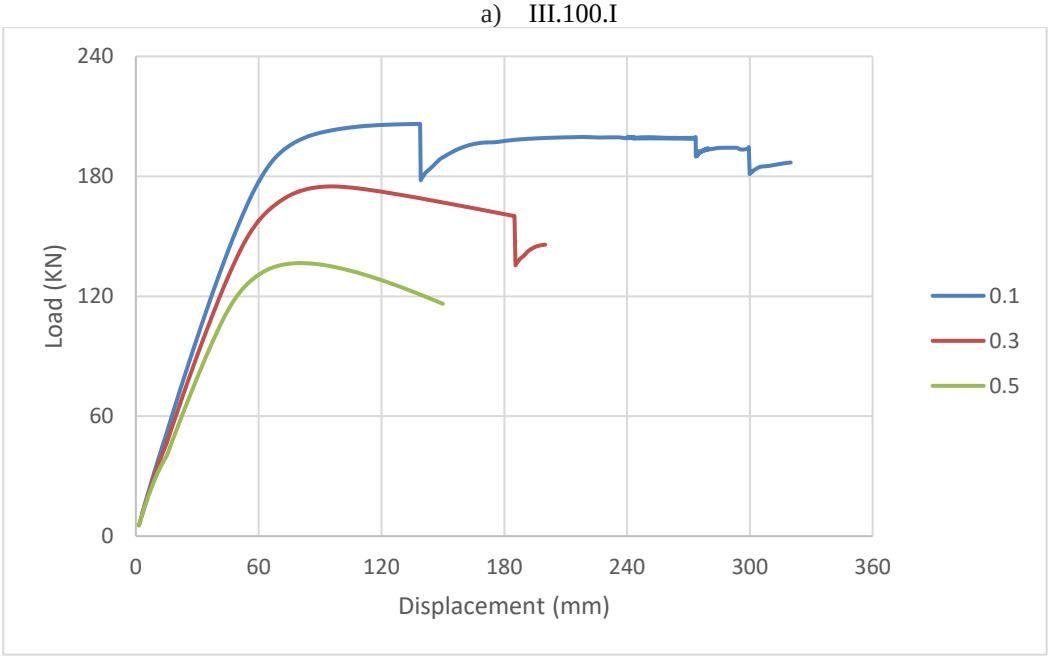

b) III.100.II

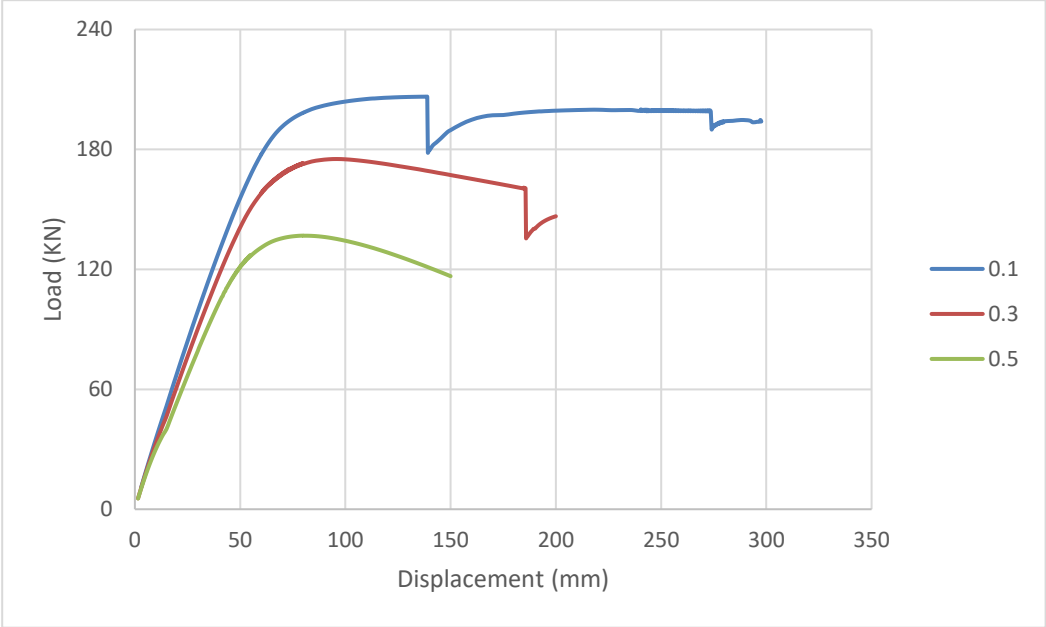

c) III.100.III

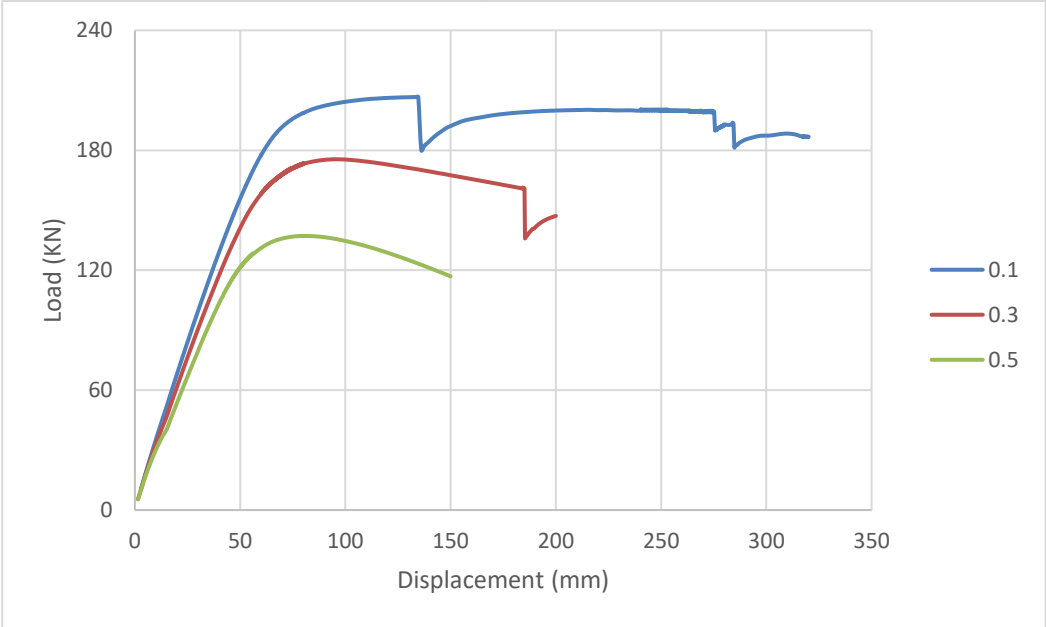

d) III.100.IV

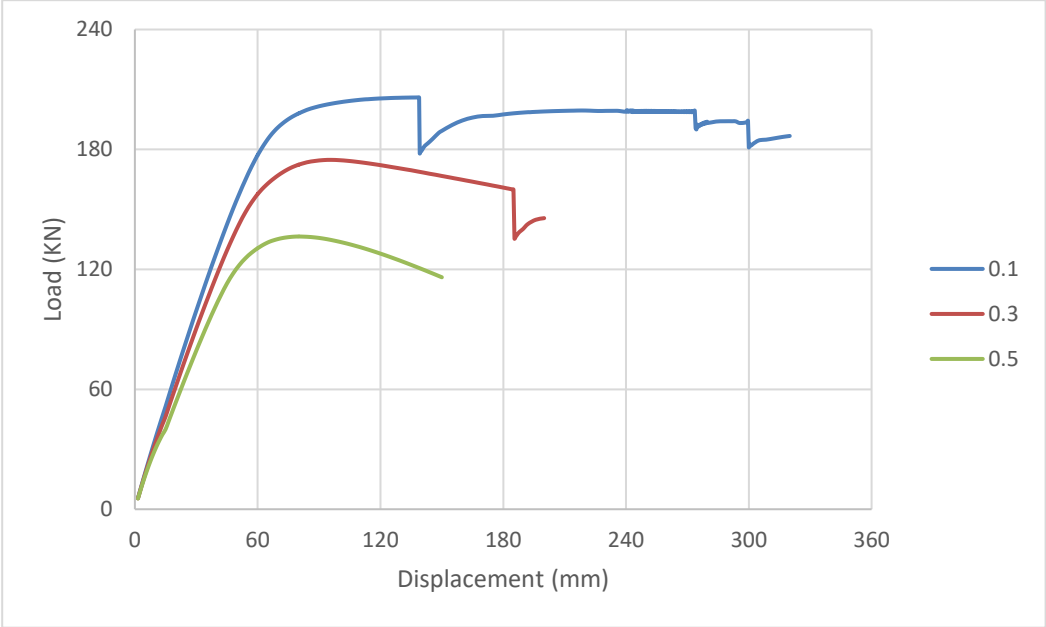

e) III.150.I

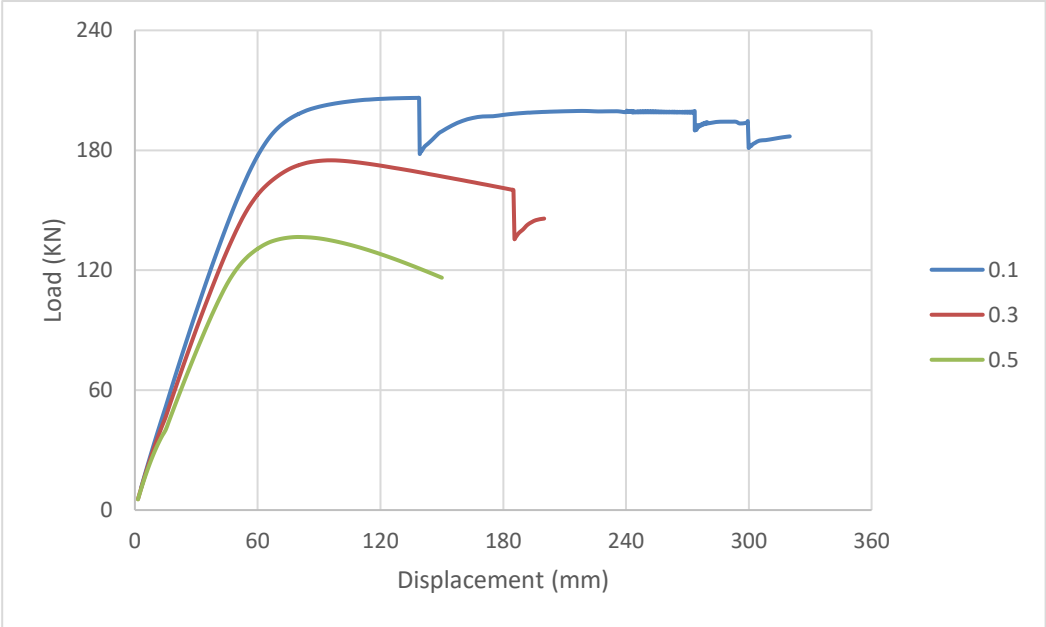

f) III.150.II

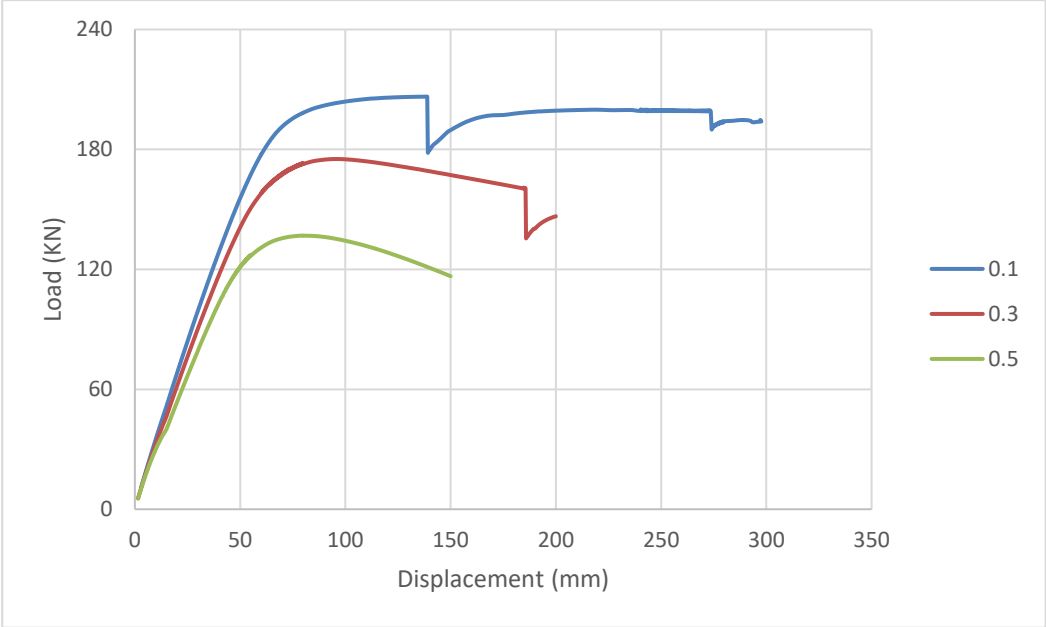

g) III.150.III

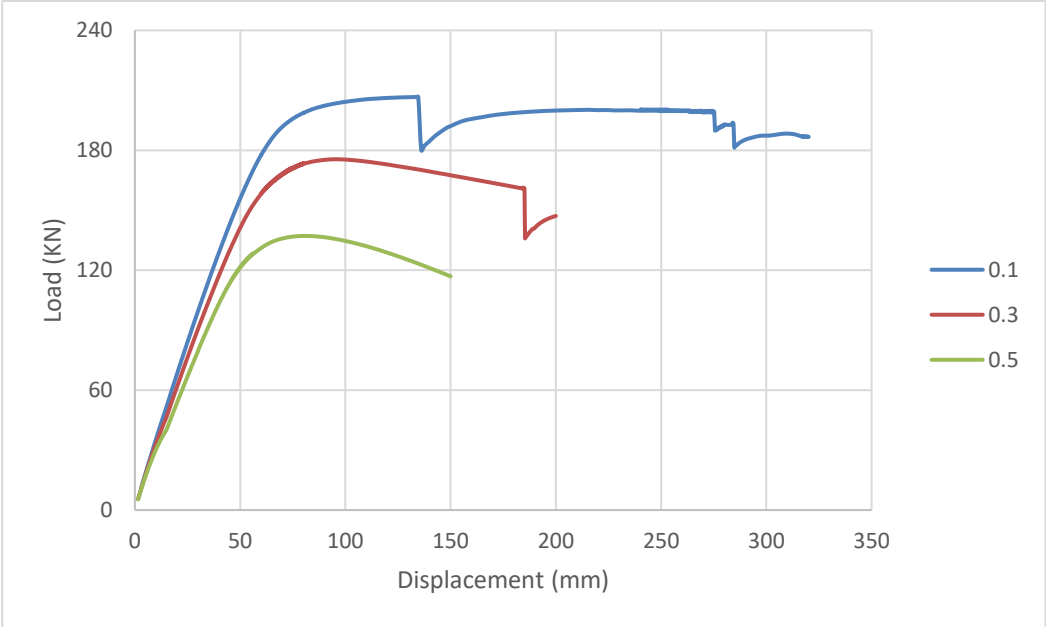

h) III.150.IV

Figure IV.4: Comparison of skeleton curves of the longitudinal and transversal bars.

IV.3.3 Dissipated energy

Energy dissipation is a relatively important parameter to evaluate the cyclic performance of a member of the structure. Dissipated energy is calculated from the lateral load-displacement curve as the area enclosed by the hysteretic hoops. The calculated results are given in Table IV.1. As shown in Figure IV.5, it can be found that the energy dissipation gradually grows up with the increase in reinforcement bars ratio. Specimens with a 0.5 axial load ratio have the poorest energy dissipation capacity. Meanwhile, the plastic work done each cycle for specimens with 4ϕ16, 8ϕ16, 4ϕ20 and 8ϕ20 is similar. The dissipated energy for specimens with 0.1 axial load ratio and 4ϕ16, 8ϕ16, 4ϕ20 and 8ϕ20 bars is near

380KN.m, 382KN.m, 382KN.m and 384KN.m respectively. Compared with the energy dissipation capacity of FEC columns with different spacing between transversal bars, it can be found that the specimens with 100mm spacing have higher energy than others.

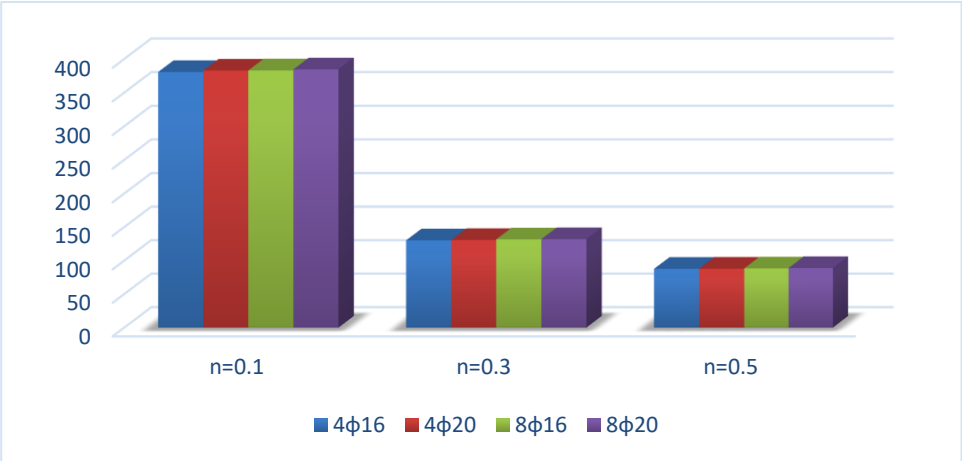

a) FEC columns with 100mm spacing

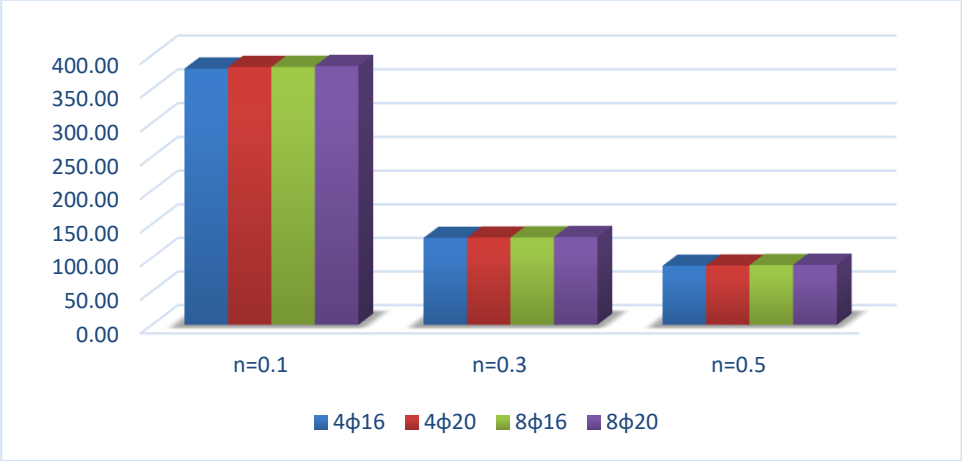

b) FEC columns with 150mm spacing

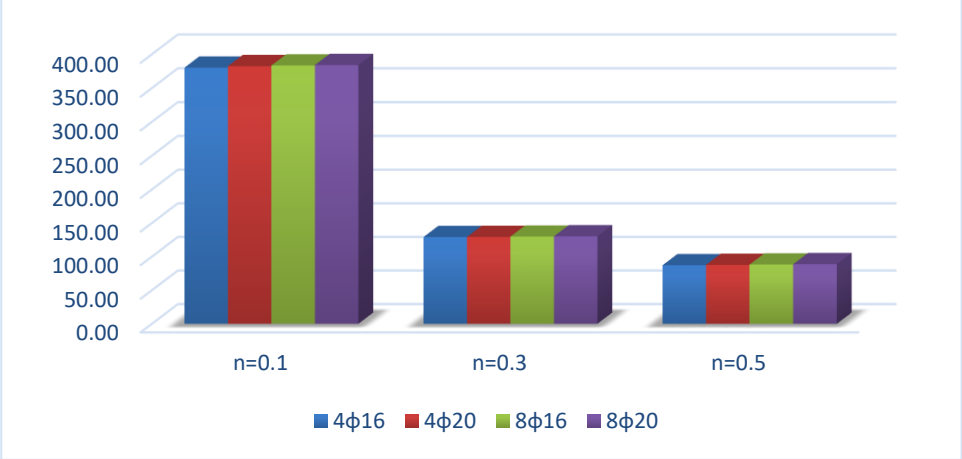

c) FEC columns with 200mm spacing

Figure IV.5: Energy dissipation of longitudinal and transversal bars effects.

IV.3.4 Ductility Factor

It is used to determine the cyclic or seismic behaviour of a structure's elements as well as their deformation capability. The ductility factor μ of a specimen is defined as the ratio of the ultimate displacement to the yield displacement $\mu=\Delta_u/\Delta_y$, Where, Δ_u is the ultimate displacement corresponding to ultimate load P_u and Δ_y is the yielding of the structural steel section displacement corresponding to yield load P_y. The calculated ductility ratio is given in Table IV.1. In order to highlight the ductility ratio of the FEC columns as compared to different transversal bars spacing specimens, a comparison between the ductility of groups was identified in Figure IV.6. It can be found that the FEC columns with 8ϕ20 have the highest ductility compared with the others FEC columns. The ductility for specimens with a 0.1 axial load ratio is near 3.8. This can be noted that the spacing between transversal bars didn't affect the ductility of the FEC columns.

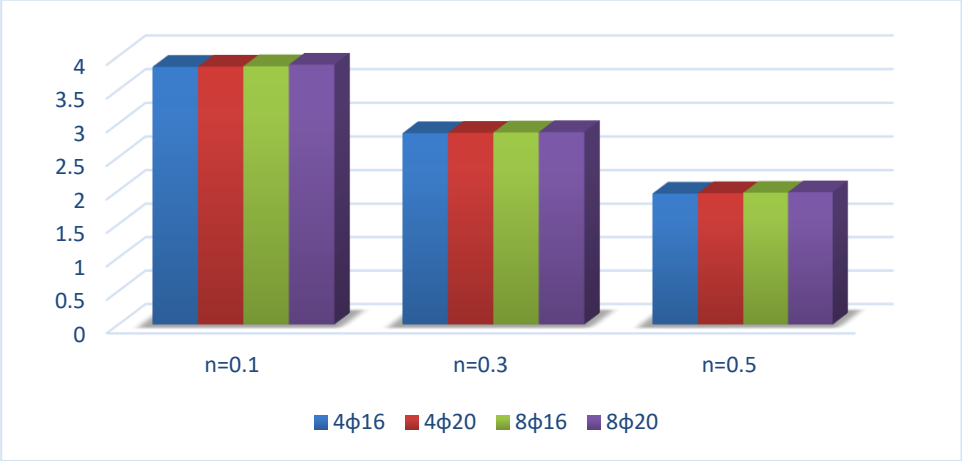

a) FEC columns with 100mm spacing

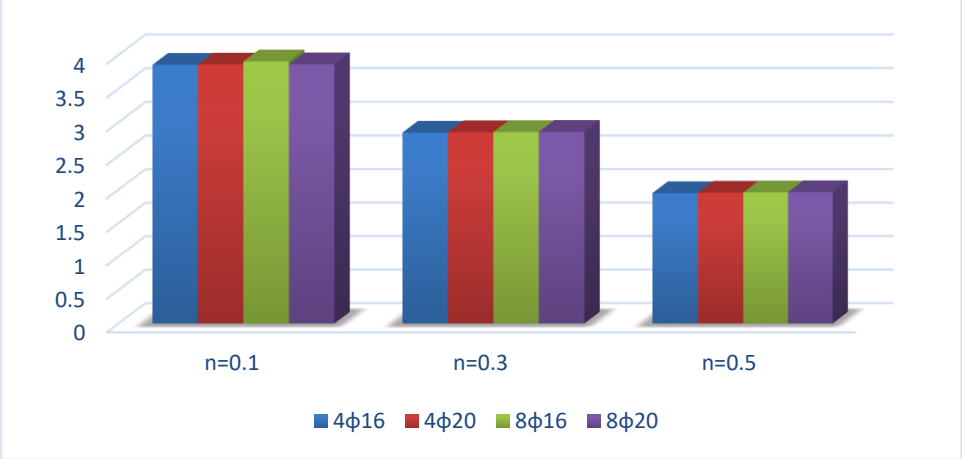

b) FEC columns with 150mm spacing

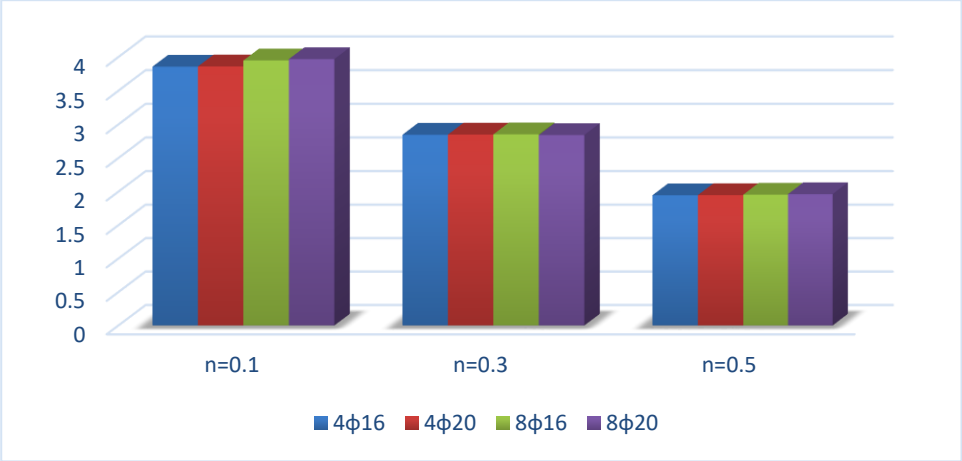

c) FEC columns with 200mm spacing

Figure IV.6:Ductility of the effect of longitudinal and transversal bars.

IV.3.5 Structural stiffness

Established by the numerical results, the main value of the rigidity of a column at the ith drift has been evaluated by the following ratio (IV.1):

$$K_i = \frac{|+P_i|+|-P_i|}{|+\Delta_i|+|-\Delta_i|} \qquad \text{(IV.1)}$$

where $+\Delta_i$ and $-\Delta_i$ are the peak displacements of the cycle at the ith lateral displacement level in two reversal directions respectively, $+P_i$ and $-P_i$ are the loads corresponding to the peak displacements respectively, [21]. As shown in Figure IV.7, Figure IV.8 and Figure IV.9, the stiffness of specimens almost remained constant before reaching the yield displacement Δ_y. This indicates that the specimens are in the elastic stage. Subsequently, the specimens experience a significant reduction in stiffness as the curves gradually go down until the failure occurs.

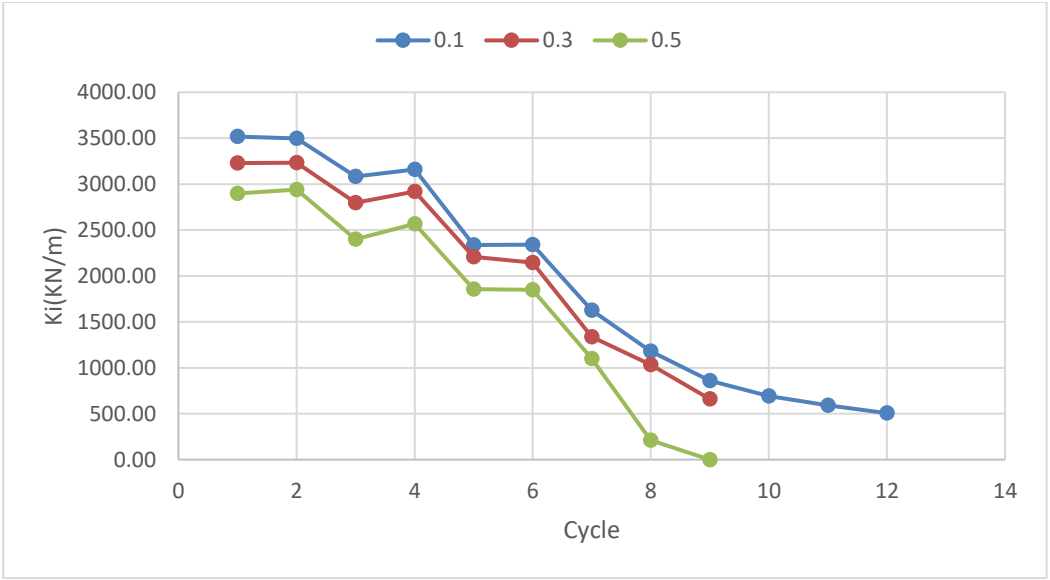

a) 4ϕ16

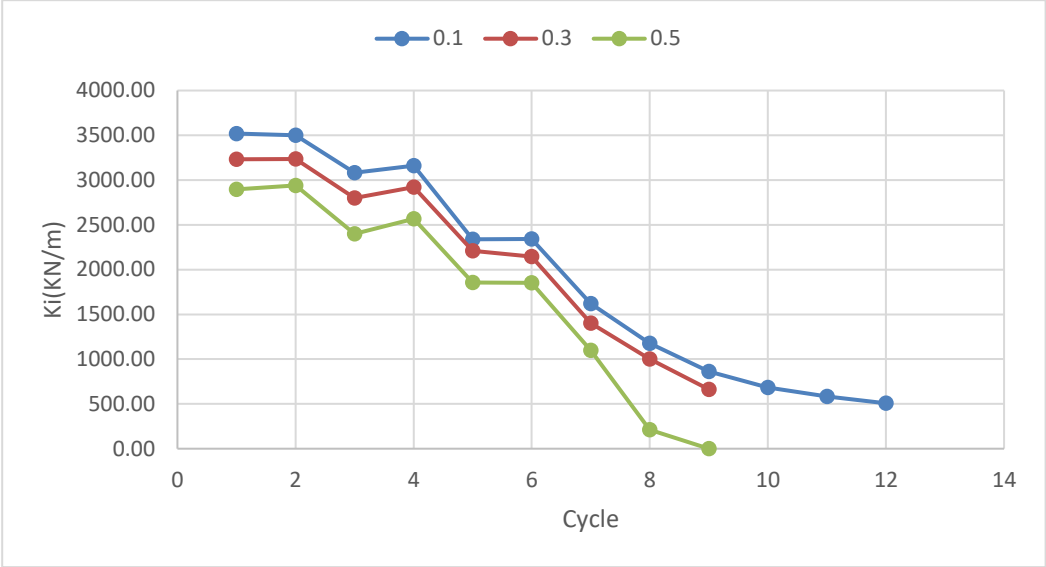

b) 4ϕ20

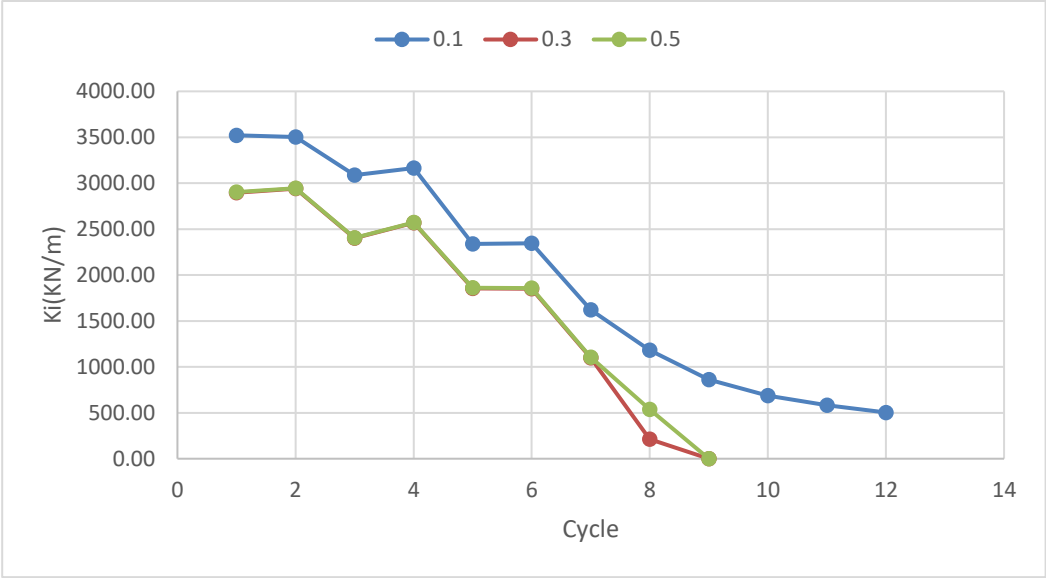

c) 8ϕ16

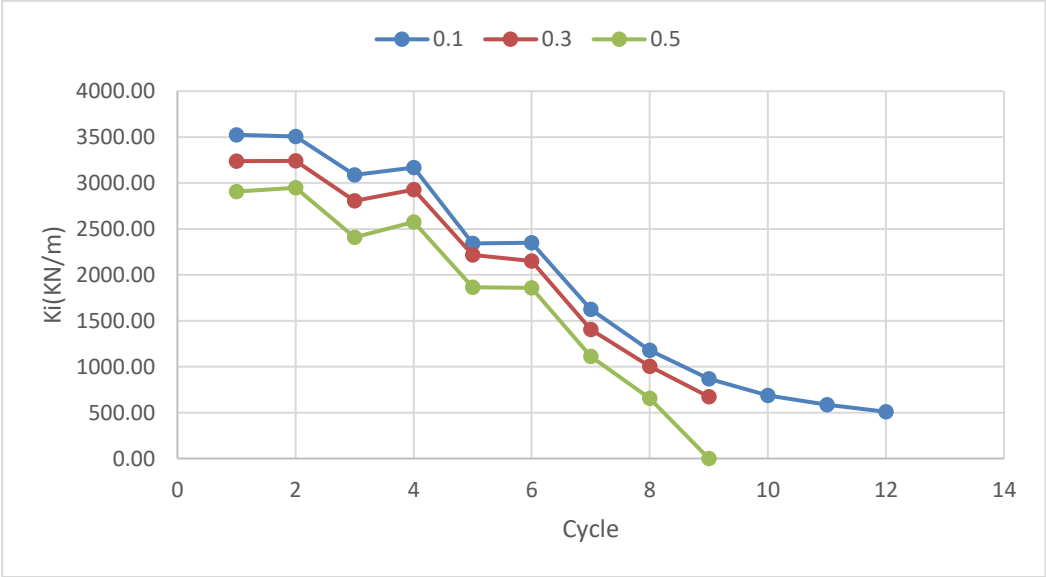

d) 8ϕ20

Figure IV.7: Structural stiffness of FEC columns with 100mm spacing.

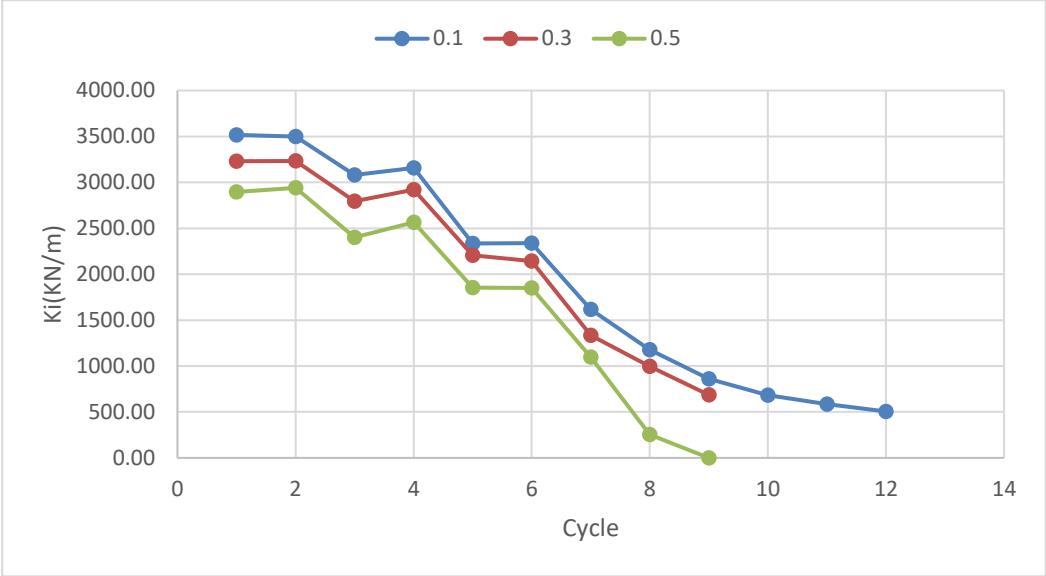

a) 4ϕ16

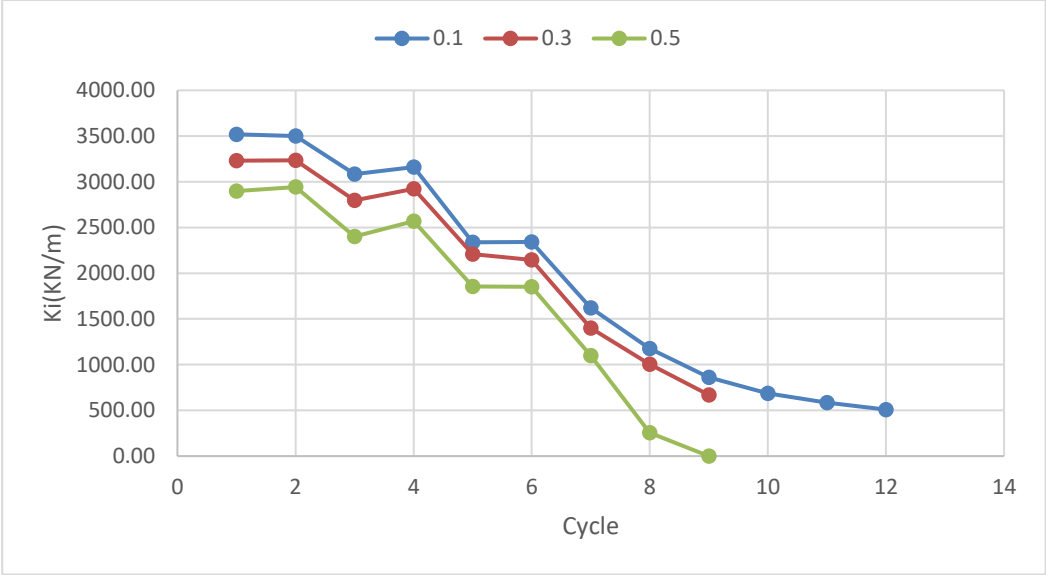

b) 4ϕ20

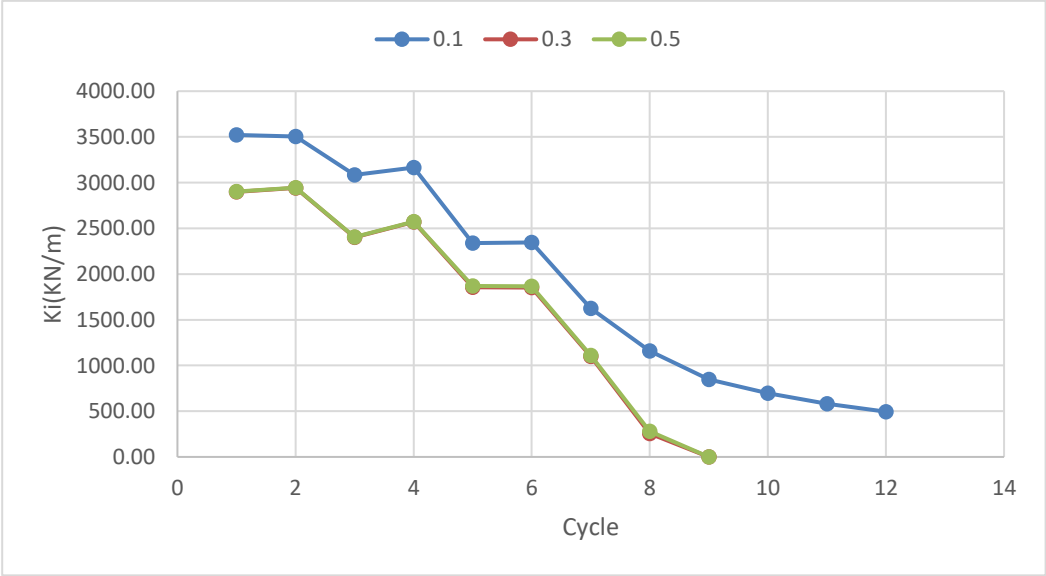

c) 8ϕ16

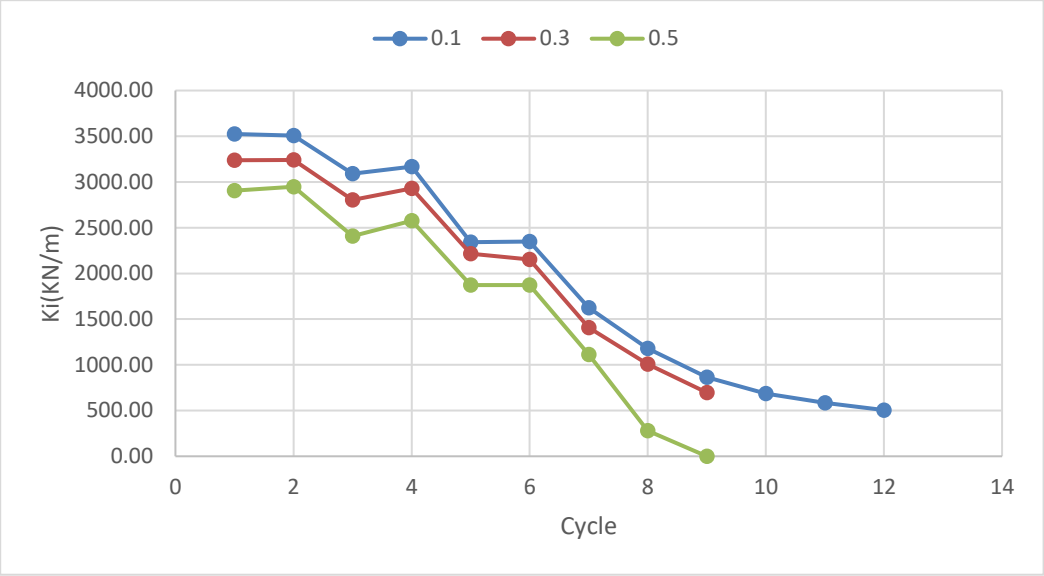

d) 8ϕ20

Figure IV.8: Structural stiffness of FEC columns with 150mm spacing.

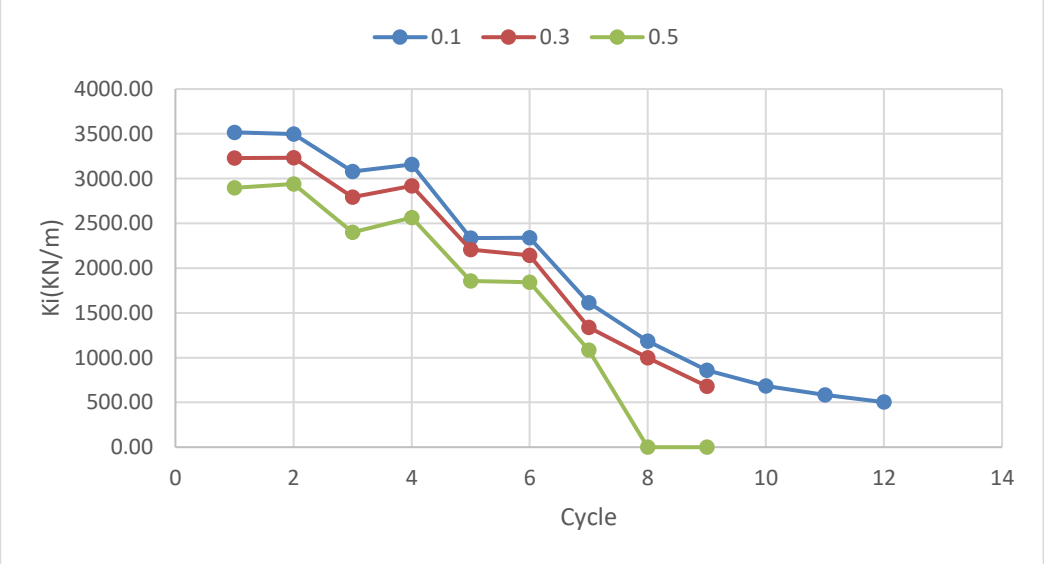

a) 4ϕ16

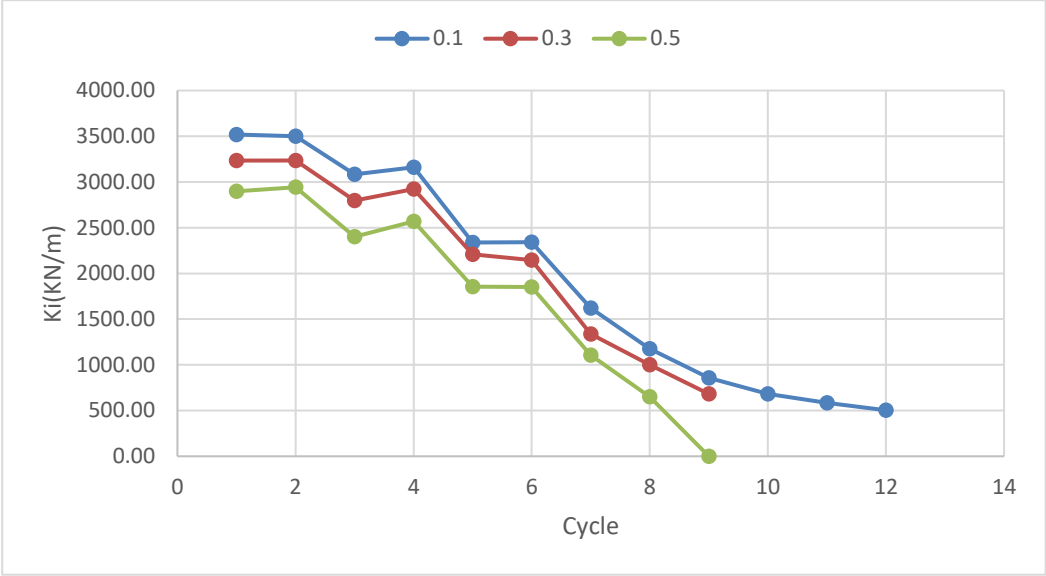

b) 4ϕ20

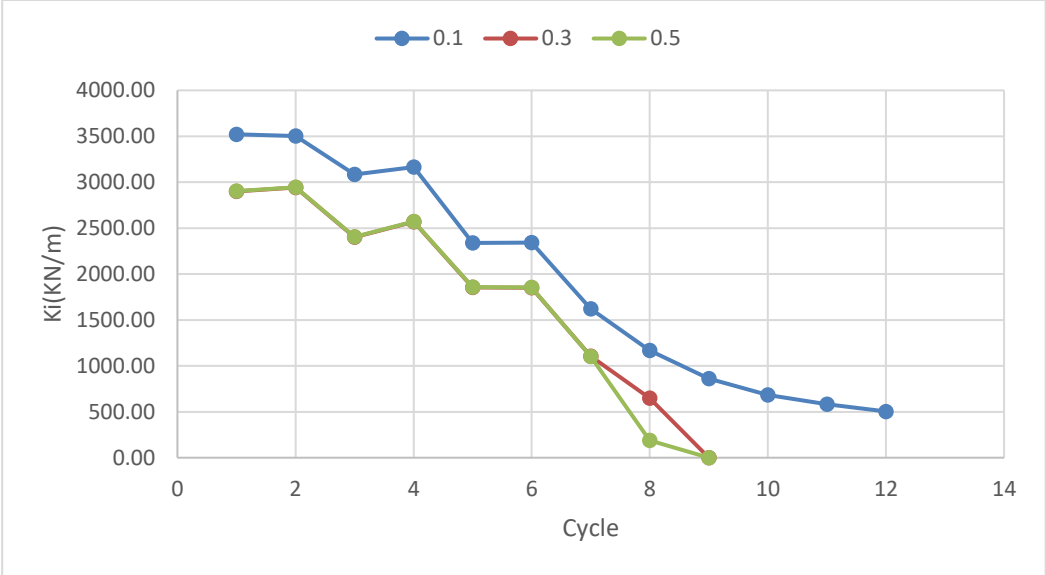

c) 8ϕ16

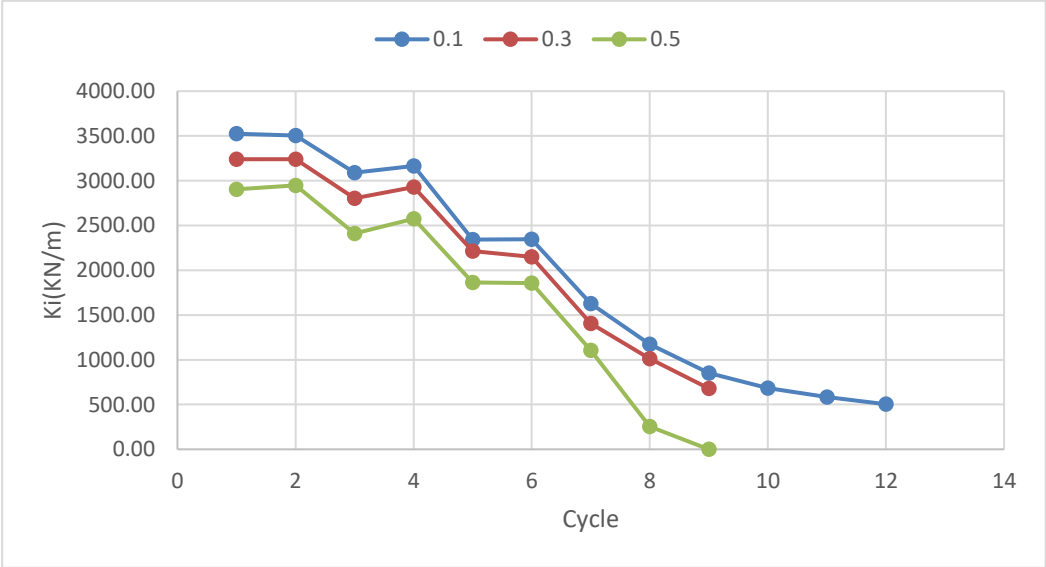

d) 8ϕ20

Figure IV.9: Structural stiffness of FEC columns with 200mm spacing.

IV.4 Conclusion

In this chapter, various parametric studies for FEC columns were investigated. The main variables parametric considered in the test program were the applied axial load ratio, longitudinal reinforming bars, and transversal reinforming bars. By comparing FEC columns with various parametric the following conclusions have been drawn:

- The longitudinal and transversal reinforcement bars have a slight effect on the FEC columns. This is because the capacity of the reinforcement bars is dominated by the load-bearing ability of the steel section.
- As the longitudinal and transversal reinforcement bars ratio increases, the FEC columns become strong and rigid.
- Spacing 100mm between transversal bars attained the highest peak load, ductility, energy dissipation, higher initial stiffness and stiffness degradation much better than the others.
- Specimens with a 0.5 ratio of axial load have the lowest peak load and initial stiffness, while the other two specimens exhibit a 10.35%-27.73% increase in peak load, 50.31%-95.92% increase in initial stiffness and 13.74%-15.62% increase in ductility.
- The axial compression ratio has a significant effect on the FEC columns.

A proposed connected reinforcement design in FEC columns is and presented in the next chapter. The numerical models were developed to provide structural designers with advanced analysis and design tools that can be used to design safe and economical composite buildings. Furthermore, the proposed numerical models allow the designer to analyse and design FEC columns made with a new type of connection between steel and concrete.

Chapter V
A PROPOSED CONNECTED REINFORCEMENT DESIGN IN FEC COLUMNS

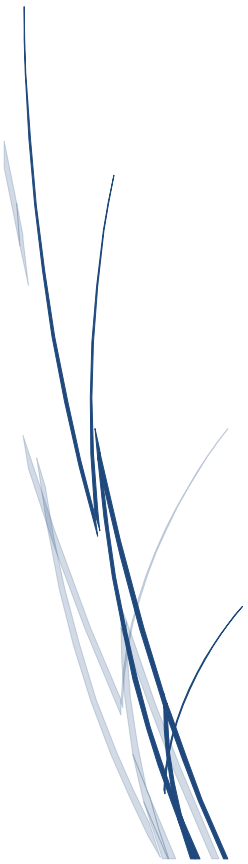

CHAPTER V
A PROPOSED CONNECTED REINFORCEMENT DESIGN IN FEC COLUMNS

V.1 Introduction

In this chapter, the development and characterisation process of the novel type of connection between steel and concrete dedicated to fully encased composite columns are described. In the scope of the performed investigation, the development process of concept, the analysis of non-mechanical shear connection means, numerical simulations and derivation of the analytical model for the resistance of connectors were done. The proposed novel solution of connection between steel and concrete interface was developed for FEC columns application and has an aim to be applicable to the regular composite columns and heavy composite column used in high-rise buildings.

V.2 Design of parametric study

Shear connectors are the most common solution to ensure the assembly of steel structures with concrete in composite structures. In this regard, this chapter proposes novel connecting designs for FEC columns. FEC column without connectors built to comparison with the proposed connection as indicated in Figure V.1(a). Headed stud shear connectors are among the most popular types of connection devices used in composite constructions. To this end, stud shear connectors were added at the steel-concrete interface to develop structures that combine the advantages of steel and reinforced concrete at the FEC columns as indicated in Figure V.1(b), the bending considered is defined with respect to the strong axis y-y. New steel-concrete connection designs are proposed in this study to increase the cyclic strength and performance of FEC columns. Figure V.1(c) shows the first proposed design which is bars welded to the steel's flange. For the second design, bars were welded to the steel's web as seen in Figure V.1 (d). Since that the manufacturing of the composite column is industrial, the aim of this work is to connect by welding the concrete reinforcement bars to the steel section to be used as shear connectors and stirrups at the same time. With bars welded to the steel's flange with the stirrup as seen in Figure V.1(e) and bars welded to the steel's flange side with the stirrup as seen in Figure V.1(f).

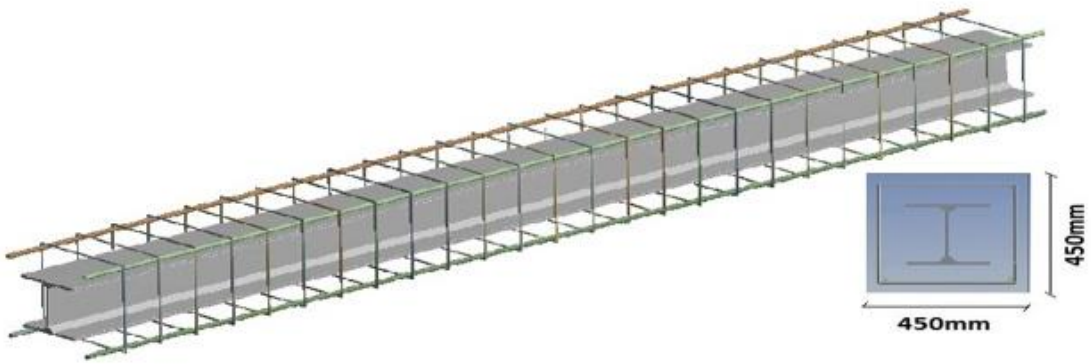

a) FEC.450x450

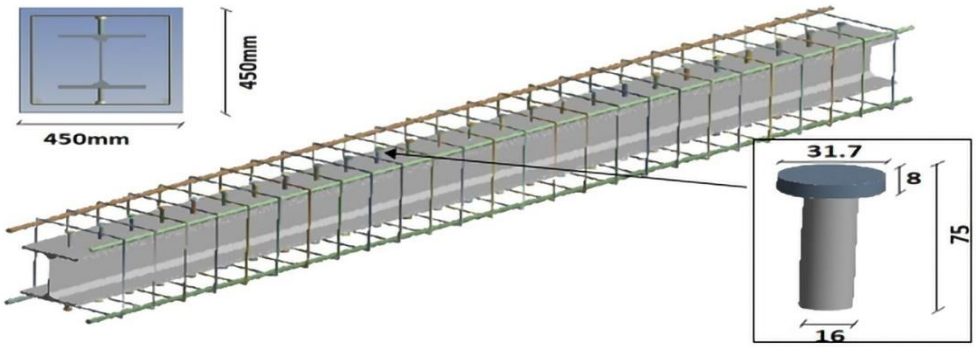

b) FEC.S.150

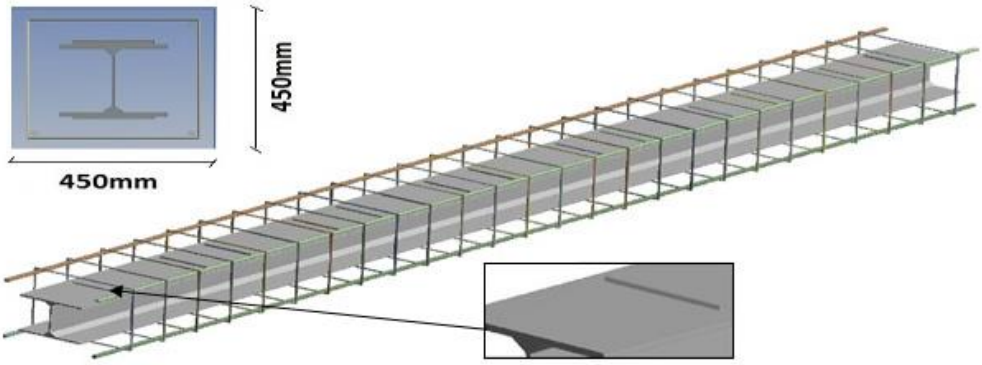

c) C1

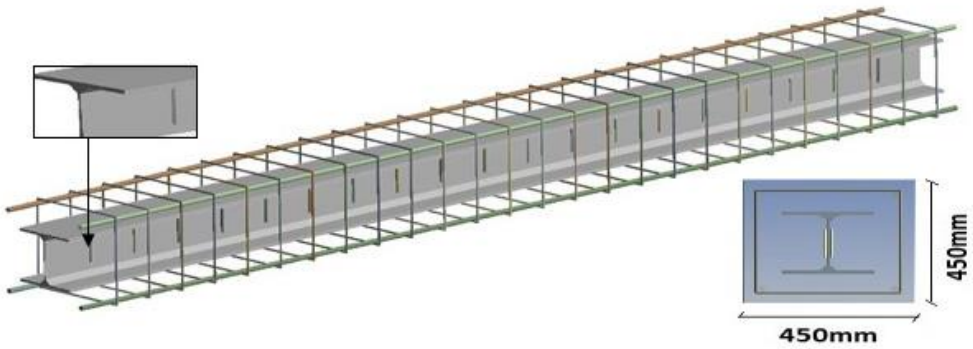

d) C2

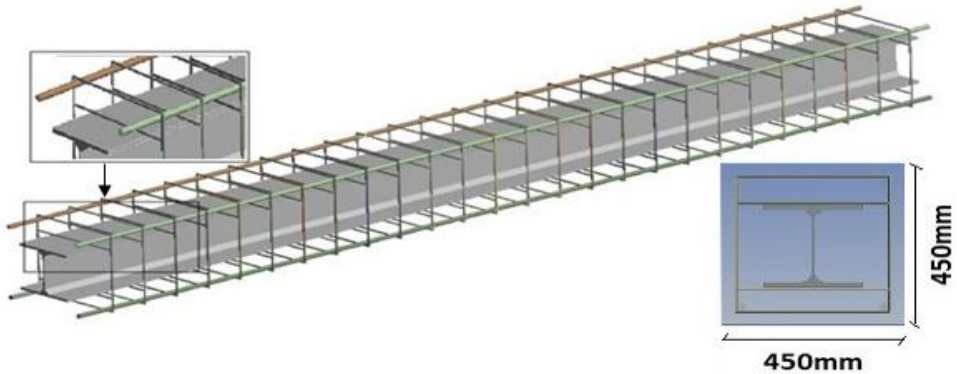

e) C3

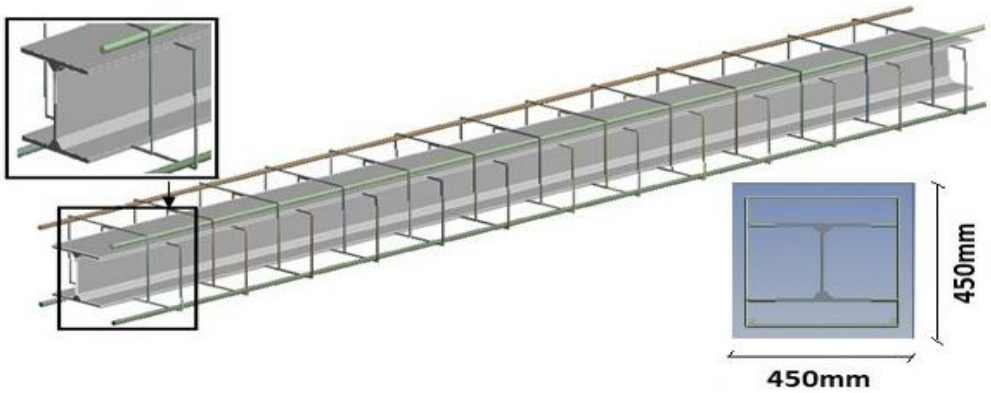

f) C4

Figure V.1: Dimensions of certain composite columns that have been proposed.

V.3Results and discussion

The cyclic response parameters of composite columns with the effect of the connexion between steel and concrete interface is shown in Table V.1. The obtained numerical results of the FEC column with proposed designs (C1, C2, C3, C4) show better results than the FEC column without connectors and the FEC column with stud connector in terms of energy dissipation, load capacity, stiffness, stiffness degradation and ductility, as described in the following section.

Table V.1: Summary of the numerical results of connection between steel and concrete.

Specimens	P_m (KN)	Δ_y (mm)	Δ_u (mm)	P_y (KN)	P_u (KN)	E (KN.m)	μ	K_y (KN/m)
FEC.450x450	198.65	64.2	200	194.24	164.34	378.45	3.12	3025.55
FEC.S.150	201.59	55	200	170.8	170.79	390.91	3.64	3105.46
FEC.C1.100	209.56	45.4	200	164.61	181.37	363.04	4.41	3625.77
FEC.C1.150	203.99	53	200	167.36	168.69	374.43	3.77	3157.74
FEC.C1.200	200.28	53.94	200	168.31	165.38	385.13	3.71	3120.32
FEC.C1.250	200.19	54.03	200	168.03	168.01	381.54	3.70	3109.94
FEC.C2.100	199.8	55.05	200	167.3	160.58	386.37	3.63	3039.06
FEC.C2.150	199.56	55.25	200	167.52	159.15	381.84	3.62	3032.04
FEC.C2.200	199.39	55	200	165.34	160.15	376.8	3.64	3006.18
FEC.C2.250	199.16	55	200	165.01	161.58	373.63	3.64	3000.18
FEC.C3.100	233.77	46.94	200	181.21	174.72	392.78	4.26	3860.46
FEC.C3.150	216.79	48	200	176.5	169.3	394.91	4.17	3677.08
FEC.C3.200	203.13	50.06	200	168.93	159.45	388.17	4.00	3374.55
FEC.C3.250	200.23	54	200	168.34	192.03	303.49	3.70	3117.41
FEC.C4.100	204.94	51.76	200	168.15	168.3	390.12	3.86	3248.65
FEC.C4.150	203.5	51.89	200	167.8	164.35	389.84	3.85	3233.76
FEC.C4.200	202.03	52.1	200	167.31	160.58	387.29	3.84	3211.32
FEC.C4.250	201.93	52.5	160	166.56	179.42	127.44	3.05	3172.57

V.3.1 Hysteresis Curves

The load-displacement hysteresis curve for a composite column with directly welded bars to structural steel for a connection with concrete subjected to cyclic loading is shown in Figure V.2. The hysteresis curves' behaviour is symmetric along the horizontal axis as illustrated in this figure. The peak loads recorded pattern for both the push and pull cycles was almost the same. The lateral load and lateral displacement are mostly linear in the elastic phase, and the loading and unloading curves are almost similar, indicating that residual deformation after unloading is negligible and the energy dissipation capacity is low. Hysteretic curves show obvious nonlinearity in the elastic-plastic stage, and the slope gradually decreases after reaching the peak load. An obvious residual deformation was noticed since the displacement could not return to its original position after unloading. The energy dissipation capacity was also gradually improved throughout the elastic-plastic stage. Table V.1 also includes the results of the peak load investigation. The usage of suggested designs in the composite column could increase the peak load of the composite column by 2.62 % in the first design, 0.46 % in the second design, and 3.07 % in the fourth design, according to an overall analysis of these hysteresis curves. Furthermore, when the bars are welded to the transversal bars in the third design, the peak load is increased by 8.37 %. It has also been shown that the length of the composite area and the strength capability have a direct relationship. The energy dissipation capacity and ductility were both improved by increasing the spacing between the welded bars. Nevertheless, all specimens with the exception of FEC.C3.250, which failed in the 11th cycle and FEC.C4.250, which failed in the 8th cycle due to the steel section connection being disconnected, resisted the whole cyclic applied.

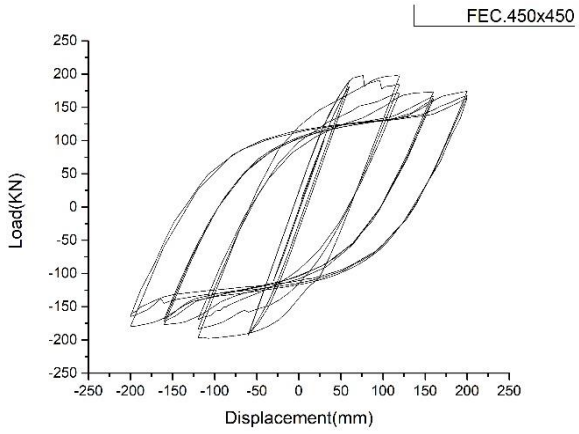

a) FEC.450x450

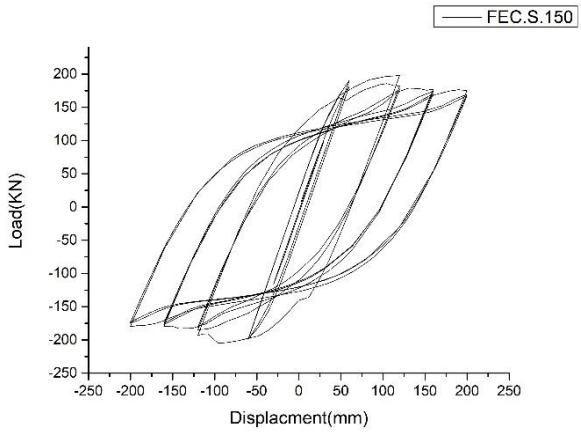

b) FEC.S.150

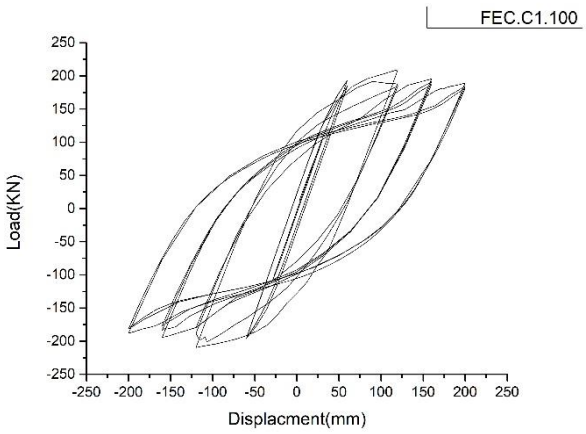

c) FEC.C1.100

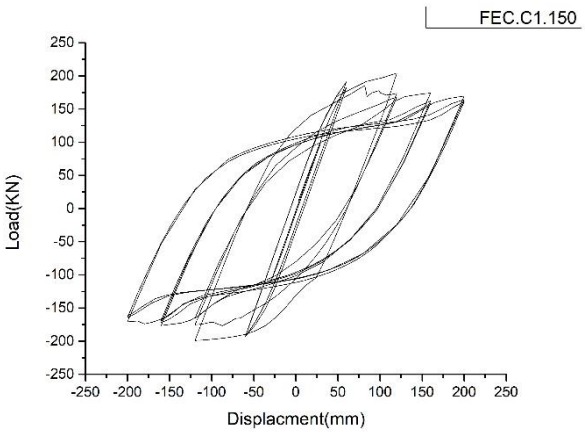

d) FEC.C1.150

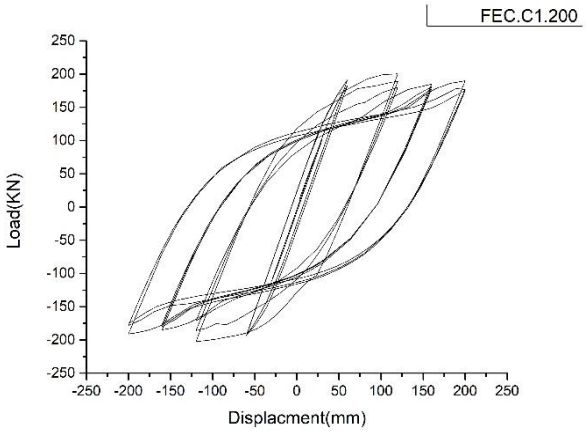

e) FEC.C1.200

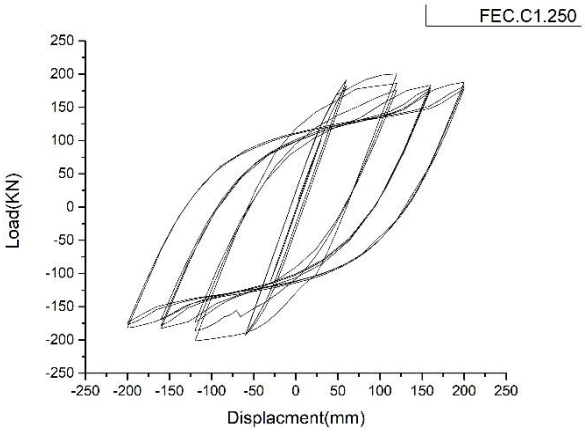

f) FEC.C1.250

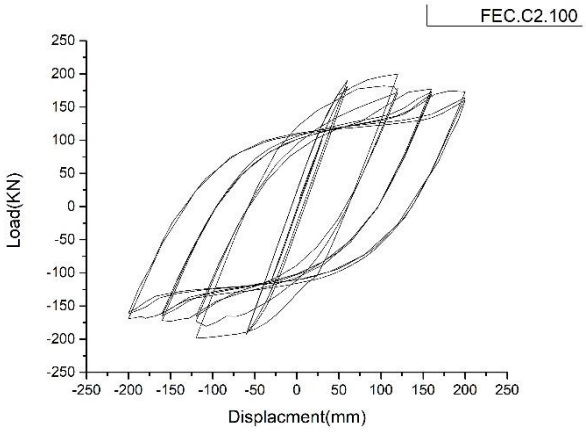

g) FEC.C2.100

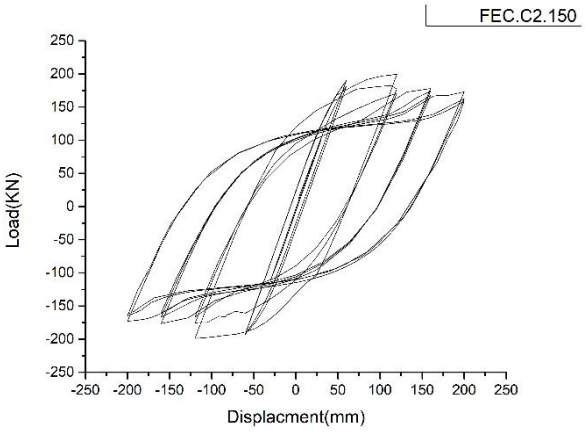

h) FEC.C2.150

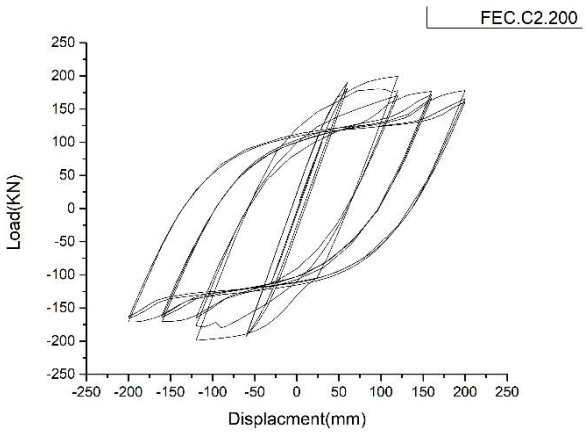

i) FEC.C2.200

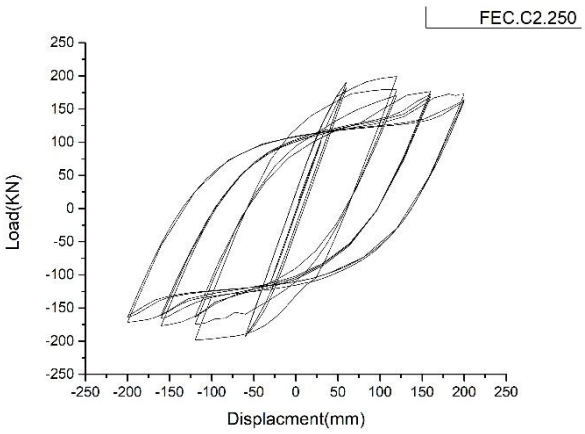

j) FEC.C2.250

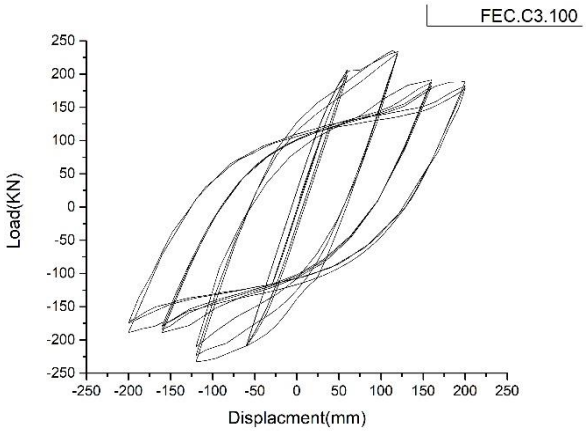

k) FEC.C3.100

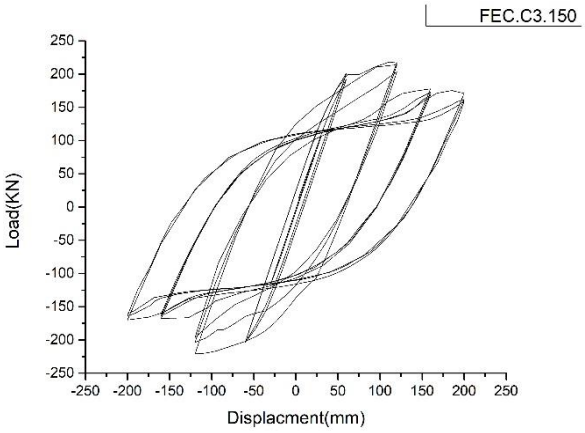

l) FEC.C3.150

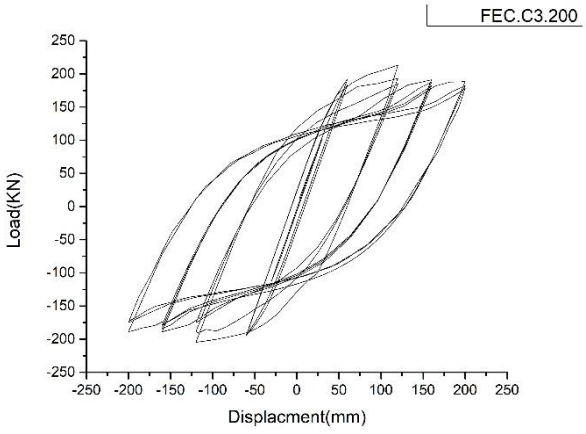

m) FEC.C3.200

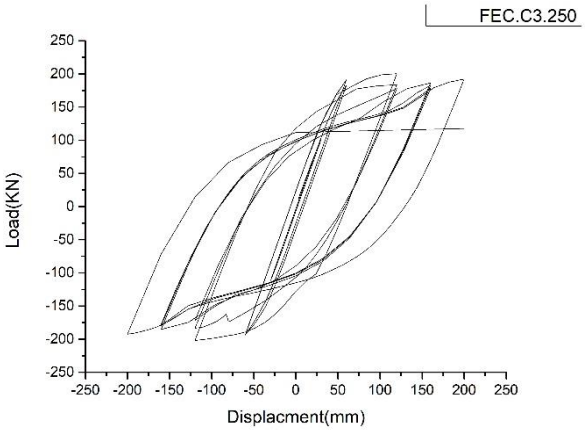

n) FEC.C3.250

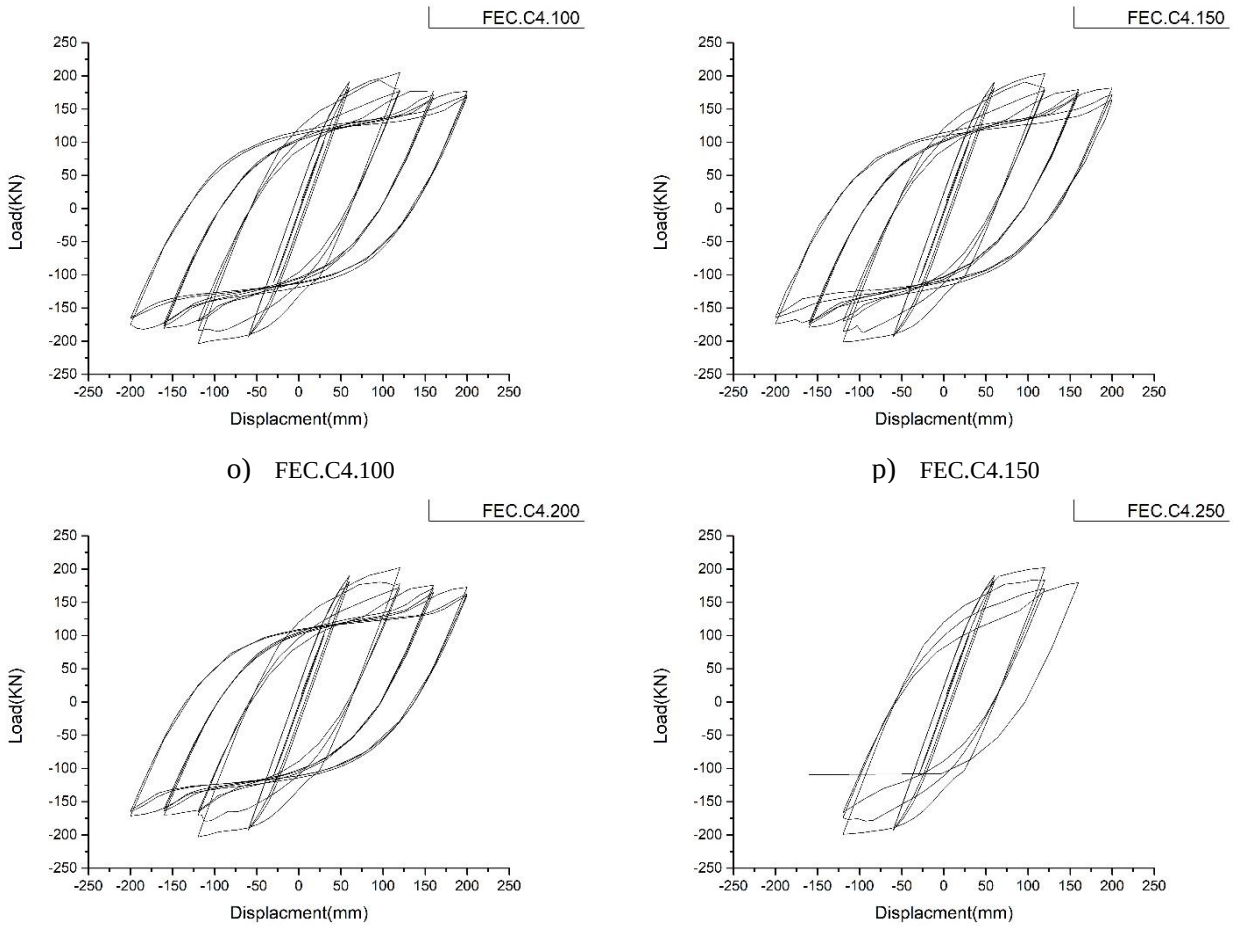

o) FEC.C4.100 p) FEC.C4.150

q) FEC.C4.200 r) FEC.C4.250

Figure V.2: Hysteresis curves of the effect of connectors

V.3.2 Skeleton Curves

To compare models, envelope curves were constructed by connecting the peak point's lateral load and the corresponding horizontal displacement from the first cycle of each loading level, as shown in Figure V.3. The peak load P_m and the initial stiffness K_y of each specimen were listed in Table V.1. These envelope curves illustrate that these specimens experienced elastic and elastic-plastic stages. In the elastic stage, the relation between horizontal load and displacement is almost linear, but the slope of these curves is different from each other. As the horizontal displacement continued to increase, the specimens entered the elastic-plastic stage, which shows obvious nonlinear behaviour. For the specimens FEC.C2.100-250 and FEC.C4.100-250, the lateral load changes slightly with the increase of the displacement after yielding load, which shows good deformation capacity. As expected, the envelope curves of specimens FEC.C2.100-250 has the lowest peak load and both initial stiffness and ductility. It can be found that the improvement in this design does not significantly affect the peak load. This is because the capacity of the connection is dominated by the load-bearing ability of the column. However, the lateral load decreases abruptly after yielding load for specimen FEC.C1.150 and FEC.C3.150. For test specimen FEC.C3.250 and FEC.C4.250, it experienced a small elastic-plastic stage, which shows a

significant reduction in deformation capacity. By comparing specimens with different spacing between the welded bars, it can be observed that the influence of increasing spacing between welded bars for type C1 significantly reduced both initial stiffness and ductility by 21.91% and 14.32% respectively, also for type C3 by 8.32% and 4.08%. In contrast, it decreased slightly for C2 on both initial stiffness and ductility by 0.85% and 0.45% respectively, also for type C4 by 1.21% and 0.40%.

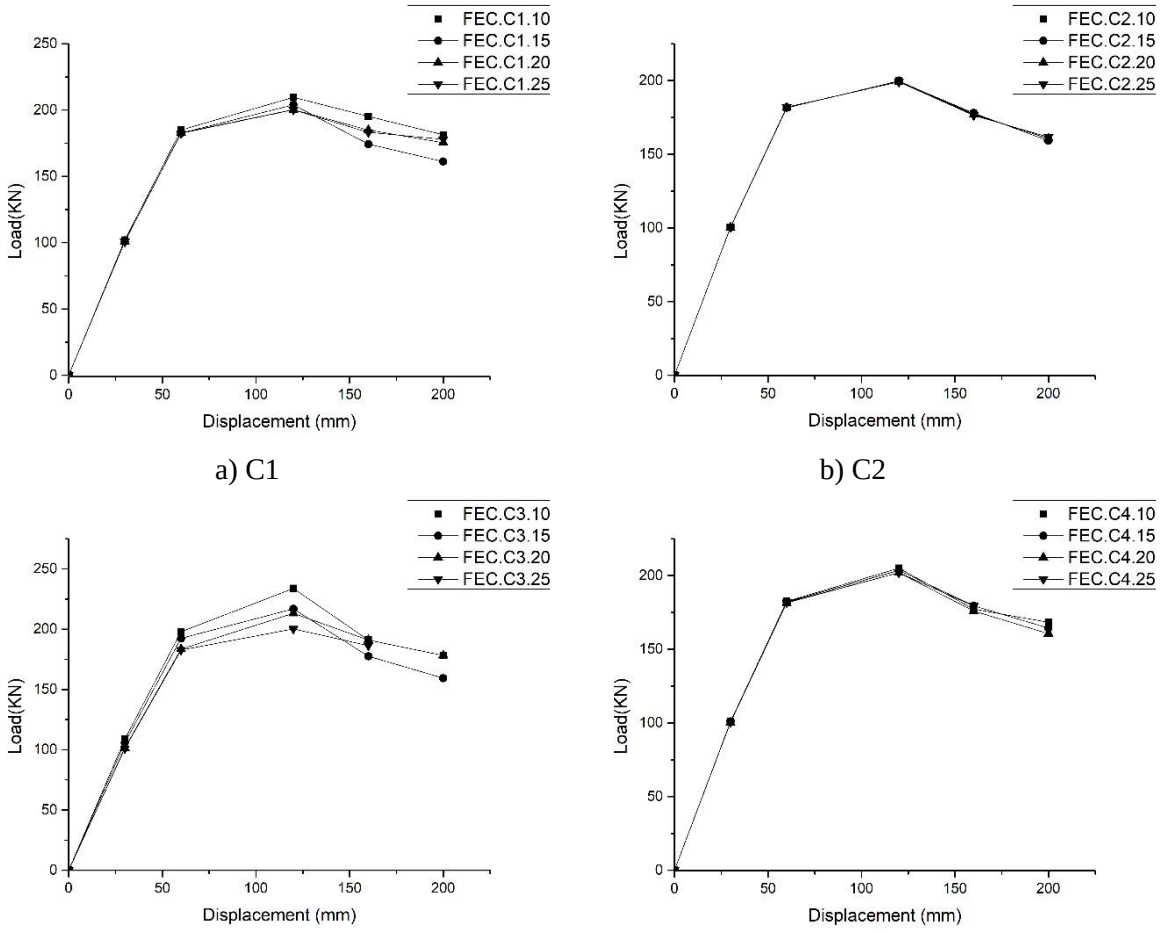

Figure V.3: Load-displacement envelope curves for the effect of connectors.

V.3.3 Dissipated energy

The calculated results are given in Table V.1. A comparison between energy dissipation of different designs specimens is presented in Figure V.4. As shown in this figure, the energy dissipation in C2, C3 and C4 grows up with the decrease in the spacing of the welded bars. In contrast, in C1 the energy dissipation grows up with the increase in the spacing of the welded bars. Therefore, the dissipated energy is noticeably smaller than that of other specimens. Meanwhile, the plastic work done each cycle for specimens FEC.C2.100-250, FEC.C3.100-200 and FEC.C4.100-200 is similar. Since the ductility of C3 and C4 is greater than C2, the former two designs have higher dissipated energy. As shown in Figure V.4, it can be demonstrated that the energy dissipation capacity of the connection to the FEC column is improved by 0.89%, 4.17%, and 2.92% for C2, C3, and C4 respectively and deteriorated by 1.07% for the C1.

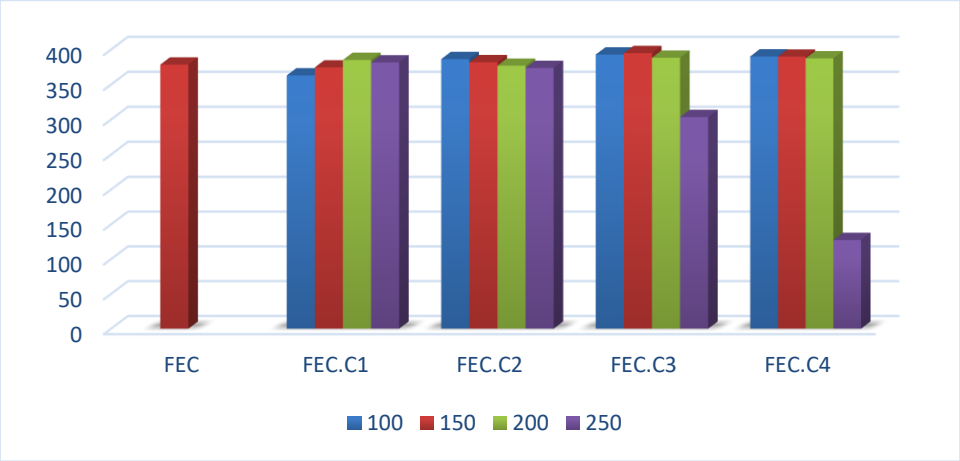

Figure V.4: Energy dissipation comparison between (i) FEC.C1, (ii) FEC.C2, (iii) FEC.C3, and (iv) FEC.C4.

V.3.4 Ductility Factor

The ductility ratio for all models indicated in this study is given in Table V.1. The results show that the ductility ratio is increased by decreasing the spacing between the welded bars. Specimens FEC.C1.100 and FEC.C3.100 have higher ductility than the other specimens. The specimens FEC.C2.100-250 have the smallest ductility and are almost the same, which indicates that in this type of design, the yielding of the column did not affect by the spacing between the welded bars. However, the corresponding yielding displacement is greatly influenced by the spacing between the welded bars and the design of the connection. Moreover, the comparison among all presented specimens in this effect is indicated in Figure V.5 shows that the ductility increased by 17.24%, 13.81%, 25.18% and 18.96% for C1, C2, C3, and C4 respectively.

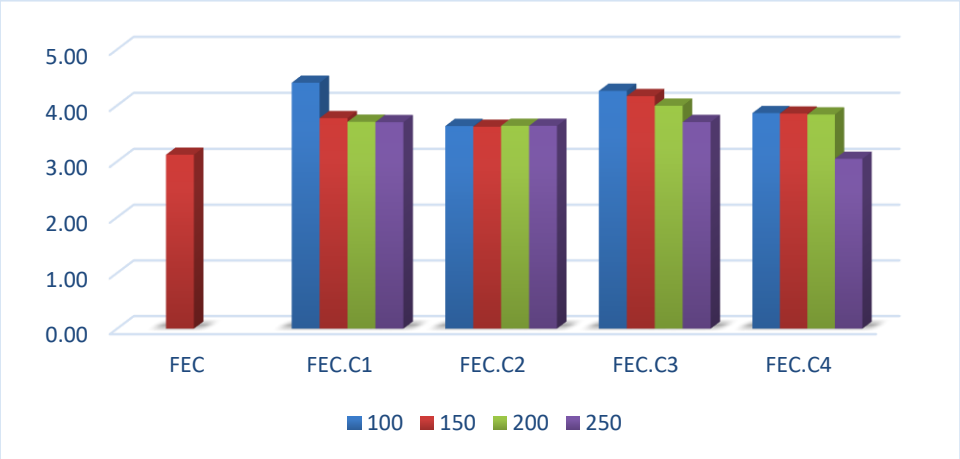

Figure V.5: Ductility comparison between (i) FEC.C1, (ii) FEC.C2, (iii) FEC.C3, and (iv) FEC.C4.

V.3.5 Structural stiffness

The stiffness degraded almost symmetrically in a positive and negative direction during the cyclic loading process. Figure V.6 shows a comparison between stiffness degradation of different designs and different spacing between the welded bars. The stiffness deteriorated significantly after the 4th cycle. It can be found that the initial stiffness of specimens increases by decreasing of spacing between the welded bars. The comparison results show that the stiffness has degraded by 47.34%, 48.02%, 45.43% and 47.59%, for C1, C2, C3 and C4, respectively. It can be concluded that the C3 specimens exhibited significantly higher initial stiffness and stiffness degradation much better than the other types of designs. The spacing between the welded bars has a significant influence on the stiffness degradation by 2.87%, 0.14%, 5.78% and 0.38%, for the C1, C2, C3 and C4, respectively.

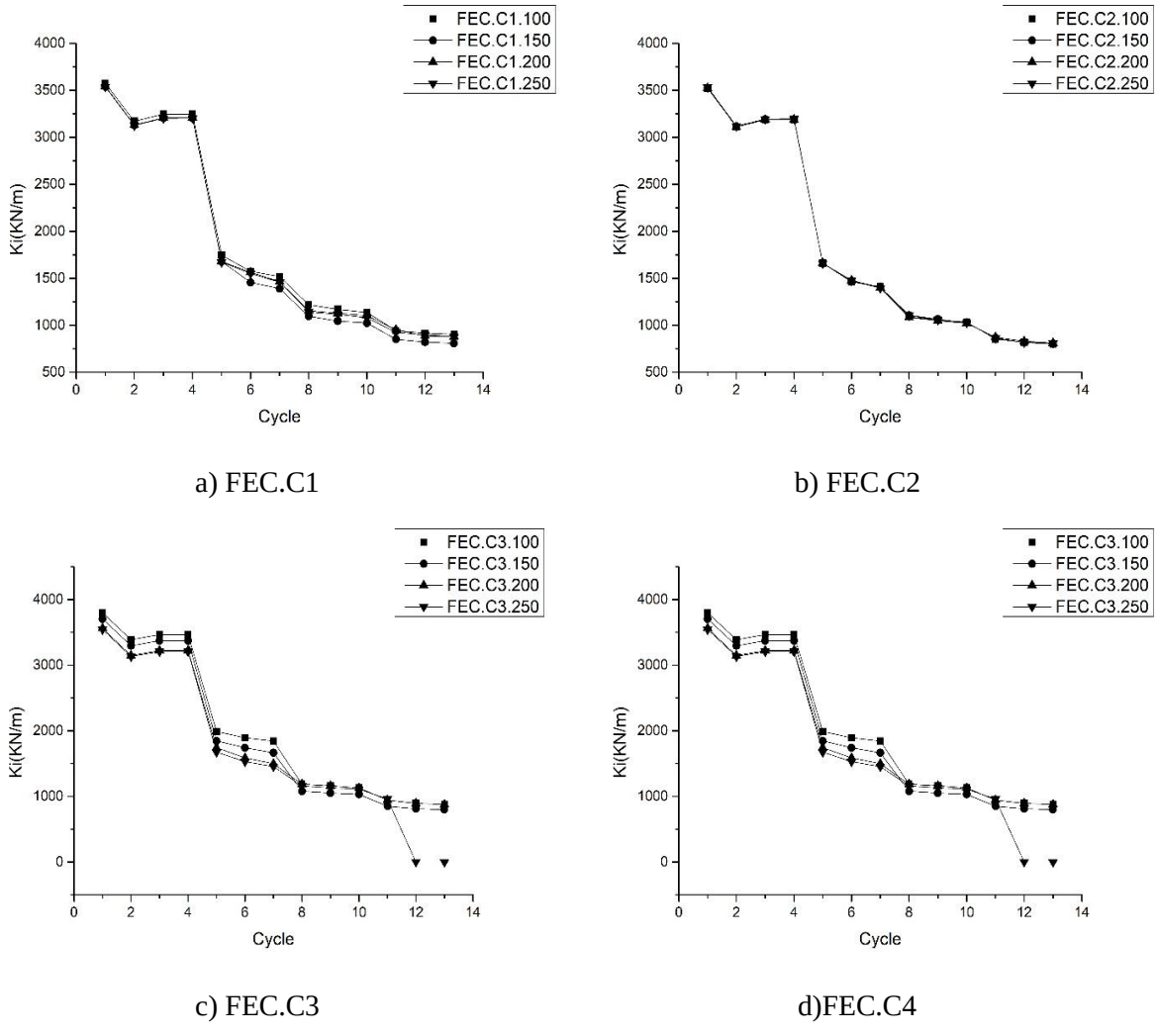

a) FEC.C1 b) FEC.C2

c) FEC.C3 d)FEC.C4

Figure V.6: Stiffness degradation curves of the effect of the connectors.

V.4 Comparison of FEC with stud and with proposed designs

To evaluate the numerical results and highlight the efficiency of the proposed designs, the proposed designs (C1, C2, C3, C4) were compared. This comparison was divided into two parts. In the first part

of the work, the effects of the different proposed designs were compared with FEC without connectors and effects of different bars welded spacing as described in the previous sections. In the second part of the work, a comparison between FEC with proposed designs and with stud connector was compared in terms of:

- Load capacity increased by 1.18%, 7.01% and 0.94% for C1, C3, C4 respectively and decreased by 1.02% for C2.
- Ductility improved by 3.64%, 12.73%, 5.65% for C1, C3, C4 respectively and reduced by 0.45% for C2.
- Energy dissipation decreased by 4.40%, 2.37%, 0.27% for C1, C2, C4 respectively and increased by 1.01% for C3.
- Stiffness initial improved by 1.66%, 15.55%, 3.97% for C1, C3, C4 respectively and reduced by 2.42% for C2.

V.5 Conclusion

In this chapter, novel connecting designs for FEC columns is proposed. Four different types of concrete-steel connections have been suggested and investigated: (i)C1 Bars are welded to the steel's flange, (ii)C2 Bars are welded to the steel's web, (iii)C3 Bars are welded to the steel's flange and the stirrup, and (iv) C4 Bars are welded to the steel's flange side and the stirrup. On structural steel, the aforementioned designs are easier to design, manufacture and install. At the same time, C3 and C4 utilize as connections and stirrups. By comparing FEC columns with and without shear connectors, a series of tests were employed to understand the behaviour of the suggested designs under cyclic loads. Besides, the FEC columns welded with the concrete reinforcement bars to the steel section, considering their position at a different spacing in the structural steel were compared. In addition, a comparison between FEC with studs and with proposed designs was also considered. As a result of this investigation, the following conclusions have been drawn:

- Using the proposed designs, load capacity, energy dissipation capacity, ductility, and initial stiffness were all improved when compared to FEC columns without connectors.
- All specimens resisted the whole cyclic applied except FEC.C3.250 failed in the 11th cycle and FEC.C4.250 failed in the 8^{th} cycle due to disconnecting the welded bars of the structural steel section, which shows a significant reduction in deformation capacity.
- The plastic work done for specimens in type C2 and in type C4 is similar. About the fact that the ductility of specimens C1, C3 and C4 is greater than that of specimen C2, the former three series have higher dissipation energy.

- The lateral load changes slightly with increasing displacement after yielding load for specimens C2 and C4, indicating good deformation capacity. Specimen C2 had the lowest peak load, ductility, and initial stiffness, as expected. It can be found that the amelioration in this design does not significantly affect the peak load. Because the capacity of the connection determines the column's load-bearing capabilities. Because the load-bearing ability of the column is dominated by the capacity of the connection.

- The yielding displacement is exceedingly influenced by the decrease of spacing between the welded bars.

- The type C2 has the smallest ductility and is almost the same, which indicates that in this type of connection, the yielding of the column did not affect by the spacing between the welded bars.

- By comparing all the models, C3 attained the highest peak load, energy dissipation capacity, ductility, stiffness degradation and higher initial stiffness much better than the others. Thus, this type will be a sufficient and efficient design of connection to use in the FEC column.

- C3 and C4 designs are interesting designs of connection between steel and concrete due to their ability to use as connectors and stirrups at the same time.

According to the findings of this study, it was observed in C3 and C4 designed specimens that the welding of the bars with the steel column provides a good steel-concrete connection and therefore a better behaviour of the FEC columns subjected to cyclic loading. This new concept of FEC columns such as C3 and C4 specimens can be quite efficient in construction elements with respect to cyclic and also seismic loads.

GENERAL CONCLUSION

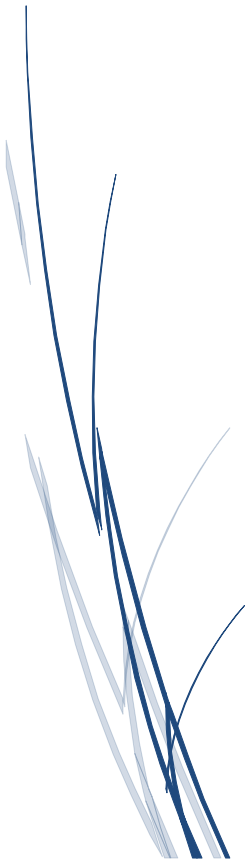

GENERAL CONCLUSION

This thesis presents extensive numerical simulation studies of the cyclic behaviour of FEC columns. The primary aim of the research is to improve knowledge and understanding of the cyclic performance of FEC columns and provide guidance for the design of cyclic resistance in FEC columns.

Prior to studying FEC columns, an investigation was conducted into the FEC columns by comparing experimental tests and finite element modelling to validate the accuracy of the numerical modelling. The investigation was a preparation for the further study of FEC columns subjected to cyclic loading and aimed to understand how cyclic loads affect the performance of FEC columns. Then, a series of cyclic tests were carried out for FEC columns. A total of seventy-five columns were prepared for cyclic tests. The observed results from the numerical tests were used to investigate the cyclic behaviour and the effects of several factors (cover concrete, coefficient of friction, axial load ratio, concrete reinforcement bars and boundary of condition) on the resistance performance of FEC columns. In addition, methods to improve the connection between steel and concrete performance were proposed and examined in order to comprehensively study the cyclic behaviour of FEC columns.

Some conclusions which can be drawn from the outcomes of the current research are summarized as follows:

- With an increase of the cover concrete, the displacement ductility, the energy dissipation and the stiffness increase by 11.71%, 18.93% and 50.52% receptively compared with specimen I.1. With an increase of the concrete cover, the ductility and the energy dissipation of a specimen tends to increase until it reaches 70 mm (c/h=0.0175). However, when the cover concrete is so large reaches 80mm (c/h=0.02) in the analysed specimens, the displacement ductility and the energy dissipation decrease by 27.33%, 24.97% receptively, and the stiffness decreases seriously due to the absence of the reinforcement bars in cover concrete.

- After the load reaches the ultimate load, the hysteretic curves of the columns are plumped and affected by the spalling of cover concrete. Specimens (I.1-I.7) exhibit good ductility, energy dissipation capacity and good rigidity, counter to specimen I.8 that failed to complete the test, it reached the failure mode at the end of the 10th cycle because the concrete cover is too high and the outer concrete is without reinforcement.

- With an increase of the coefficient of friction between steel and concrete, the ductility, the energy dissipation and the stiffness increase by 12.62%, 7.82% and 7.11% receptively. However, when the coefficient of friction reaches 0.6, it gives a better energy dissipation. It proves that the columns with a 0.6 coefficient of friction exhibit favourable cyclic behaviour.

- The coefficient of friction has an important effect on the cyclic behaviour of composite columns. The cyclic behaviour worsens when the coefficient of friction is decreased and it improves when

the coefficient is increased, especially under 0.6.

- The longitudinal and transversal reinforcement bars have a slight effect on the FEC columns. This is because the capacity of the reinforcement bars is dominated by the load-bearing ability of the steel section.
- As the longitudinal and transversal reinforcement bars ratio increases, the FEC columns become strong and rigid.
- Spacing 100mm between transversal bars attained the highest peak load, ductility, energy dissipation, higher initial stiffness and stiffness degradation much better than the others.
- Specimens with a 0.5 ratio of axial load have the lowest peak load and initial stiffness, while the other two specimens exhibit a 10.35%-27.73% increase in peak load, 50.31%-95.92% increase in initial stiffness and 13.74%-15.62% increase in ductility.
- The axial compression ratio has a significant effect on the FEC columns.
- Stiffness degradation showed similar responses with different boundary conditions.
- The boundary condition has a significant effect on the FEC columns, boundary condition (fixed-free) has the highest peak load, ductility, energy dissipation and higher initial stiffness much better than fixed-fixed.
- Using the proposed designs, load capacity, energy dissipation capacity, ductility, and initial stiffness were all improved when compared to FEC columns without connectors.
- All specimens resisted the whole cyclic applied except FEC.C3.250 failed in the 11th cycle and FEC.C4.250 failed in the 8^{th} cycle due to disconnecting the welded bars of the structural steel section, which shows a significant reduction in deformation capacity.
- The plastic work done for specimens in type C2 and in type C4 is similar. About the fact that the ductility of specimens C1, C3 and C4 is greater than that of specimen C2, the former three series have higher dissipation energy.
- The lateral load changes slightly with increasing displacement after yielding load for specimens C2 and C4, indicating good deformation capacity. Specimen C2 had the lowest peak load, ductility, and initial stiffness, as expected. It can be found that the amelioration in this design does not significantly affect the peak load. Because the capacity of the connection determines the column's load-bearing capabilities. Because the load-bearing ability of the column is dominated by the capacity of the connection.

- The yielding displacement is exceedingly influenced by the decrease of spacing between the welded bars.
- The type C2 has the smallest ductility and is almost the same, which indicates that in this type of connection, the yielding of the column did not affect by the spacing between the welded bars.
- By comparing all the models, C3 attained the highest peak load, energy dissipation capacity, ductility, stiffness degradation and higher initial stiffness much better than the others. Thus, this type will be a sufficient and efficient design of connection to use in the FEC column.

According to the findings of this study, it was observed that the cover concrete 70 mm (c/h=0.0175) have the highest cyclic peak load, ductility, energy dissipation initial stiffness and less stiffness degradation compared with the other cover concrete ratio. The studying of the coefficient of friction proves that the columns with a 0.6 coefficient of friction exhibit favourable cyclic behaviour. C3 and C4 designs are interesting designs of connection between steel and concrete due to their ability to use as connectors and stirrups at the same time. There is consideration to combine steel profile and reinforcement bars in an industrial concept.

BIBLIOGRAPHY

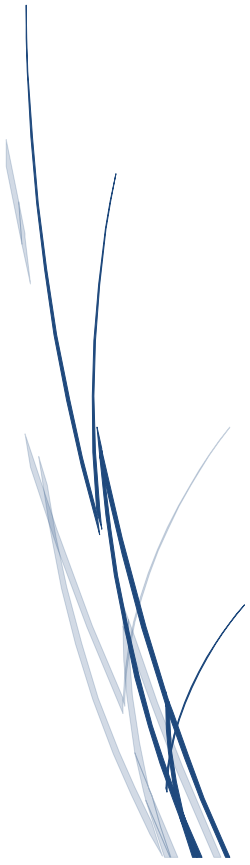

BIBLIOGRAPHY

[1] M. Aribert, C. Campiane, and V. Pacurar, "Monotonic and cyclic behavior of fully encased Composite columns and dissipative interpretation for seismic design," *Swets&Zeitlinger B.V., Lise. Netherlands, Proc. STESSA 2003*, pp. 115–122, 2003.

[2] Eurocode 4, *Design of composite steel and concrete structures Part 1-1 General rules and rules for buildings EN 1994-1-1*. 2004.

[3] M. S. Rahman, "Behaviour and Strength of Fully Encased Composite Columns," no. December, 2016, pp. 1–198, 2016.

[4] R. Q. Bridge and J. W. Roderick, "Behavior of built-up composite columns.," *J. Struct. Div.*, vol. 104, pp. 1141–1155, 1978.

[5] H. Eggemann, "Developement of composite columns. Emperger's effort," *Proc. First Int. Congr. Constr. Hist.*, no. January, pp. 787–797, 2003.

[6] W.-F. Chen and S.-E. Kim, *LRFD steel design using advanced analysis*, vol. 13. CRC press, 1997.

[7] A. C. I. Committee, "Building code requirements for structural concrete (ACI 318-08) and commentary," 2008.

[8] B. I. Authority, "The New Zealand Building Code Handbook," *PO Box*, pp. 11–846, 1992.

[9] B. Ashe *et al.*, "Sustainability and the building code of Australia," 2003.

[10] T. Fukuchi and K. Ueno, "Guidelines on acoustic treatments for school buildings proposed by the Architectural Institute of Japan," 2004.

[11] A. Ataei, M. A. Bradford, and H. R. Valipour, "Experimental study of flush end plate beam-to-CFST column composite joints with deconstructable bolted shear connectors," *Eng. Struct.*, vol. 99, pp. 616–630, 2015, doi: doi.org/10.1016/j.engstruct.2015.05.012.

[12] Y. Zhang, Y. Liu, H. Xin, and J. He, "Numerical parametric study on ultimate load and ductility of concrete encased equal-leg angle steel composite columns," *Eng. Struct.*, vol. 200, p. 109679, 2019, doi: https://doi.org/10.1016/j.engstruct.2019.109679.

[13] A. Shariati, M. Shariati, N. H. R. Sulong, M. Suhatril, M. M. A. Khanouki, and M. Mahoutian, "Experimental assessment of angle shear connectors under monotonic and fully reversed cyclic loading in high strength concrete," *Constr. Build. Mater.*, vol. 52, pp. 276–283, 2014, doi: https://doi.org/10.1016/j.conbuildmat.2013.11.036.

[14] P. Lacki, J. Nawrot, A. Derlatka, and J. Winowiecka, "Numerical and experimental tests of steel-concrete composite beam with the connector made of top-hat profile," *Compos. Struct.*, vol. 211,

pp. 244–253, 2019, doi: https://doi.org/10.1016/j.compstruct.2018.12.035.

[15] M. I. Tabet-Derraz, A. Khelil, K. Hamdaoui, N. Boumechra, and M. Abdallah, “Experimental and numerical study of an innovative OMEGA-shaped connector for composite beams,” *Structures*, vol. 32, pp. 279–297, 2021, doi: https://doi.org/10.1016/j.istruc.2021.02.050.

[16] C. Odenbreit, M. Chrzanowski, R. Obiala, T. Bogdan, and H. Degée, “Characterisation of a new flat mechanical shear connection mean for steel-concrete composite columns,” *Structures*, vol. 21, pp. 122–134, 2019, doi: https://doi.org/10.1016/j.istruc.2019.03.001.

[17] G. W. Renton, “The behaviour of reinforced concrete beam-column joints under cyclic loading,” 1972.

[18] C. Chen, C. Wang, and H. Sun, “Experimental Study on Seismic Behavior of Full Encased Steel-Concrete Composite Columns,” *J. Struct. Eng.*, vol. 140, no. 6, p. 04014024, 2014, doi: 10.1061/(asce)st.1943-541x.0000951.

[19] C. Campian, Z. Nagy, and M. Pop, “Behavior of fully encased steel-concrete composite columns subjected to monotonic and cyclic loading,” *Procedia Eng.*, vol. 117, no. 1, pp. 439–451, 2015, doi: 10.1016/j.proeng.2015.08.193.

[20] W. Zhu, J. Jia, J. Gao, and F. Zhang, “Experimental study on steel reinforced high-strength concrete columns under cyclic lateral force and constant axial load,” *Eng. Struct.*, vol. 125, pp. 191–204, 2016, doi: 10.1016/j.engstruct.2016.07.018.

[21] L. Fang, B. Zhang, G. F. Jin, K. W. Li, and Z. L. Wang, “Seismic behavior of concrete-encased steel cross-shaped columns,” *J. Constr. Steel Res.*, vol. 109, pp. 24–33, 2015, doi: 10.1016/j.jcsr.2015.03.001.

[22] C. H. Xu, L. Zeng, Q. Zhou, X. Tu, and Y. Wu, “Cyclic performance of concrete-encased composite columns with T-shaped steel sections,” *Int. J. Civ. Eng.*, vol. 13, no. 4A, pp. 456–467, 2015, doi: 10.22068/IJCE.13.4.455.

[23] C. S. Shim, Y. S. Chung, and J. H. Han, “Cyclic response of concrete-encased composite columns with low steel ratio,” *Proc. Inst. Civ. Eng. Struct. Build.*, vol. 161, no. 2, pp. 77–89, 2008, doi: 10.1680/stbu.2008.161.2.77.

[24] H. L. Hsu, F. J. Jan, and J. L. Juang, “Performance of composite members subjected to axial load and bi-axial bending,” *J. Constr. Steel Res.*, vol. 65, no. 4, pp. 869–878, 2009, doi: 10.1016/j.jcsr.2008.04.006.

[25] E. Ellobody and B. Young, “Numerical simulation of concrete encased steel composite columns,” *J. Constr. Steel Res.*, vol. 67, no. 2, pp. 211–222, 2011, doi: 10.1016/j.jcsr.2010.08.003.

[26] S. Taufik and B. Tjahjono, "3D ANSYS Modeling behaviour of encased steel composite column with wide flange and hollow section," *Int. J. Mech. Appl.*, vol. 9, no. 1, pp. 10–18, 2019, doi: DOI: 10.5923/j.mechanics.20190901.02.

[27] H. Naito, M. Akiyama, and M. Suzuki, "Ductility Evaluation of Concrete-Encased Steel Bridge Piers Subjected to Lateral Cyclic Loading," *J. Bridg. Eng.*, vol. 16, no. 1, pp. 72–81, 2011, doi: 10.1061/(asce)be.1943-5592.0000120.

[28] J. Yue, J. Qian, and D. E. Beskos, "Seismic damage performance levels for concrete encased steel columns using acoustic emission tests and finite element analysis," *Eng. Struct.*, vol. 189, no. March, pp. 471–483, 2019, doi: 10.1016/j.engstruct.2019.03.077.

[29] Y. Chen, T. Wang, J. Yang, and X. Zhao, "Test and numerical simulation of partially encased composite columns subject to axial and cyclic horizontal loads," *Int. J. Steel Struct.*, vol. 10, no. 4, pp. 385–393, 2010, doi: 10.1007/BF03215846.

[30] L. H. Han, F. Y. Liao, Z. Tao, and Z. Hong, "Performance of concrete filled steel tube reinforced concrete columns subjected to cyclic bending," *J. Constr. Steel Res.*, vol. 65, no. 8–9, pp. 1607–1616, 2009, doi: 10.1016/j.jcsr.2009.03.013.

[31] P. Gajalakshmi and H. J. Helena, "Behaviour of concrete-filled steel columns subjected to lateral cyclic loading," *J. Constr. Steel Res.*, vol. 75, pp. 55–63, 2012, doi: 10.1016/j.jcsr.2012.03.006.

[32] L. H. Han, H. Huang, and X. L. Zhao, "Analytical behaviour of concrete-filled double skin steel tubular (CFDST) beam-columns under cyclic loading," *Thin-Walled Struct.*, vol. 47, no. 6–7, pp. 668–680, 2009, doi: 10.1016/j.tws.2008.11.008.

[33] W. W. Qian, W. Li, L. H. Han, and X. L. Zhao, "Analytical behavior of concrete-encased CFST columns under cyclic lateral loading," *J. Constr. Steel Res.*, vol. 120, pp. 206–220, 2016, doi: 10.1016/j.jcsr.2015.12.018.

[34] S. A. Civjan and P. Singh, "Behavior of shear studs subjected to fully reversed cyclic loading," *J. Struct. Eng.*, vol. 129, no. 11, pp. 1466–1474, 2003, doi: doi.org/10.1061/(ASCE)0733-9445(2003)129:11(1466).

[35] A. Suzuki and Y. Kimura, "Cyclic behavior of component model of composite beam subjected to fully reversed cyclic loading," *J. Struct. Eng.*, vol. 145, no. 4, p. 4019015, 2019, doi: https://doi.org/10.1061/(ASCE)ST.1943-541X.0002294.

[36] D. Lowe, K. Roy, R. Das, C. G. Clifton, and J. B. P. Lim, "Full scale experiments on splitting behaviour of concrete slabs in steel concrete composite beams with shear stud connection," *Structures*, vol. 23, pp. 126–138, 2020, doi: https://doi.org/10.1016/j.istruc.2019.10.008.

[37] J. Bonilla, L. M. Bezerra, and E. Mirambell, "Resistance of stud shear connectors in composite

beams using profiled steel sheeting," *Eng. Struct.*, vol. 187, pp. 478–489, 2019, doi: doi.org/10.1016/j.engstruct.2019.03.004.

[38] S. M. Younes, H. M. Ramadan, and S. A. Mourad, "Stiffening of short small-size circular composite steel–concrete columns with shear connectors," *J. Adv. Res.*, vol. 7, no. 3, pp. 525–538, 2016, doi: https://doi.org/10.1016/j.jare.2015.08.001.

[39] R. Rahnavard, C. Rebelo, H. D. Craveiro, and R. Napolitano, "Understanding the cyclic performance of composite steel-concrete connections on steel bridges," *Eng. Struct.*, vol. 224, p. 111213, 2020, doi: https://doi.org/10.1016/j.engstruct.2020.111213.

[40] S. De Nardin and A. El Debs, "Shear transfer mechanisms in composite columns: an experimental study," *Steel Compos. Struct.*, vol. 7, no. 5, p. 377, 2007, doi: https://doi.org/10.12989/scs.2007.7.5.377.

[41] K. Alenezi, M. M. Tahir, T. Alhajri, M. R. K. Badr, and J. Mirza, "Behavior of shear connectors in composite column of cold-formed steel with lipped C-channel assembled with ferro-cement jacket," *Constr. Build. Mater.*, vol. 84, pp. 39–45, 2015, doi: doi.org/10.1016/j.conbuildmat.2015.03.015.

[42] L. Guo, J. Wang, W. Wang, and M. Duan, "Seismic evaluation and calculation models of CFDST column blind bolted to composite beam joints with partial shear interaction," *Eng. Struct.*, vol. 196, p. 109269, 2019, doi: doi.org/10.1016/j.engstruct.2019.06.005.

[43] J. Zhang, X. Hu, Q. Sun, Y. Zhang, W. Zhu, and L. Li, "Experimental study on seismic performance of glulam-concrete composite beam-to-column joints," *Compos. Struct.*, vol. 236, no. December 2019, p. 111864, 2020, doi: 10.1016/j.compstruct.2020.111864.

[44] L. R. dos Santos, H. de Sousa Cardoso, R. B. Caldas, and L. F. Grilo, "Finite element model for bolted shear connectors in concrete-filled steel tubular columns," *Eng. Struct.*, vol. 203, p. 109863, 2020, doi: https://doi.org/10.1016/j.engstruct.2019.109863.

[45] L. R. dos Santos, R. B. Caldas, L. F. Grilo, H. Carvalho, and R. H. Fakury, "Design procedure to bearing concrete failure in concrete-filled steel tube columns with bolted shear connectors," *Eng. Struct.*, vol. 232, p. 111910, 2021, doi: https://doi.org/10.1016/j.engstruct.2021.111910.

[46] B. Mou, Y. Liu, P. Wei, F. Zhao, W. Chenglong, and N. Ning, "Numerical investigation and design method of bolted beam-column joint panel with eccentricity in beam depths," *J. Constr. Steel Res.*, vol. 180, p. 106568, 2021, doi: https://doi.org/10.1016/j.jcsr.2021.106568.

[47] A. A. Chiniforush, A. Ataei, and M. A. Bradford, "Experimental study of deconstructable bolt shear connectors subjected to cyclic loading," *J. Constr. Steel Res.*, vol. 183, p. 106741, 2021.

[48] M. Shariati, N. H. R. Sulong, M. Suhatril, A. Shariati, M. M. A. Khanouki, and H. Sinaei,

"Comparison of behaviour between channel and angle shear connectors under monotonic and fully reversed cyclic loading," *Constr. Build. Mater.*, vol. 38, pp. 582–593, 2013, doi: https://doi.org/10.1016/j.conbuildmat.2012.07.050.

[49] M. Shariati, N. H. R. Sulong, A. Shariati, and A. B. H. Kueh, "Comparative performance of channel and angle shear connectors in high strength concrete composites: An experimental study," *Constr. Build. Mater.*, vol. 120, pp. 382–392, 2016, doi: https://doi.org/10.1016/j.conbuildmat.2016.05.102.

[50] P. Helbrych, M. Major, and J. Nawrot, "Numerical and experimental analysis of a shear connection made using a top-hat profile," *Civ. Environ. Eng. reports*, vol. 26, no. 3, pp. 69–78, 2017, doi: https://doi.org/10.1515/ceer-2017-0036.

[51] ANSYS, "APDL, Release 15.0." 2013.

[52] S. P. Hussan and A. Bashir, "Analysis of Earthquake Resistant Properties of RC Core Steel Composite Columns & RCC Sections Using Finite Element Analysis," *Int. J. Eng. Trends Technol.*, vol. 28, no. 7, pp. 359–364, 2015.

[53] B. J. Si, Z. G. Sun, Q. H. Ai, D. S. Wang, and Q. X. Wang, "Experiments and simulation of flexural-shear dominated RC bridge piers under reversed cyclic loading," 2008.

[54] N. Seres, "Numerical modelling of shear connection between concrete slab and sheeting deck," 2008.

[55] M. M. Arrahmane, "Analyse numérique des poutres composites acier-béton simplement appuyées : étude de l'interface dalle-profil," 2015.

[56] S. S. Patil, A. N. Shaikh, and B. R. Niranjan, "Non Linear Finite Element Method of Analysis of Reinforced Concrete Deep Beam," *Int. J. Mod. Eng. Res.*, vol. 2, no. 6, pp. 4622–4628, 2012.

[57] A. M. Ibrahim and M. S. Mahmood, "Finite element modeling of reinforced concrete beams strengthened with FRP laminates," *Eur. J. Sci. Res.*, vol. 30, no. 4, pp. 526–541, 2009.

[58] Fauzan, R. Kurniawan, and Z. Al Jauhari, "Finite Element Analysis of CES Composite Columns," *Int. J. Civ. Eng. Technol.*, vol. 8, no. 10, pp. 979–987, 2017.

[59] A. John, U. K. G, and U. S, "Analytical study on stress-strain behaviour of reinforced concrete column," *Int. J. Civ. Eng. Technol.*, pp. 45–55, 2014.

[60] A. B. Alsamawi, N. Boumechra, and K. Hamdaoui, "Numerical Parametric Study of Fully Encased Composite Columns Subjected to Cyclic Loading," *Civ. Eng. J.*, vol. 8, no. 01, pp. 45–59, 2022, doi: http://dx.doi.org/10.28991/CEJ-2022-08-01-04.

[61] A. Alsamawi and N. Boumechra, "Behaviour of fully encased composite columns under cyclic loads," *ce/papers*, vol. 4, no. 2–4, pp. 564–569, 2021, doi: https://doi.org/10.1002/cepa.1331.

[62] P. Fuschi, M. Dutko, D. Perić, and D. R. J. Owen, “On numerical integration of the five-parameter model for concrete,” *Comput. Struct.*, vol. 53, no. 4, pp. 825–838, 1994, doi: doi.org/10.1016/0045-7949(94)90371-9.

[63] W. P. Zhao, “Local bond-slip numerical simulation based on ANSYS contact analysis,” *2011 Int. Conf. Electr. Technol. Civ. Eng. ICETCE 2011 - Proc.*, vol. 0, pp. 438–441, 2011, doi: 10.1109/ICETCE.2011.5775869.

[64] A. M. Ibrahim, S. K. Mohaisen, and Q. W. Ahmed, “Finite element modeling of composite steel-concrete beams with external prestressing,” *Int. J. Civ. Struct. Eng.*, vol. 3, no. 1, pp. 101–116, 2012.

[65] S. De Nardin, F. M. Almeida Filho, J. Oliveira Filho, V. G. Haach, and A. L. H. C. El Debs, “Non-linear analisys of the bond strength behavior on the steel-concrete interface by numerical models and pull-out tests,” in *Proceedings of the Structures Congress and Exposition*, 2005, pp. 1077–1088, doi: 10.1061/40753(171)107.

[66] Eurocode 3, *Design of steel structures Part 1-1 General rules and rules for buildings EN 1993-1-1*. 2004.

[67] Eurocode 2, *Design of concrete structures - Part 1-1: General rules and rules for buildings EN 1992-1-1*. 2004.

[68] C. Xu, L. Zeng, Q. Zhou, X. Tu, and Y. Wu, “Cyclic performance of concrete-encased composite columns with T- shaped steel sections,” vol. 13, no. 4, 2015.

[69] H. Krawinkler, *Guidelines for cyclic seismic testing of components of steel structures*, vol. 24. Applied Technology Council, 1992.

LIST OF PUBLICATIONS

Based on the work described in this thesis, the following list of publications have been made until the day of publication of the thesis:

Journal Articles

1. A. Alsamawi and N. Boumechra, "Behaviour of fully encased composite columns under cyclic loads," ce/papers, vol. 4, no. 2–4, pp. 564–569, 2021, https://doi.org/10.1002/cepa.1331.

2. Alsamawi N. Boumechra and K. Hamdaoui, "Numerical parametric study of fully encased composite columns subjected to cyclic loading" Civil engineering journal, vol. 8, no. 01, pp. 45–59, 2022, http://dx.doi.org/10.28991/CEJ-2022-08-01-04 .

3. A. Alsamawi, N. Boumechra and K. Hamdaoui, "Novel types of connection between steel and concrete in fully encased composite columns under cyclic loading", Eur J Environ Civ Eng.:1-19. https://doi:10.1080/19648189.2022.2066184

4. A. Alsamawi, N. Boumechra, K. Hamdaoui, E. Alkebsi and H. Basri (2022). "Numerical investigation of fully encased composite columns subjected to combined axial and cyclic loading". Int J Adv Sci Res Innov. 2022;5(1):39-53. https://doi:10.21608/IJASRI.2022.228573.

5. A. Alsamawi, N. Boumechra, A. Almutawakel, E. Alkebsi, H. Basri and H. Charrak, "Numerical investigation of fully encased composite columns with web or flange shear connectors under cyclic loading". (In the publishing stage)

6. A. Alsamawi, N. Boumechra, A. Almutawakel, E. Alkebsi, H. Basri and H. Charrak, "Analysis performance of fully encased composite columns with web or flange shear connectors under cyclic loading". (In the publishing stage)

Refereed Conference Papers

1. A. Alsamawi and N. Boumechra (2021). "Behaviour of fully encased composite columns under cyclic loads". *Proceedings of the 9th European Conference on Steel Structures*, Sheffield, United Kingdom,2021.

2. A. Alsamawi, N. Boumechra, A. Almutawakel, E. Alkebsi, H. Basri and H. Charrak (2021). Numerical investigation of fully encased composite columns with web or flange shear connectors under cyclic loading. *Proceedings of the first International Conference on Energy, Thermofluids and Materials Engineering*, Biskra, Algeria, 2021.

3. A. Alsamawi, N. Boumechra, K. Hamdaoui, E. Alkebsi and H. Basri (2022). "Numerical investigation of fully encased composite columns subjected to combined axial and cyclic loading". *Proceedings of the 4th International Conference on Engineering Science and Technology*, Luxor, Egypt, 2022.

Behaviour of composite steel-concrete columns subjected to cyclic loads

Abstract: For multi-floors buildings, the columns are generally of a composite steel-concrete design, either fully encased or partially encased and often tubular filled with reinforced concrete. Their composition in two materials whose constitutive laws are different induces a complexity in its behaviour, resistance and its dimensioning compared to the static and dynamic loads. Eurocode 4 presents the analytical tools for the calculation and sizing of composite columns subjected mainly to static loads. Several works, especially experimental ones, have been carried out to understand the behaviour of composite columns with respect to cyclic loads. The complexity in the response of this system reveals the interaction between the two materials, the elastoplastic constitutive law of steel, the specific constitutive law of concrete, the effect of friction, the effect of cover concrete, the effect of axial load ratio, the effects of concrete reinforcement bars, boundary conditions as well as the proposed new type of connection between steel and concrete interface. All these aspects will be taken into account in the study of this structural system. The work to be accomplished is a detailed numerical study of the behaviour of the composite column subjected to combined axial load and cyclic loads by evaluating the effect of all the parameters mentioned previously. In order to be able to develop analytical tools facilitating the engineer and the designer the calculation and the evaluation of the resistance of the composite column in relation to dynamic and seismic actions.

Keywords: Fully encased composite columns, Coefficient of friction, Cover concrete, Shear connector, Cyclic loading, Hysteresis curves.

سلوك الأعمدة الخرسانية الفولاذية المركبة المعرضة لأحمال دورية

ملخص: بالنسبة للمباني متعددة الطوابق ، تكون الأعمدة بشكل عام من تصميم مركب من الحديد الصلب والخرسانة ، إما مغطاة بالكامل أو مغطاة جزئيًا وغالبًا ما تكون أنبوبية مملوءة بالخرسانة المسلحة. يؤدي تكوينها في مادتين تختلف قوانينهما التأسيسية إلى تعقيد في سلوكها ومقاومتها وأبعادها مقارنة بالأحمال الثابتة والديناميكية. يقدم Eurocode 4الأدوات التحليلية لحساب وحجم الأعمدة المركبة المعرضة أساسًا لأحمال ثابتة. تم تنفيذ العديد من الأعمال ، وخاصة الأعمال التجريبية ، لفهم سلوك الأعمدة المركبة فيما يتعلق بالأحمال الدورية. يكشف التعقيد في استجابة هذا النظام عن التفاعل بين المادتين ، القانون التأسيسي للصلب المرنة ، القانون التأسيسي المحدد للخرسانة ، تأثير الاحتكاك ، تأثير الخرسانة المغطاة ، تأثير نسبة الحمل المحوري ، التأثيرات من قضبان التسليح الخرسانية وظروف الحدود ونوع التوصيل الجديد المقترح بين الفولاذ والواجهة الخرسانية. ستؤخذ كل هذه الجوانب في الاعتبار عند دراسة هذا النظام الهيكلي. العمل المراد إنجازه عبارة عن دراسة عددية مفصلة لسلوك العمود المركب المعرض للحمل المحوري المشترك والأحمال الدورية من خلال تقييم تأثير جميع المعلمات المذكورة سابقاً. من أجل التمكن من تطوير أدوات تحليلية تسهل على المهندس والمصمم حساب وتقييم مقاومة العمود المركب فيما يتعلق بالإجراءات الديناميكية والزلزالية.

الكلمات المفتاحية: أعمدة مركبة مغلفة بالكامل ، معامل الاحتكاك ، غطاء الخرسانة ، موصل القص ، التحميل الدوري ، منحنيات التباطؤ

Comportement des poteaux mixtes acier-béton soumis à des charges cycliques

Résume : Pour les bâtiments à plusieurs étages les poteaux sont en général de conception mixte acier-béton, soit enrobés, soit semi-enrobés et souvent tubulaires remplis de béton armé. Leur composition en deux matériaux dont les lois de comportement sont différentes induit une complexité dans son comportement, résistance et son dimensionnement par rapport aux charges statiques et dynamiques. L'Eurocode EC4 présente les outils analytiques pour le calcul et le dimensionnement des poteaux mixtes soumis surtout aux charges statiques. Plusieurs travaux, surtout expérimentaux ont été menés pour comprendre le comportement des poteaux mixtes par rapport aux charges cycliques. La complexité dans la réponse de ce système fait apparaitre l'interaction entre les deux matériaux, la loi de comportement élasto-plastique de l'acier, la loi de comportement spécifique du béton, l'effet du frottement, l'effet de l'enrobage du béton, l'effet du rapport de charge axiale, les effets des barres d'armature en béton, les conditions aux limites ainsi que le nouveau type de connexion proposé entre l'interface de l'acier et du béton. Tous ces aspects serons pris en compte dans l'étude de ce système structural. Le travail à accomplir est une étude numérique détaillée du comportement du poteau mixte soumis aux charge axiale et charges cycliques combinées en évaluant l'effet de tous les paramètres cites précédemment, ceci pour pouvoir développer des outils analytiques facilitant a l'ingénieur et au concepteur le calcul et l'évaluation de la résistance du poteau mixte par rapport aux actions dynamiques et sismiques.

Mots clés : Poteaux mixte totalement enrobés, Coefficient de frottement, Béton enrobage, Connecteur de cisaillement, Chargement cyclique, Courbes d'hystérésis.